Functional analysis of the flagellar type III secretion apparatus in *Salmonella enterica* serovar Typhimurium.

Von der Fakultät für Lebenswissenschaften
der Technischen Universität Carolo-Wilhelmina zu Braunschweig
zur Erlangung des Grades eines
Doktors der Naturwissenschaften
(Dr. rer. nat.)
genehmigte

D i s s e r t a t i o n

von Florian Daniel Fabiani
aus Albertville, Frankreich

1. Referentin: Prof. Dr. Petra Dersch
2. Referentin: Prof. Dr. Susanne Engelmann
eingereicht am: 08.05.2017
mündliche Prüfung (Disputation) am: 03.07.2017

Druckjahr 2017

Vorveröffentlichungen der Dissertation

Teilergebnisse aus dieser Arbeit wurden mit Genehmigung der Fakultät für Lebenswissenschaften, vertreten durch die Mentorin der Arbeit,
in folgenden Beiträgen vorab veröffentlicht:

Tagungsbeiträge

***Fabiani F.D.**, Barlag B., Hensel M., und Erhardt M.*: Functional analysis of the flagellar Type III secretion apparatus in *Salmonella enterica* serovar Typhimurium. (Poster). North Regio Day on Infection, NoRDI V, Braunschweig (2014).

***Fabiani F.D.**, Barlag B., Hensel M., und Erhardt M.*: Functional analysis of the *Salmonella* Typhimurium flagellar Type III secretion apparatus protein FliO. (Poster). BLAST XIII meeting, Tuscon, Arizona (2015).

***Fabiani F.D.**, Renault T., Barlag B.,Dietsche T., Wagner S., Hensel M., und Erhardt M.*: Functional analysis of the flagellar Type III secretion protein FliO in *Salmonella* Typhimurium. (Poster). Type III secretion system meeting, Tübingen (2016).

Acknowledgment:

I would like to thank the persons who´s help was crucial and without whom I couldn't have achieve this thesis.

First of all, I thank Dr. Marc Erhardt, for giving me the opportunity to work in his team. During these three and a half years, I really enjoyed working under his supervision on a fascinating project. I learned a lot at his side, he has always been extremely inspiring, supportive and was a great boss.

I would like to thank my mentor Prof. Dr. Petra Dersch for her support and her input and advice as a member of the thesis committee as well as during our constructive group meetings.

I am also grateful to Prof. Dr. Susanne Engelmann, for her helpful participation in the thesis committee meetings and for reviewing this thesis, and to Prof. Dr. André Fleißner for holding the chair during my defense. I would also like to thanks Prof. Dr. Emmanuelle Charpentier for her contribution to the early thesis committee meetings.

Thank you to the "HZI International Graduate School for Infection Research" and the Helmholtz association for funding my thesis, administrative help, and financial support for courses, external stays and participation at international conferences.

I am grateful to Prof. Dr. Samuel Wagner, Tobias Dietsche, Prof. Dr. Michael Hensel, and Dr. Britta Peters for productive collaborations and expert scientific support.

Obviously, I'd like to thank my colleagues from the IBIS group and friends. More especially, my office-mates Julia Horstmann, Dr. Caroline Kühne and Imke Spöring, for the friendly atmosphere, for constructive discussions and ideas, for helping me with every weird German administrative stuff, and for enduring my occasional bad mood. Many thanks to my "chaperone Post-doc" Dr. Thibaud Renault, for teaching me so much, for his help, for always keeping me motivated, and for our - not only scientific - great discussions. Thanks to Nadine Körner for her essential technical support, and to Karen Freier for her help and interest in the project.

I am grateful to the members of the MIBI group, for their questions and remarks during our joined group meetings, in particular to Jörn "Jörny" Hoßmann and Franziska Schuster, for pleasant and productive talks.

Special thanks to Imke, Julia, Jörn, Thibaud and Marc for valuable corrections of this work.

Merci beaucoup à mes parents, pour m'avoir permis d'arriver jusqu'ici et toujours avoir été là pour moi, pendant trente ans. Merci d'avoir cru en moi.

Finally, thank you Frieda, for your love, your moral support, for being there for me when I need help, and because you always keep me thinking straight.

Contents

List of figures V
List of Tables VI
List of abbreviations VI
Amino acid abbreviations VIII
Summary IX
Zusammenfassung X
1. Introduction 1
1.1. The Salmonella genus and associated diseases 1
1.2. Infection cycle and virulence factors of S. enterica 2
1.3. Type III secretion systems in Salmonella 5
1.4. The functional components of the flagellar T3SS 11
1.5. Objectives 13
2. Results 15
2.1. Genetic determination of the essential components for export by the fT3SS apparatus 15
2.1.1. Hook-β-lactamase fusion base assay 16
2.1.2. Construction of a minimal type III secretion plasmid 17
2.1.3. The minimal T3SS complement single operon deletion 21
2.1.4. Reconstitution of flagellar substrate export with minimal plasmids 24
2.1.5. Construction of a chromosomally encoded minimal type III secretion apparatus 25
2.1.6. Flagellar export reconstitution and definition of a minimal set of essential proteins 27
2.2. Unraveling the role of FliO 31
2.2.1. FliO function is related to FliP expression 32
2.2.2. FliO protects FliP from proteolysis 34
2.2.3. FliP membrane integration is not influenced by FliO 37
2.2.4. Lon is responsible for FliP proteolysis 39
2.2.5. FliO is not localized in the export apparatus 41
2.2.6. FliO is required for FliP oligomer assembly in flagellar formation 45
2.3. The role of the N-terminal signal peptide of FliP 49
2.3.1. Construction of cleavage site mutants 49
2.3.2. Cleavage is crucial for motility 51
2.3.3. Both cleavage and the presence of the signal peptide are important for FliP stability 52
2.3.4. The signal peptide facilitates membrane integration 54
2.3.5. Cleavage might be involved in the folding process 55
2.3.6. Cleavage is essential for proper assembly of the basal body 57
3. Discussion 59

3.1. FliF, FlhBA and FliOPQR are sufficient to assemble a functional T3SS export apparatus ..59
3.2. FliO act as a flagellum-specific chaperone facilitating the assembly of the export gate 61
3.3. Signal peptide enhances FliP membrane insertion and must be cleaved for flagellum assembly 63
3.4. FliO and the signal peptide probably got lost during injectisome evolution.....64
4. Conclusions 67
5. Materials and Methods 69
5.1 Material, buffers and chemicals.....69
5.2 Antibodies.....73
5.3 Bacterial strains, plasmids and media 73
5.4 Strain constructions 73
5.4.1 Proof reading amplification 84
5.4.2 Amplification with Go-Taq® polymerase 84
5.4.3 Colony PCR 85
5.4.4 Plasmid purifications 85
5.4.5 Enzymatic restriction digest 85
5.4.6 Vector dephosphorylation 85
5.4.7 Insert phosphorylation. 86
5.4.8 Agarose gel electrophoresis 86
5.4.9 Gel extraction 87
5.4.10 DNA concentration measurement 87
5.4.11 Ligation 87
5.4.12 Chemically competent cells preparation 87
5.4.13 Electro-competent cells preparation 87
5.4.14 Electroporation 88
5.4.15 PCR based fusion 88
5.4.16 Gibson assembly® 88
5.4.17 Chromosomal integration of CRIM plasmids 89
5.4.18 FRT recombination 89
5.4.19 λ-red recombination for tetRA insertion 89
5.4.20 λ-red recombination for tetRA replacement 90
5.4.21 P22 transduction 90
5.4.22 DNA-sequencing 91
5.5 Motility assay 91
5.6 Flagella staining – Immunofluorescence 91
5.7 Minimal Inhibitory Concentration assay 91

5.8 Secretion assay **92**
5.9 Protein stability assay **93**
5.10 TCA precipitation **93**
5.11 Cell fractionation assay **93**
5.12 SDS polyacrylamide gel **94**
5.13 TCE staining **95**
5.14 Western blot **95**
5.15 Stripping of Western blot membrane **95**
5.16 Protein levels quantification **95**
5.17 Large scale crude membrane preparation **96**
5.18 Sucrose gradient **96**
5.19 FliP pull down **97**
5.20 Blue Native PAGE **98**
5.21 Mass spectrometry analysis **98**
5.22 FliO localization by super-resolution microscopy **99**
5.23 Single molecule localization and tracking **100**
5.24 Single cysteine labelling **100**
6. References 101

List of figures

FIGURE 1: INVASION OF THE INTESTINAL EPITHELIUM BY SALMONELLA TYPHIMURIUM. 4
FIGURE 2: FLAGELLAR GENE EXPRESSION AND FLAGELLAR ASSEMBLY. 6
FIGURE 3: COMPARISON OF THE STRUCTURES OF THE FLAGELLUM AND THE INJECTISOME. 8
FIGURE 4: PREDICTED TOPOLOGY OF THE EXPORT GATE COMPONENTS. 12
FIGURE 4: SCHEMATIC REPRESENTATION OF THE FLGE-BLA REPORTER SYSTEM. 16
FIGURE 5: FUSION OF FLIOPQR WITH THE TERMINATORS REGION OF PEM726 BY PCR-BASED FUSION. 18
FIGURE 6: CONSTRUCTION OF MINIMAL T3SS PLASMIDS.. 19
FIGURE 7: FLAGELLAR OPERONS INDUCTION ON PEM1271 AND PEM2273.. 20
FIGURE 8: CHROMOSOMALLY ENCODED PEM2273 FAILED TO COMPLEMENT SINGLE OPERONS DELETIONS. 22
FIGURE 9: EPISOMALLY ENCODED PEM2273 COMPLEMENTS SINGLE FLAGELLAR OPERON DELETIONS.. 23
FIGURE 10: PEM2273 DOES NOT ALLOW RECONSTITUTION OF FLAGELLAR EXPORT. A) EXAMPLE OF MIC ASSAY 24
FIGURE 11: ORGANIZATION OF THE FLAGELLAR OPERONS AT THEIR NATIVE LOCI OF S. ENTERICA TYPHIMURIUM LT2. 26
FIGURE 12: FLIOPQR FLHBA AND FLIF ARE SUFFICIENT TO RESTORE FLAGELLAR EXPORT. 28
FIGURE 13: FLGE-BLA EXPRESSION IS SIMILAR IN ALL STRAINS. 29
FIGURE 14: FLIO IS DISPENSABLE UPON FLIP OVEREXPRESSION.. 30
FIGURE 15: FLIP IS HIGHLY CONSERVED AMONG SPECIES.. 33
FIGURE 16: OVEREXPRESSION OF FLIP COMPLEMENTS FLIO DELETION.. 34
FIGURE 17: FLIP IS UNSTABLE IN ABSENCE OF FLIO.. 35
FIGURE 18: FLIO ACTS ON FLIP STABILITY AT THE PROTEIN LEVEL. 36
FIGURE 19: FLIO IS ALSO INVOLVED IN FLHA STABILITY. 37
FIGURE 20: FLIP MEMBRANE INTEGRATION IS INDEPENDENT ON FLIO. 38
FIGURE 21: LON IS INVOLVED IN FLIP STABILITY. 40
FIGURE 22: LON DEPENDENT PROTEOLYSIS OCCURS AT THE MEMBRANE. 41
FIGURE 23: HALOTAG AND SNAP-TAG FUSION DO NOT AFFECT EXPORT AND FLAGELLAR FORMATION. 42
FIGURE 24: FLIO DOES NOT CO-LOCALIZE WITH THE BASAL BODIES.. 43
FIGURE 25: FLIO IS FREELY DIFFUSING IN THE MEMBRANE. 44
FIGURE 26: FLIO IS REQUIRED FOR FLIP COMPLEXES ASSEMBLY. 46
FIGURE 27: FLIO PHYSICALLY INTERACTS WITH FLIP BUT IS ABSENT OF THE BASAL BODY. 48
FIGURE 28: SCHEMATIC VIEW OF THE CLEAVAGE SITE MUTANTS USED IN THIS STUDY. 50
FIGURE 29: SIGNAL PEPTIDE CLEAVAGE IS CRUCIAL FOR MOTILITY. 52
FIGURE 30: THE PRESENCE OF THE SIGNAL PEPTIDE AND CLEAVAGE EFFICIENCY INFLUENCE FLIP STABILITY. 53
FIGURE 31: THE SIGNAL PEPTIDE INFLUENCES MEMBRANE INSERTION. 54
FIGURE 32: SIGNAL PEPTIDE CLEAVAGE INFLUENCES THE FLIP TOPOLOGY. 56
FIGURE 33: CLEAVAGE IS CRUCIAL FOR FLIP COMPLEXES FORMATION.. 58
FIGURE 35: FLIO FACILITATES FLIP ASSEMBLY WITHIN THE IMEA COMPLEX.. 62

List of Tables

TABLE 1: LIST OF THE PROTEINS OF THE FT3SS AND THEIR HOMOLOGS IN THE INJECTISOME. 10
TABLE 2: EXAMPLES OF FLIO HOMOLOGS IN MULTIPLE PHYLA OF THE BACTERIAL DOMAIN. 65
TABLE 3: LIST OF ANTIBIOTICS AND OTHER ADDITIVES 69
TABLE 4: LIST OF MEDIA AND BUFFERS 70
TABLE 5: LIST OF ANTIBODIES USED IN THIS STUDY 73
TABLE 6: LIST OF STRAINS USED FOR THIS STUDY 74
TABLE 7: LIST OF PLASMIDS USED IN THIS STUDY 79
TABLE 8: LIST OF PRIMERS USED FOR PLASMIDS AND STRAINS CONSTRUCTION IN THIS STUDY 80
TABLE 9: PCR AMPLIFICATION WITH PROOF READING POLYMERASE 84
TABLE 10: PCR AMPLIFICATION WITH GO-TAQ POLYMERASE 84
TABLE 11: PCR AMPLIFICATION WITH GO-TAQ POLYMERASE 85
TABLE 12: DEPHOSPHORYLATION 86
TABLE 13: PHOSPHORYLATION 86
TABLE 14: GIBSON ASSEMBLY REACTION 88
TABLE 15: AMPICILLIN DILUTIONS FOR MIC ASSAY 92
TABLE 16: SDS GELS COMPOSITION 94
TABLE 17: SUCROSE GRADIENT COMPOSITION 96

List of abbreviations

AAA+	ATPases Associated with diverse cellular Activities
Amp	Ampicillin
AnTc	Anhydrotetracycline
APS	Ammonium persulfate
Ara	Arabinose
ATP	Adenosine triphosphate
att	Bacteriophage attachment site
Bla	B-lactamase
BN-PAGE	Blue Native polyacrylamide gel electrophoresis
bp	Base pair
°C	Degree Celsius
CCD	Charge-coupled device
CID	Collision-induced dissociation
Cm	Chloramphenicol
C-ring	Cytoplasmic ring
CCW	Counter clockwise
CW	Clockwise
DAPI	4',6-diamidino-2-phenylindole
DDM	n-Dodecyl-β-D-maltopyranoside
DNA	Deoxyribonucleic acid
dNTP	Deoxyribonucleoside triphosphate
dSTORM	Direct stochastic optical reconstruction microscopy
DTT	Dithiothreitol
ECL	Enhanced chemiluminescence
EDTA	Ethylenediaminetetraacetic acid
EtBr	Ethidium bromide
FCF	FRT-chloramphenicol-FRT cassette
FKF	FRT-kanamycin-FRT cassette
FM-64	N-(3-Triethylammoniumpropyl)-4-(6-(4-(Diethylamino) Phenyl) Hexatrienyl) Pyridinium Dibromide
FRT	Flippase recognition target

fT3SS	Flagellar specific type III secretion system
gDNA	Genomic DNA
H	Hour
HA	Human influenza hemagglutinin
HBB	Hook basal body
HRP	Horseradish peroxidase
IC_{50}	half maximal inhibitory concentration
IM	Inner membrane
IPTG	Isopropyl β-D-1-thiogalactopyranoside
Kan	Kanamycin
kDa	Kilo Dalton
L	Liter
LB	Lysogeny broth
LC-MS/MS	Liquid chromatography tandem mass spectrometry
Log	Logarithm
L-ring	LPS-ring
M	Meter
M	Molar
MBP	Maltose-binding protein
MCP	Methyl-acepting chemotaxis protein
MIC	Minimal inhibitory concentration
min	Minute
ml	Milliliter
mM	Millimolar
MQ-water	Milli-Q™ water
MSD	Mean square displacement
MS-ring	Membrane-Supramembrane-ring
n	Number of sample
NaSal	Sodium salicylate
NC	Needle complex
nm	Nanometer
OD_{600}	Optical density at 600 nm
OD unit	Equivalent of 1 ml of culture at OD_{600} =1
OM	Outer membrane
ON culture	Overnight culture
-P	Phosphorylated
PCR	Polymerase chain reaction
PEG	Polyethylene glycol
PFA	Paraformaldehyde
PG	Peptidoglycan
PMF	Proto-motive force
P-ring	Peptidoglycan-ring
PVDF	polyvinylidene difluoride
RNA	Ribonucleic acid
s	Second
SCAM	Substituted-Cysteine Accessibility Method
SCV	Salmonella Containing Vacuole
SD	Standard deviation
SDS	Sodium dodecyl sulfate
SDS-PAGE	SDS-polyacrylamide gel electrophoresis
SOC	Super Optimal broth with Catabolite repression
SP	Signal peptide
Spc	Spectinomycin
SPI	Salmonella Pathogenicity Island
SRM	Super Resolution Microscopy
SRP	Signal recognition particle

Tc	Tetracycline
TCA	Trichloroacetic acid
TCE	Trichloroethylene
TEMED	Tetramethylethylenediamine
TBF	Transformation buffer
TM	Transmembrane domain
TPM	Transcript per million
TIRF	Total internal reflection fluorescence microscopy
T_x	Time point x
T3SS	Type III secretion system
V	Volt
VAP	Vacuole-associated actin polymerization
vc	Vector control
vT3SS	Virulence-associated Type III secretion system
W	Watt
WT	Wild-type
::	Insertion
α	Anti
Δ	Deletion of the gene X
ΔpH	pH gradient
ΔΨ	Electrical potential gradient
µl	Microliter
µM	Micromolar

Amino acid abbreviations

Amino Acid	3-letter	1-letter
Alanine	Ala	A
Arginine	Arg	R
Asparagine	Asn	N
Aspartic acid	Asp	D
Cysteine	Cys	C
Glutamic acid	Glu	E
Glutamine	Gln	Q
Glycine	Gly	G
Histidine	His	H
Isoleucine	Ile	I
Leucine	Leu	L
Lysine	Lys	K
Methionine	Met	M
Phenylalanine	Phe	F
Proline	Pro	P
Serine	Ser	S
Threonine	Thr	T
Tryptophan	Trp	W
Tyrosine	Tyr	Y
Valine	Val	V

Summary

The ability of many bacteria to swim trough liquids or swarm over surfaces is not only essential to access more favorable environments but is also crucial for many pathogens to establish a successful infection. Swimming and swarming motility is dependent on a macromolecular propeller, the flagellum. Flagellum synthesis requires the translocation of thousands of flagellar subunits across the bacterial cell envelope. This export process depends on a complex nanomachine located at the base of the flagellum, the flagellar Type III secretion system (fT3SS). This apparatus is highly similar to the virulence associated T3SS (vT3SS) used by many Gramm-negative pathogens to inject toxins into the host cell. The fT3SS is composed of six cytoplasmic and seven membrane proteins previously described as essential for export. FliGMN and FliHIJ form the cytoplasmic ring and the flagellar specific ATPase complex, respectively. FlhBA and FliOPQR form the export gate surrounded by the MS-ring made of FliF. Except for FliO, the membrane components are highly conserved among species, and have clear homologs in the vT3SS. Despite intense study on the function and the synthesis of the flagellum, the molecular details of protein export via the fT3SS is poorly understood. It remains unclear which proteins are essential for flagellar substrate export and the function of several of them is unknown. In this thesis, we contributed to untangle the mechanism underlying flagellar Type III secretion.

In the first part, we aimed to reconstitute a minimal T3SS apparatus, only composed of proteins required and sufficient for export. We uncoupled export of flagellar substrate from synthesis, to measure export in a plasmid- and a chromosomally-encoded minimal T3SS. We determined that FlhBA, FliF and FliPQR are essential and that FliO is only dispensable in presence of excess FliP.

In the second part, we further investigated the functional link between FliO and FliP. We demonstrated that FliO prevents Lon-mediated proteolysis of FliP and that FliO facilitates the formations of FliP complexes required for flagellar assembly. We observed that FliO is not part of the completed flagellum. We propose that FliO acts as a specific chaperone for flagellar assembly.

In the last part, we examined the role of the cleavable signal peptide of FliP, which is absent in the vT3SS homolog of FliP, and the effect of its cleavage on motility and flagellar synthesis. We observed that the presence of the signal peptide enhances FliP expression but is not crucial for motility, while cleavage is required for flagellar assembly.

Zusammenfassung

Motilität ermöglicht es vielen Bakterien sich nicht nur zu Bereichen mit vorteilhaften Wachstumsbedingungen zu bewegen, sondern ist bei vielen Pathogenen für eine erfolgreiche Infektion des Wirts notwendig. Schwimm- und Schwärmmotilität ist von einem makromolekularen Propeller, dem Flagellum, abhängig. Die Synthese des Flagellums erfordert den Transport von tausenden Untereinheiten durch die bakterielle Zellhülle. Dieser Transport wird von einer komplexen Nanomaschine, dem flagellaren Typ-III-Sekretionssystem (fT3SS), bewerkstelligt. Das fT3SS ähnelt dem Virulenz-assoziierten T3SS (vT3SS), das von Pathogenen verwendet wird, um Toxine in eine eukaryotische Zelle zu injizieren, stark. Das fT3SS setzt sich aus sechs zytoplasmatischen und sieben Membranproteinen zusammen. FliGMN bilden den zytoplasmatischen Ring und FliHIJ den ATPase-Komplex. Der MS-Ring aus FliF umgibt den aus FlhBA und FliOPQR zusammengesetzten Exportkanal. Außer FliO sind die Membranproteine in verschiedenen Spezies hoch konserviert und haben jeweils ein Homolog im vT3SS. Trotz intensiver Forschung zur Funktion und Synthese des Flagellums sind die Details des Proteinexports durch das fT3SS noch nicht gut verstanden. Es ist unklar welche Proteine essentiell für den flagellaren Substratexport sind. Außerdem ist die Funktion einiger Proteine unbekannt. Diese Arbeit soll dazu beitragen den Mechanismus des Typ-III-Sekretionssystems aufzuklären.

Zunächst wurde versucht ein minimales T3SS zu konstruieren, das nur aus Proteinen besteht, die notwendig und hinreichend für den flagellaren Export sind. Der Export von flagellarem Substrat wurde von der Synthese entkoppelt, um die Exportrate von Plasmid- und chromosomal codierten minimalen T3SS zu messen. Es wurde ermittelt, dass FlhBA, FliF und FliPQR essentiell sind und FliO nur in Gegenwart eines Überschusses an FliP entbehrlich ist.

Anschließend wurde der funktionelle Zusammenhang von FliO und FliP tiefergehend untersucht. Es konnte gezeigt werden, dass FliO die Proteolyse von FliP durch die Lon-Protease verhindert. Es wurde bewiesen, dass FliO die Bildung des zur Synthese des Flagellums notwendigen FliP-Komplexes begünstigt. Außerdem wurde beobachtet, dass FliO im fertiggestellten Flagellum nicht vorhanden ist. Es wird postuliert, dass FliO als spezifisches Chaperon die Synthese des Flagellums ermöglicht.

Abschließend wurden die Funktion des Signalpeptides von FliP und der Effekt, den dessen Abspaltung auf Flagellensynthese und Motilität hat, erforscht. Es wurde beobachtet, dass das Signalpeptid zwar die Expression von FliP verbessert, seine Abwesenheit die Motilität jedoch nur wenig beeinträchtigt. Es konnte gezeigt werden, dass die Abspaltung des Signalpetides für die Synthese des Flagellums notwendig ist.

1. Introduction

Bacterial pathogens have always been a major threat to public health. Since the antiquity until the beginning of the 20th century, pandemics such as the plague of Athens, the black death, the great plague, the cholera and tuberculosis pandemics have been responsible for hundreds of millions of deaths [1,2]. Therefore, the invention of vaccines and most notably the discovery of antibiotics in the 1940's, were seen as a revolution. This view was comforted with the rapid decrease of a multitude of diseases such as smallpox, tuberculosis and tetanus. Both scientists and political authorities were convinced that infectious diseases would be quickly eradicated [3]. However, over- or misuse of antibiotics increased the selective pressure on bacterial pathogens, leading to the selection of resistant bacteria. Thereafter, resistance to antimicrobial drugs rapidly spread among species. Furthermore, the appearance of the Human immunodeficiency virus led to the reemergence of many bacterial infections [4–6]. Recently, the world health organization issued a list of 12 bacterial pathogens of major concern, on which research and development of new antimicrobial drugs should prioritize. This list of concerning bacteria includes *Salmonella, Pseudomonas* and other *Enterobacteriaceae* [7]. Therefore, better understanding of these bacteria and their pathogenesis is crucial for the discovery of effective new drugs. In this thesis, we investigate a protein export system, the Type III secretion system (T3SS), which is crucial for the pathogenicity *Salmonella enterica*. This system is highly conserved among many Gram-negative pathogens and required for both motility and virulence.

1.1.The *Salmonella* genus and associated diseases

Salmonellae are Gram-negative, 2 to 5 µm long rod shaped, flagellated and facultative anaerobic enteric bacteria responsible for typhoidal and non-typhoidal salmonellosis in both humans and animals [8,9]. The nomenclature of the *Salmonella* genus is complex. The genus can be divided into two species; the cold-blooded animals commensal *S. bongori*, and *S. enterica,* mostly affecting warm-blooded animals. The *S. enterica* species regroups about 2,500 different serovars classified based on the chemical composition of the lipopolysaccharide (O antigen) and the protein content of the flagella (H antigens) [10,11]. Many of these serovars are major human foodborne pathogens, such as *S. enterica* serovar Typhi (*S*. Typhi) and. *S. enterica* serovar Typhimurium (*S*. Tm). *S.* Typhi is responsible for typhoid fever, an invasive systemic illness with frequent lethal outcome, and

S. Typhimurium is the causative agent of non-typhoidal salmonellosis, a usually self-limiting gastroenteritis, which in some cases can evolve into life-threatening septicemia in susceptible individuals [12]. Whereas *S.* Typhi is human-restricted, *S.* Typhimurium also causes a typhoid fever-like syndrome in murine hosts. The global burden of typhoid fever was estimated to 21.6 million cases and about 215,000 fatalities per year in 2004 [13]. For non-typhoidal *Salmonellae,* studies estimated a total of 93 million cases of gastroenteritis and 3.4 million of invasive salmonellosis cases responsible for 155,000 and 680,000 deaths, respectively [14,15]. Although these diseases have less dramatic consequences in developed countries, they have important socio-economic implications. For instance, the annual cost of *Salmonella* infections was evaluated to be approximately 3 billion dollars for the US alone [16]. Furthermore, the prevalence of multidrug resistant strains dramatically increased in the last 30 years making *Salmonella enterica* a major public health problem [17]. In this work, we focus on *S.* Typhimurium.

1.2.Infection cycle and virulence factors of *S. enterica*

Salmonellae enter the gastro-intestinal tract mainly upon ingestion of contaminated water or food. They survive the low pH in the stomach and colonize the intestine where they cross the epithelial barrier and cause gastro-intestinal disease. Several virulence factors and determinants, encoded on the chromosome, on genomic islands acquired by horizontal gene transfer, the *Salmonella* Pathogenicity Islands (SPIs), or on plasmids, are required at different stages to establish a successful infection [18].

After entering the intestinal lumen, *Salmonellae* must rapidly reach the epithelium to trigger infection. Flagellar motility and chemotaxis play a crucial role in this process. *Salmonella* harbors several chemoreceptors and expresses four to five peritrichous flagella. These long macromolecular helical filaments, powered by a rotary motor at their base, rotate in a counter-clockwise manner and form a bundle. This bundle acts as a propeller, allowing bacteria to swim through liquid environments. Flagellar rotation is coupled to temporal sensing of environmental conditions. *Salmonella* harbors multiple chemoreceptors, also known as methyl-accepting chemotaxis proteins (MCPs), which sense the presence of chemoattractant and repellant such as sugars or amino acids present in the mucus, but also the pH, the oxygen concentration and the temperature. These MCPs form complexes with the adapter protein CheW and the histidine kinase CheA [19–21]. In presence of repellant or in absence of attractant, CheA is autophosphorylated and transfers

its phosphoryl group on the chemotaxis response regulator CheY. Subsequently, CheY~P binds to the flagellar rotor. Upon binding, the rotor, which is located at the base of the flagellum, switches direction from counterclockwise to clockwise. This process results in disruption of the flagellar bundle, and the bacterium tumbles. When the bundle reforms, the bacterium starts swimming forward in a new direction. This results in a random walk biased towards beneficial conditions [22,23]. In the lumen, this mechanism allows *Salmonella* to swim through a thick layer of mucus towards the epithelium and establishes initial contact with the target cells [24,25] (Figure 1 I). Motility also provides a better access to nutrients and thus enhances colonization of the intestinal epithelium [26].

Once in contact with the epithelium (Figure 1 II), the bacteria adhere to the surface of their target cells through fimbrial as well as non-fimbrial adhesins [27–29]. *S.* Typhimurium mainly targets specialized epithelial cells, the M-cells, located in the Payer´s patches, which transport antigens from the lumen to the lymphoid tissue [30,31]. However, *Salmonella* also invades non-phagocytic epithelial cells [32]. Directly after adhesion, bacteria use a needle-like complex, encoded on the SPI-1, the so-called SPI-1 injectisome, to initiate invasion of the host cell [33]. This needle complex forms a pore in the eukaryotic cell wall and injects effectors directly into the host cytosol. These effectors, such as SopE and SopD, interact with eukaryotic small Rho-GTPases, inducing a dramatic actin rearrangement [34,35]. This rearrangement leads to formation of membrane ruffles (Figure 1 III) and engulfment of *Salmonella* into the host cell. Bacteria are then incorporated by micropinocytosis into large vesicles, the *Salmonella* containing vacuoles (SCVs) [32,36]. The delivery of the effectors also induces production of pro-inflammatory cytokines and recruitment of phagocytes. The resulting intestinal inflammation and the invasion induce epithelial cell damage and fluid secretion responsible for severe diarrhea [37]. Inflammation facilitates access to nutrients and is therefore beneficial for *Salmonella*. However, once the levels of immune cells and antimicrobial agents are too high, inflammation becomes detrimental. Thus, several SPI-1 effectors also counter-act the pro-inflammatory effects of SopE and SopD to maintain optimal conditions.

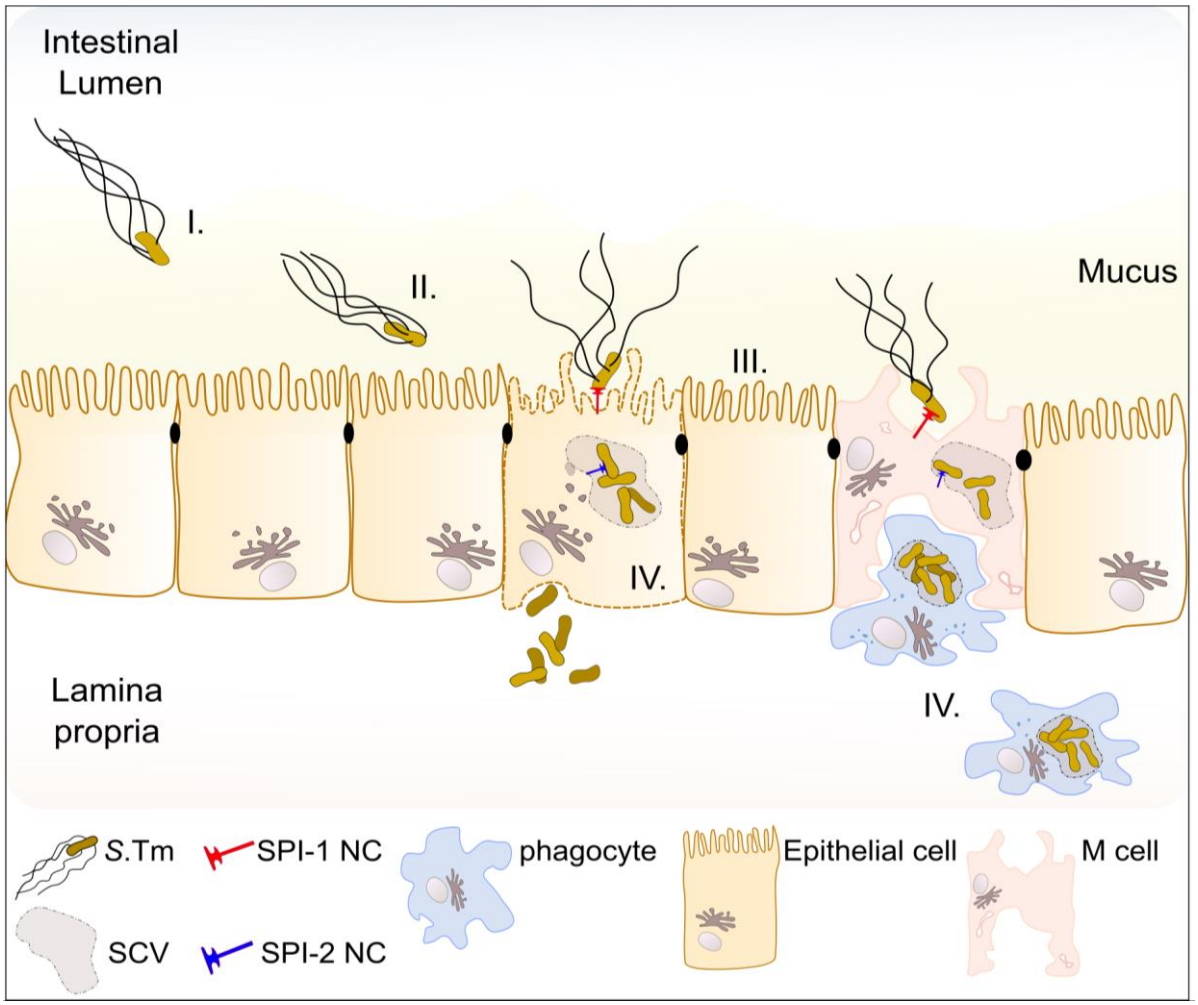

Figure 1: Invasion of the intestinal epithelium by *Salmonella* Typhimurium. I) *Salmonellae* enter the gastrointestinal tract and use peritrichous flagellation to swim across the mucus. **II)** When approaching the epithelial layer, bacteria attach to target cells using adhesins. **III)** *Salmonellae* inject toxins into M-cells or non-phagocytic epithelial cells through the SPI-1 needle complex (NC). This triggers a dramatic actin rearrangement, the so-called membrane ruffling, allowing bacteria to be engulfed in the eukaryotic cells. **IV)** After engulfment, bacteria prevent maturation of the vesicle and fusion with the phagosome by secreting effector proteins in the cytosol using the SPI-2 needle complex. *Salmonellae* then multiply in the SCVs, before being either released in the *lamina propria* or engulfed by phagocytes, facilitating spreading to target organs**.**

After internalization, maturation of the vesicle and fusion with the lysosome would normally lead to delivery of free radicals and antimicrobial enzymes inside the SCV. In order to escape this fate, *Salmonella* assembles a second needle-like complex encoded on SPI-2 [38]. This second injectisome enables delivery of several effectors in the cytosol, such as SsaB (SpiC). SsaB inhibits intracellular trafficking, therefore preventing fusion with the lysosome [39] (Figure 1 IV). Other SPI-2 effectors induce *Salmonella* induced filaments (SIFs) and the formation of an actin network surrounding the SCVs, also called vacuole-associated actin polymerization (VAP). These processes maintain the integrity of the SCVs and allow them to migrate to the vicinity of the Golgi apparatus to intercept

transport vesicles as a source of nutrients [18]. Therefore, SCVs become an ideal niche for *Salmonellae* to survive and replicate within the epithelium (Figure 1). Consequently, SCVs migrate towards the basolateral membrane and bacteria enter the *lamina propria,* where they are engulfed by phagocytes once again.

In healthy individuals, *Salmonella* does not disseminate and the disease remains self-limited. The destruction of the epithelium, resulting from internalization and subsequent inflammation, causes severe diarrhea, nausea and abdominal cramps, which are the major symptoms in non-invasive salmonellosis. In susceptible individuals however, such as children, pregnant women or immunocompromised patients, *S. Typhimurium* can disseminate systematically and colonize the liver and the spleen, where it preferentially replicates. In order to escape from the intestinal epithelium, SPI-1 and SPI-2 secreted effectors activate caspase-1 and caspase-3 pathways to trigger apoptosis. Programmed cell death, in opposition to necrosis, prevents the release of intracellular content, allowing bacteria to be taken up by phagocytes in a non-inflammatory fashion. Once taken up, bacteria can survive within phagocytes and disseminate through the lymphatic system towards the liver and the spleen [18]. In mice, this process usually takes between 12 and 24 hours [18,40]. Interestingly, *Salmonella* developed another and more direct way to disseminate. Once *Salmonella* is engulfed by CD18+ monocytes, the SPI-2 secreted effector SfrH manipulates the motility machinery of the cell to directly penetrate the blood stream and reach the target organs in approximately 15 minutes [40]. *Salmonella* dissemination to lymphatic organs and bacteremia lead to a severe systemic disease similar to typhoid fever, and occasionally even meningitis, dramatically decreasing the survival chances.

1.3.Type III secretion systems in *Salmonella*

Nearly all critical steps of the infection cycle, including approach, invasion, survival and dissemination are dependent on three highly sophisticated nanomachines; the SPI-1 and SPI-2 injectisomes and the flagellum. Interestingly, these three crucial virulence factors are evolutionary related. The assembly of the flagellum is dependent on protein export via the flagellar T3SS (fT3SS), which is highly homologous to the virulence associated T3SS (vT3SS) required for needle complex (NC) formation and effector secretion. Phylogenetic studies suggest that the last common ancestor of vT3SS arose from a flagellum and evolved into a eukaryotic specific toxin delivery system [41].

The flagellum is composed of three main substructures: (i) the basal body, (ii) a flexible hook, and (iii) a long and rigid helical filament. The basal body, starting in the cytosol and spanning the inner membrane (IM) and the outer (OM) membrane, host the T3SS and the flagellar motor. The hook transmits the torque from the motor to the filament. The injectisome is made of two parts consisting of (i) a basal body harboring the secretion machinery, (ii) a short and straight needle required for delivery in the target cell [42]. Both organelles are made of 20 to 30 different proteins and display many structural similarities. The overall architecture of each structure is depicted in Figure 3 and the different proteins and their degree of homology is described in Table 1. Each injectisome has its own nomenclature. Here, we use the nomenclature corresponding to SPI-1 vT3SS to compare the structure and the assembly of the needle complex and the flagellum.

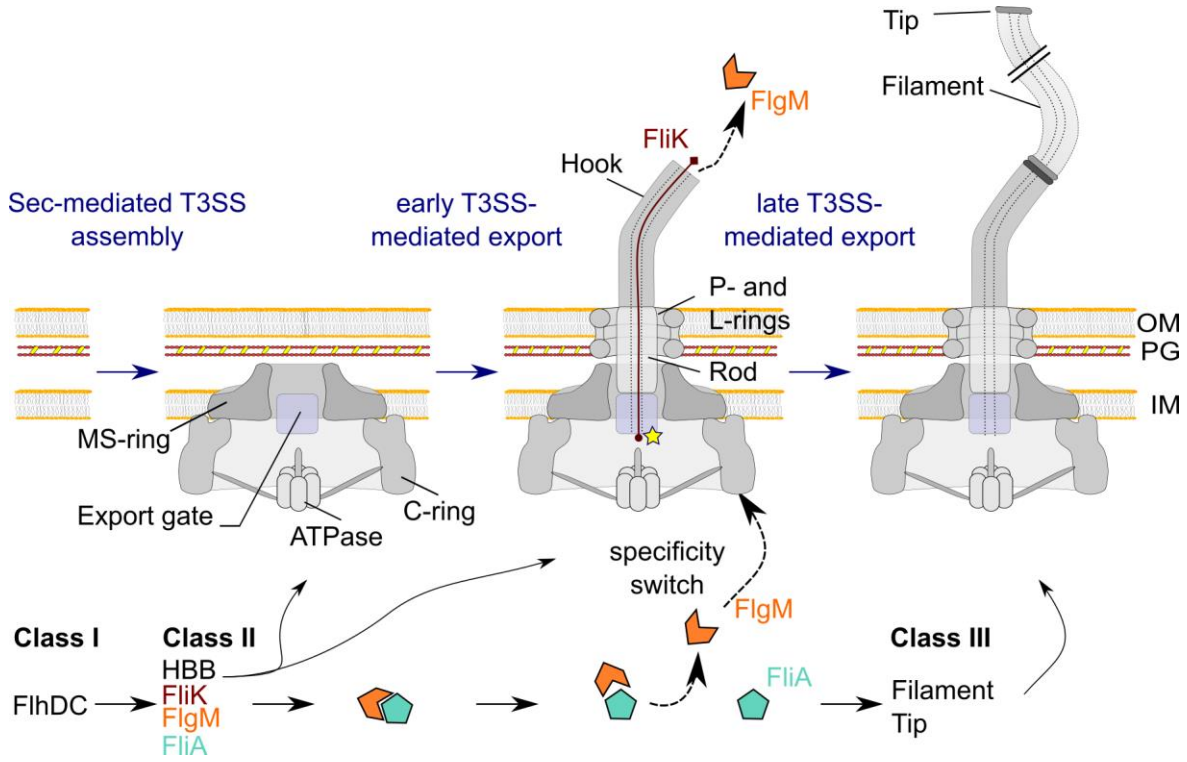

Figure 2: Flagellar gene expression and flagellar assembly Flagellar synthesis starts with FlhDC mediated activation of the Class 2 promoters. Subsequently, the proteins of the hook basal body (HBB) complex, the molecular ruler FliK, the sigma factor FliA, and its cognate anti-sigma factor FlgM are synthetized. The membrane components of the basal body are inserted in a Sec-dependent manner. Upon completion of the T3SS, the more distal components of the basal body are translocated across the membrane through the export apparatus. When length of the hook reaches 55 nm, the C-terminus of FliK interacts with the export gate and induces a specificity switch between early and late substrate. Consequently, FlgM is exported leading to the activation of Class 3 promoter by FliA. Finally, the filament and the tip proteins are expressed and translocated to the distal end of the structure, where they polymerize.

Flagellar assembly is a complex process controlled by at transcriptional hierarchy (Figure 2). Flagellar genes are organized in 14 operons, which are under the control of three promoter classes. On top of the hierarchy, the *flhDC* operon is under control of a Class 1 promoter and codes for the master regulator complex $FlhD_4C_2$, which activates σ^{70}-dependent transcription from Class 2 promoters. The expression of $FlhD_4C_2$ is tightly controlled at transcriptional and post-transcriptional levels by several positive and negative regulators including RflP (a.k.a YdiV), RflM, and RtsB [43–45]. The Class 2 operons include the genes coding for the hook basal body (HBB) proteins. Assembly of the flagellum starts with the MS-ring, made of the protein FliF, spanning the inner membrane [46–48]. The integral membrane proteins FliO, FliP, FliR, FliQ, FlhA, and FlhB assemble at the center of the MS-ring and form the export gate, where substrate proteins are translocated across the inner membrane [49]. It remains unclear whether the export gate assembles after MS-ring completion or in an independent manner. The assembly of the membrane components occur presumably co-translationally and is dependent of the Sec pathway, as for the majority of bacterial inner membrane proteins [47,50]. The nascent polypeptide is recognized by the signal recognition particle (SRP), which targets the ribosome/peptide complex to the Sec-translocon. The protein is integrated into the lipid bilayer from the Sec-translocon, where it folds into the native conformation. Misfolded proteins are then identified and degraded [51].

After completion of the MS-ring, FliG forms, with FliM and FliN, a multimeric ring in the cytosol termed C-ring, which is tightly associated with the MS-ring [52]. The C-ring constitutes the rotor component of the flagellar motor. At the base of the structure, the cytosolic proteins FliHIJ form an ATPase complex. This complex is highly similar to the F_OF_1 ATP synthase [48]. Together, the export gate, the ATPase complex, the C-ring and the MS-ring compose the T3SS apparatus. Once assembled, the T3SS export apparatus allows translocation of the building blocks of the more distal parts of the structure across the inner membrane, through a narrow channel. The flagellar inner rod, made of FlgBCFG, assembles from the periplasm to the outer membrane. The rod-capping protein FlgJ forms a whole in the outer membrane and enables subunits polymerization at the distal end of the structure [53,54]. The Rod is surrounded by the P- and L-ring, which span the peptidoglycan (PG) and the OM, and are made of FlgI and FlgH, respectively. Polymerization of FlgE subunits in a helical oligomer starts directly after basal body completion, forming a flexible hook. FlgE subunits are exported to the growing end of the

structure, where polymerization is facilitated by the hook capping protein FlgD [55], until the hook reaches a length of approximately 55 nm [56,57]. This length is controlled by a molecular ruler, FliK, which is infrequently secreted during hook polymerization [58]. When the appropriate length is reached, the C-terminal end of FliK interacts with the export gate and the specificity of the apparatus changes from early to late substrates. Therefore, the anti-sigma factor FlgM, sequestering the flagellar specific sigma factor FliA (σ^{28}), is secreted, and released σ^{28} is free to activate the expression of Class 3 operons [59].

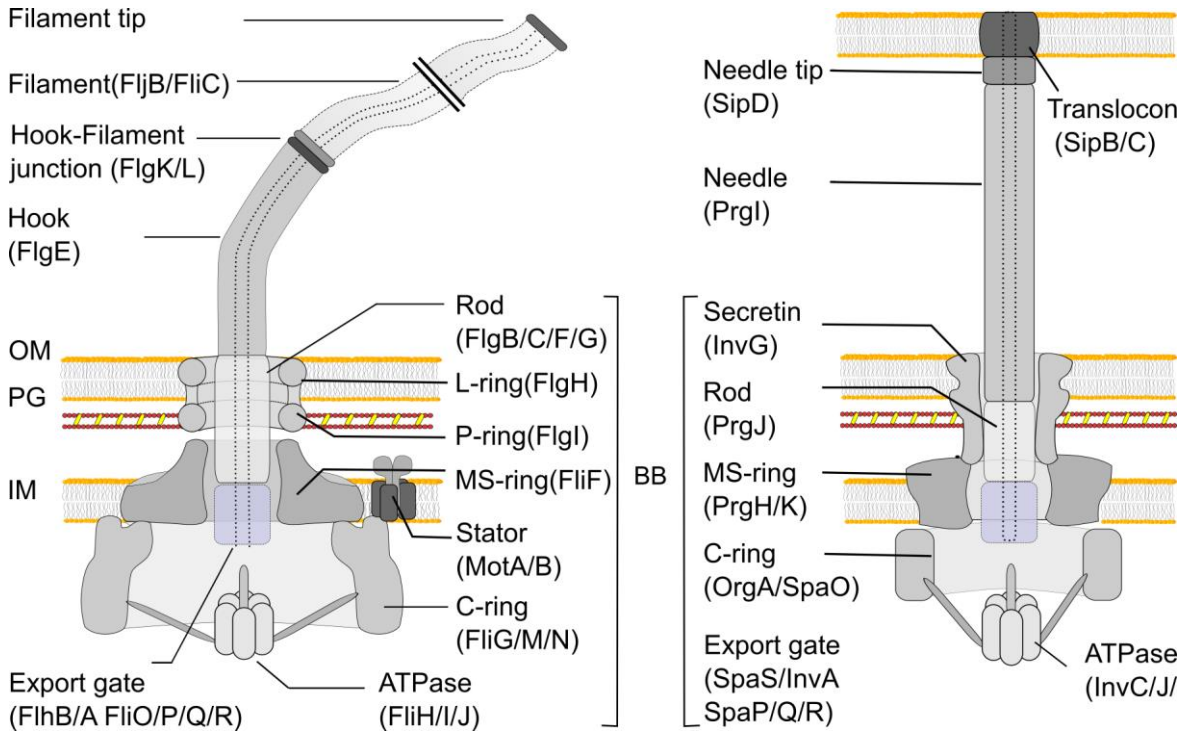

Figure 3: Comparison of the structures of the flagellum and the injectisome. Left: the flagellum is composed of three sub-structures; the basal body, starting from the cytosol and spanning both membranes, the flexible hook and the long helical filament. Right: the injectisome is made of a basal body including a secretin ring spanning the peptidoglycan and the OM, and a needle/translocon complex for delivery of toxins into the host. At the base of each structure, the export gate, the MS- and C-rings and the ATPase constitute the Type III secretion apparatus.

The hook-filament junction proteins are then expressed and assemble at the end of the hook and the polymerization of a 10-15 µm long and rigid helical filament starts. This filament is a homo-polymer made of 20,000 to 30,000 flagellin subunits, either FliC or FljB. A single bacterium synthetizes only one of these flagellin at a given time. This process, called flagellar phase variation, is depending on the recurrent inversion of a DNA fragment containing the *fljB* promoter (P*fljB*), the H segment. In one orientation, P*fljB* drives the expression of the two genes of the *fljBA* operon, the flagellin encoding gene *fljB,* and *fljA*, which codes for a negative regulator of FliC expression. In the other orientation, *fljB* and

fljA are not transcribed, thus allowing the expression of FliC. The inversion of the H segment is mediated by the DNA invertase Hin.

At its distal extremity, the filament is covered with a cap made of FliD. In parallel with filament synthesis, σ^{28} also activates the transcription of the *motAB* operon, encoding the stator components of the flagellar motor MotA and MotB. These proteins form inner-membrane proton channel associated with the basal body and anchored in the periplasm. Through interaction with the rotor, the MotAB channel transform the energy of proton flux into rotational torque. After completion of the motor, made of the stator and the rotor, the torque is transmitted to the filament through the hook, and the flagellum is functional.

The assembly of the needle complex (NC) shares similarities with that of the flagellum, but also displays important differences. As in the flagellum, assembly starts with the formation of the T3SS apparatus and is initiated at the inner membrane with the coordinated assembly of the export gate and the MS-ring [60]. The vT3SS export gate is composed of the integral membrane proteins SpaP, SpaQ, and SpaR, closely related to FliP, FliQ, and FliR, respectively, are incorporated first, followed by InvA and SpaS, the NC homologs of FlhA and FlhB [60]. Interestingly, no FliO homolog is present in the injectisome. The export gate probably serves as nucleation point for MS-ring assembly. The MS-ring is not only composed of one but two different proteins, PrgH and PrgK, exhibiting partial structural and sequence similarities with FliF [42,61]. In the needle complex, however, MS-ring polymerization happens in concert with the assembly of a homo-polymeric ring of secretins (InvG) in the periplasm [62]. This pore forming protein ring spans the PG and the OM and is not homologous with the flagellar P- and L-ring proteins. Indeed, this ring is homologous to that found in the Type IV pilus [41]. The other structures of the vT3SS apparatus are highly homologous to the fT3SS and assemble in a comparable way. Instead of a C-ring, the injectisome possess six cytosolic pods loosely associated with the IM. These pods are mainly composed of SpaO, a homolog of the FliMN building block, and OrgA, which does not have homologs in the flagellum [63,64]. The ATPase complex, made of InvC, InvI, and OrgB, displays a high conservation with the flagellar and the F_OF_1 ATPase complexes [42,48,65,66]. As for the flagellum, after completion of a functional T3SS apparatus, structural subunits are translocated across the IM for further formation of the needle. Secretion of the inner rod protein PrgJ, the needle filament protein PrgI, and the needle length regulator InvJ occur simultaneously. The inner rod assembles at the base of

the NC. The needle filament subunits polymerize at the distal end, trigger opening of the secretin and elongate extracellularly [62]. The molecular ruler InvJ controls the needle length in a similar fashion as FliK, and its interaction with SpaS induces a secretion specificity switch between early and late substrates [67]. This switch results in secretion of the needle tip subunits SipD polymerizing at the top of the needle. Upon cell contact, SipB and SipC are secreted and form a pore within the host cell membrane allowing delivery of the effectors into the host cytosol [62].

Flagellar protein	**SPI-1 homolog**	**Function**	**Degree of similarity**
FliF	PrgH	outer MS-ring	High
	OrgK	inner MS-ring	Low
FliG	-	C-ring protein /switch complex	-
FliH	OrgB	Stator	Medium
FliI	InvC	ATPase	High
FliJ	InvI	Stalk	Low
FliK	InvJ	hook/needle length regulator	Low
FliL	unknown	Unknown	-
FliM	SpaO	C-ring protein	Low
FliN			
FliO	-	minor export gate protein?	-
FliP	SpaP	minor export gate protein	High
FliQ	SpaQ	minor export gate protein?	High
FliR	SpaR	minor export gate protein	High
FlhA	InvA	major export gate protein / PMF	High
FlhB	SpaS	major export gate protein / specificity switch	High

Table 1: List of the proteins of the fT3SS and their homologs in the injectisome. The table was modified from Wagner and Diepold, 2014 [42]. FliF has been shown to be homologous to a fusion of PrgH and PrgK [42,61]. FliG has no clear homolog in the injectisome, but shares high similarities to the magnesium transporter MgtE [68]

1.4.The functional components of the flagellar T3SS

In both structures, the T3S apparatus is the cornerstone of the assembly process and is strictly required for effector secretion. In this work, we focus on the flagellar T3SS. As described above, the fT3SS is composed of 6 cytosolic and 7 membrane proteins that form the MS-ring, the export gate, the C-ring and the ATPase complex. The MS-ring is made of 26 subunits of the integral membrane protein FliF [69–71]. Spanning the IM, this ring presumably serves as scaffold protein for the export gate complex and forms, together with the C-ring, the flagellar rotor. Among the proteins of the export gate, FlhA and FlhB are the best characterized. FlhA consists of a large hydrophobic N-terminal transmembrane domain, a conserved cytoplasmic loop between TM4 and TM5, and a hydrophilic cytoplasmic C-terminal domain separated by a linker. The N-terminal domain is composed of eight transmembrane α-helices and directly interacts with FliF. FlhA cytosolic domain is thought to form a platform for substrates delivery to the export gate. The TM domain and the cytosolic loop are both important for coupling proton motive force (PMF), which combines the pH gradient (ΔpH) and the electrical potential gradient (ΔΨ) across the membrane, with flagellar substrate export [72–75]. FlhA is therefore a crucial player in the secretion process. Stepwise photobleaching analysis revealed the presence of 9 FlhA subunits, consistent with the formation of a nonameric ring of FlhA spanning the IM and extending in the cytosol, as observed for the FlhA homolog in the vT3SS of *Shigella,* MxiA, [69,76]. FlhB is composed of four transmembrane domains at its N-terminal end and a large cytosolic C-terminal domain. Upon interaction with FliK, the cytosolic domain of FlhB undergoes conformational change in FlhB responsible for a switch of specificity between early and late substrates [56,77]. Less is known about FliO, FliP, FliQ and FliR, beside that they are highly hydrophobic and relatively small proteins of 13, 25, 10 and 26 kDa respectively [78]. Their exact role and the stoichiometry remain unknown, but previous studies indicated that they are essential for secretion and form a structure at the center of the MS ring which might be the export channel [79]. However, evidence of their presence in the basal body exist only for FliP and FliR [78,80]. The topology of these components is depicted in Figure 4 based on prediction by Ohnishi et al. and after correction of FliO, FliR and FliP topology according to our recent findings and unpublished data.

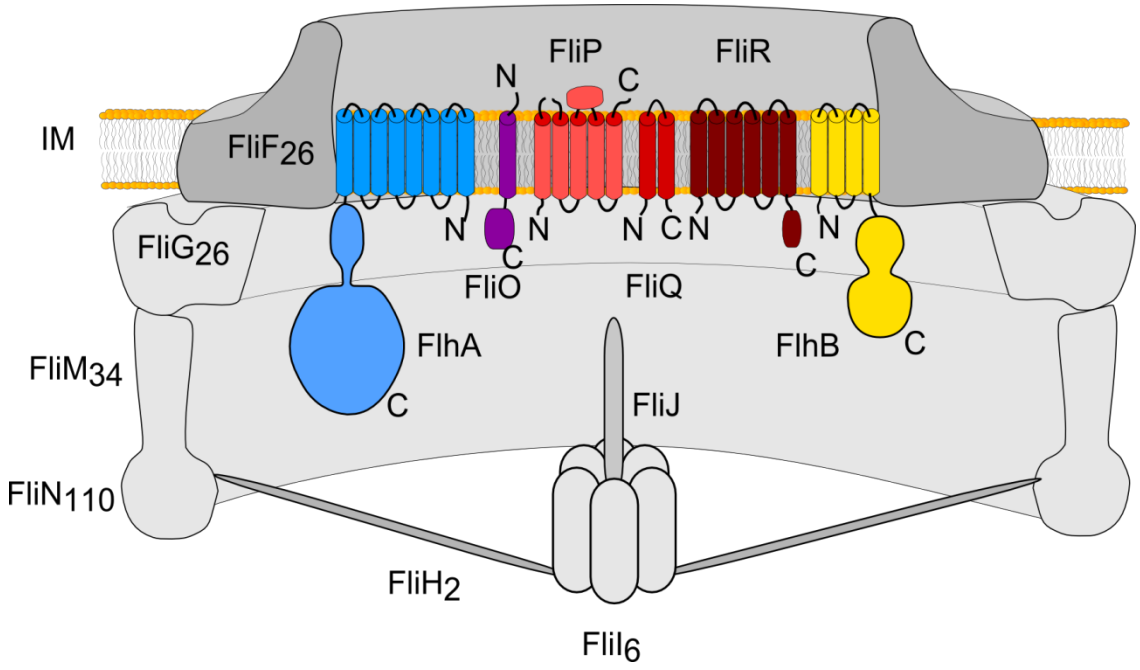

Figure 4: Predicted topology of the export gate components. The topology of the membrane components of the flagellar Type III secretion system as predicted by Ohnishi et al. [78]. FliO topology was corrected according to the observation of Barker *et al.* [81] and FliR topology after Van Arnam *et al.*[58]. FliP topology has been corrected according to the results of SCAM analysis performed in our lab (Renault *et al.*, unpublished). These are only schematic representations. The sizes and the forms of the domains are schematic and do not correspond to any experimental data.

On the cytoplasmic face of the MS-ring, FliG interacts with FliF as well as with the rest of the C-ring made of FliM and FliN. Together, the MS- and C-rings form the rotor/switch complex responsible for flagellar rotation [52]. FliG also directly interacts with the MotAB stator complex, a proton channel coupling the PMF with torque generation. FliM, linking FliG and FliN, is directly involved in the rotation direction switch [82]. Upon binding of phosphorylated CheY, FliM undergoes a conformational change, transmitted to FliG, and induces a directional change of the rotation from counterclockwise (CCW) to clockwise (CW) [83]. At the base of the C-ring, FliN has been shown to participate in the secretion process by interacting with FliH. This interaction allows targeting of the FliHIJ ATPase complex to the basal body, facilitating therefore its interaction with the export gate. Hence, the C-ring does not only contribute to flagellar rotation, but act as a docking platform for the FliHIJ ATPase [84].

As mentioned above, the FliHIJ complex resembles the F_OF_1 ATP synthase. Its ATP hydrolysis activity is dependent on the oligomerization of a hexameric ring of FliI constituting the ATPase by itself. This oligomerization is prevented in the cytosol by FliH, which forms a $FliH_2FliI$ heterotrimer. Upon interaction of FliH with FliN, FliI hexamer can form in the vicinity of the docking platform composed of FlhA and FlhB cytosolic domains. FliJ sits at the center of the FliI hexamer, stabilizing the structure. FliJ also interacts with flagellar specific substrate chaperones and FliM [48,85]. Originally, the ATPase was thought to energize export through ATP hydrolysis. However, it has been shown that the PMF is the main source of energy for secretion [86]. Export of flagellar substrates occurs in an unfolded or partially folded manner [87–89]. The ATPase allows unfolding and delivery of substrate to the export gate. Upon interaction with FlhA, FliJ also triggers an ignition key mechanism turning the inefficient ΔpH driven export gate into a highly efficient ΔΨ driven export gate [72,88].

1.5.Objectives

Despite their crucial role and intensive studies, many questions remain concerning the role, the mechanism and the importance of the proteins forming the fT3SS in flagellar substrate export, and especially concerning the core of the machinery, the export gate. A more detailed understanding of the molecular mechanism underlying type III protein secretion could provide a decisive advantage in the biological warfare not only against *Salmonella*, but also other Gram-negative pathogens using T3SS machineries as main virulence factors. In an attempt to open the fT3SS black box, we address in this thesis the following questions:

I. Which proteins of the T3SS apparatus are required and sufficient for flagellar export?

Originally, all flagellar proteins whose absence led to loss of flagella were reported as essential for export. However, recent findings demonstrated that several of these components, such as the C-ring or the ATPase complex were dispensable. Here, we uncoupled flagellar biosynthesis and T3SS-dependent export, and measured flagellar substrate export to define a minimal set of proteins essential for secretion. Using a plasmid-based and chromosome-based approach, we aimed to reconstitute a minimal T3SS apparatus only consisting of the components truly essential for the protein export function.

II. What is the function of the flagellar specific membrane protein FliO?

The core of the export apparatus is constituted of the membrane components FlhBA and FliOPQR. These proteins are highly conserved among bacterial species and have clear homologs in the vT3SS, except for FliO which is present only in the flagellum. A previous study established a relation between FliO and FliP expression. In this project, we investigated the function of FliO by analyzing its effects on FliP stability and basal body assembly. Furthermore, we observed its localization within the cell by super resolution microscopy.

III. What is the role of FliP cleavable signal peptide?

Beside the presence of FliO, another feature is specific to the flagellar T3SS export gate. The integral membrane protein FliP, presumably forming the central pore of the apparatus, carries a cleavable signal peptide (SP), which is absent in its vT3SS homolog SpaP. Here, we studied the importance of the signal peptide and the role of the signal peptide cleavage for FliP function. Using mutants deficient in cleavage or lacking the signal sequence, we studied the influence of the SP and cleavage on motility, FliP expression, stability, membrane integration, and flagellar assembly.

2. Results

2.1. Genetic determination of the essential components for export by the fT3SS apparatus

Because their deletion resulted in loss of flagella, all the components forming the MS-ring, the rotor/switch complex, the ATPase and the export gate have been described as essential for export [49,90]. However, findings that the export gate was a PMF driven exporter and that ATP hydrolysis was only required for substrate unfolding lead to reconsider the necessity of FliHIJ. Indeed, flagellar formation can occasionally occur in absence of the ATPase [86,88,91]. Furthermore, mutations in the membrane protein FliP could restore motility in strains lacking FliO [81]. Finally, the C-ring is dispensable upon upregulation of FlhDC or overproduction of FliI [92,93], although FliG was reported to be required for MS-ring and FlhA nonamer formation [69]. Therefore, it remains uncertain, which components are genuinely crucial for export under physiological conditions.

Here, we used a FlgE-β-lactamase fusion based assay, which allows to observe secretion independently on flagellar assembly. We defined a set of proteins that are strictly essential for export and aim to reconstitute a minimal T3SS apparatus. To that end, we used two different approaches. In a first approach, we constructed plasmids encoding the genes thought to be essential for the reconstitution of a functional export apparatus. In a second approach, we created strains deleted for all flagellar genes with the exceptions of those thought to be essential and compared export efficiency in presence or absence of individual components.

2.1.1. Hook-β-lactamase fusion base assay

Previous studies investigating fT3SS always used flagellation to determine whether individual proteins where required for a substrate export. However, flagellar assembly does not only depend on substrate translocation across the inner membrane. Indeed, rod and hook completion are essential for expression and polymerization of the filament subunits. In our experimental setup, described in Figure 5, the rod proteins FlgB and FlgC were deleted. In presence of a functional export apparatus, the hook protein FlgE fused to β-lactamase cannot polymerize and form the hook but is instead secreted in the periplasm, thus conferring ampicillin resistance. Export efficiency can therefore be easily measured by performing a minimal inhibitory concentration (MIC) assay [86,92].

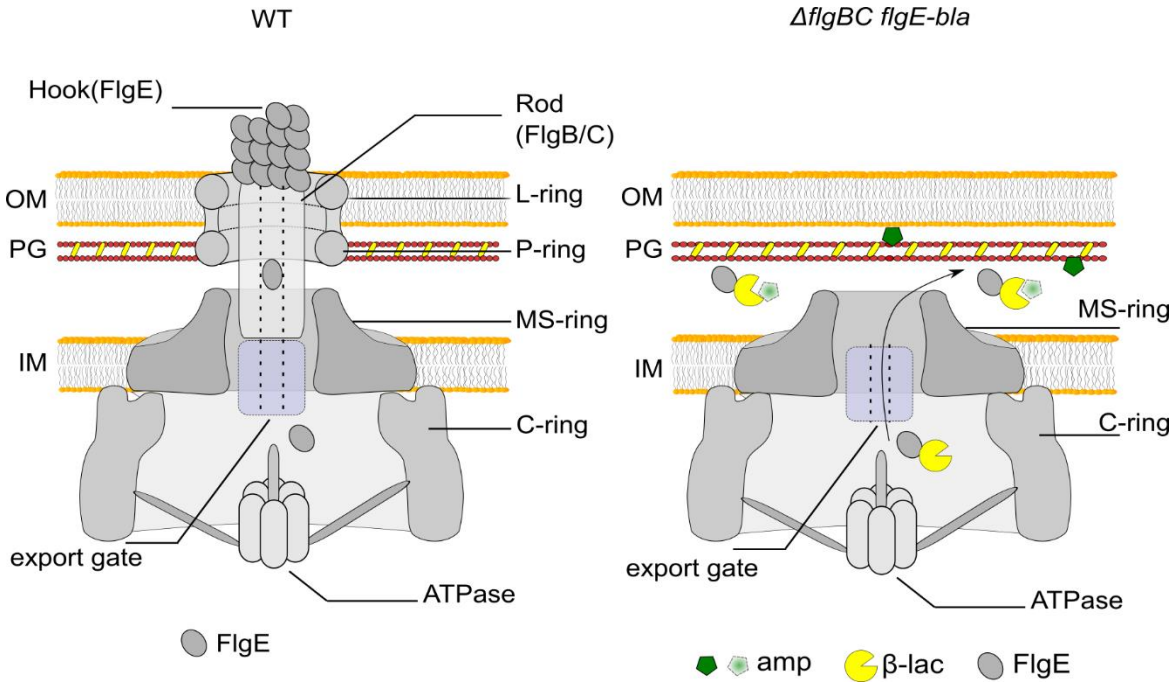

Figure 5: Schematic representation of the FlgE-Bla reporter system. Left panel: hook polymerization in WT condition. FlgE is secreted by the T3SS, travel across the OM inside the rod and polymerizes at the apical side of the growing structure. Right panel: In absence of the rod, the FlgE-Bla fusion protein is translocated in the periplasm, where the β-lactamase can degrade ampicillin.

2.1.2. Construction of a minimal type III secretion plasmid

In order to create a minimal fT3SS, we constructed several plasmids harboring different combinations of genes thought to be essential for export. As previous studies indicated that ATPase proteins FliHIJ and C-ring proteins FliMN were dispensable, those genes were excluded of the constructs created for this thesis. The C-ring protein FliG was also reported to be dispensable for export function, but the efficiency of MS-ring formation is substantially decreased in a *fliG* mutant. Therefore, two plasmids encoding *fliF*, *flhBA*, and *fliOPQR,* with and without *fliG,* were created, termed pEM1271 and pEM2273, respectively. The pTB23-*attλ* (pEM726) plasmid was used as backbone vector [94]. This plasmid is based on the conditional-replication, integration, and modular (CRIM) plasmid series, which harbors a phage λ attachment site (*attλ*) to facilitate insertion of the plasmid in the chromosome in presence of the phage integrase [95]. Chromosomal integration ensures the presence of a unique copy of each operon, preventing therefore any possible multi-copy effects. Episomal propagation at low copy numbers is also possible in a *pir*$^{+}$ background. pEM726 also harbors three different tunable promoters, which allow independent, inducible expression of the three different flagellar operons (*fliF(G), flhBA* and *fliOPQR*). This feature is critical to produce the appropriate amount of proteins required for export apparatus assembly.

pEM1271 and pEM2273 have been constructed in several complex stages which are described in Figure 7. We first generated three different plasmids, each encoding for a different flagellar operon under control of a different promoter. The *flhBA* encoding plasmid pEM897 was built by insertion of a fragment consisting of *flhBA* under control of the sodium salicylate inducible promoter P*nahG* [96]. The pEM1084 plasmid was built by insertion of *fliF* under control of the *tetA* promoter. For the construction of the *fliOPQR* encoding plasmid, we used a PCR fusion approach to create a fragment consisting of *fliOPQR,* the terminator region and a suitable restriction site (Figure 6).

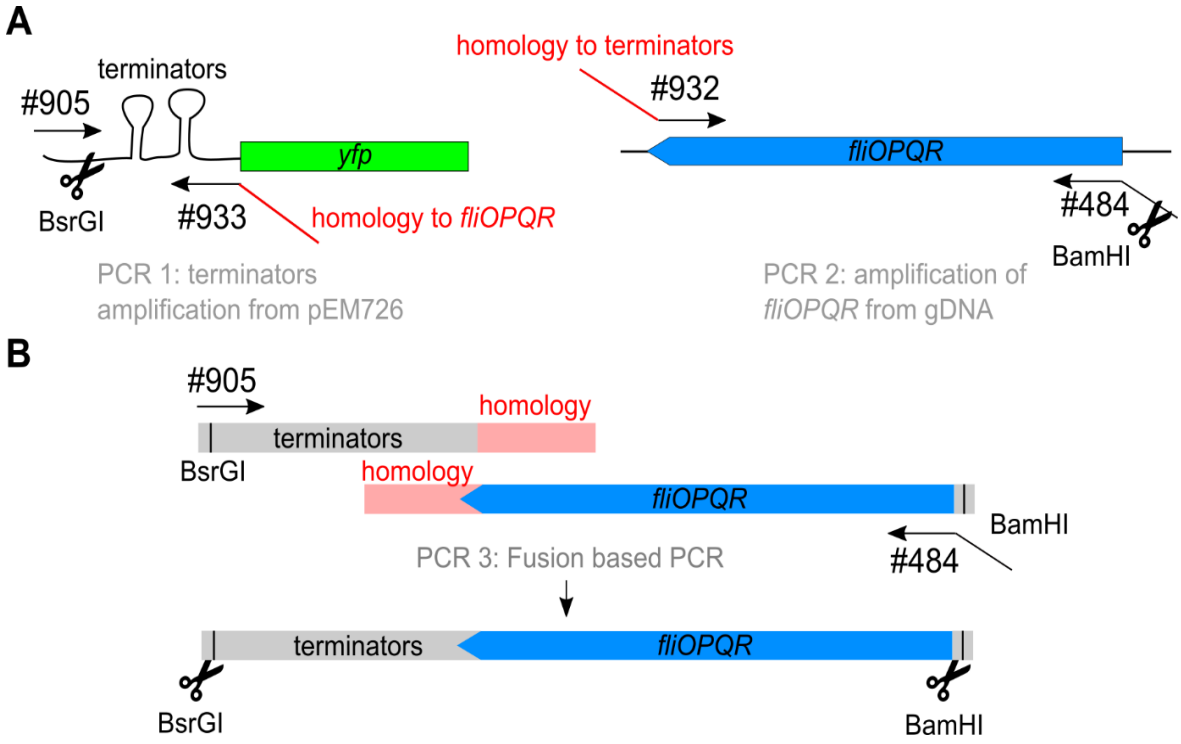

Figure 6: Fusion of *fliOPQR* with the terminators region of pEM726 by PCR-based fusion. A) Two fragments were individually amplified using one primer containing homology with the other fragment. The primer binding upstream of *fliOPQR* harbored a BamHI restriction site for later cloning purposes. The BsrGI site was already present downstream of the terminators region. B) Both fragments were fused as described in the materials and methods section.

This fragment was first sub-cloned blunt-end into pBR322. We then combined the three plasmids by consecutive insertion of *fliF* and *fliOPQR* in the plasmid carrying *flhBA*. The resulting plasmid encoded all three operons and was termed pEM1271. Finally, we used Gibson assembly®, a cloning method allowing the fusion of multiple DNA fragments, to introduce *fliG* directly downstream of *fliF*. The resulting plasmid, encoding for *fliFG*, *flhBA,* and *fliOPQR,* was termed pEM2273. Both plasmids were either propagated as episome or integrated into the chromosome using phage λ integrase.

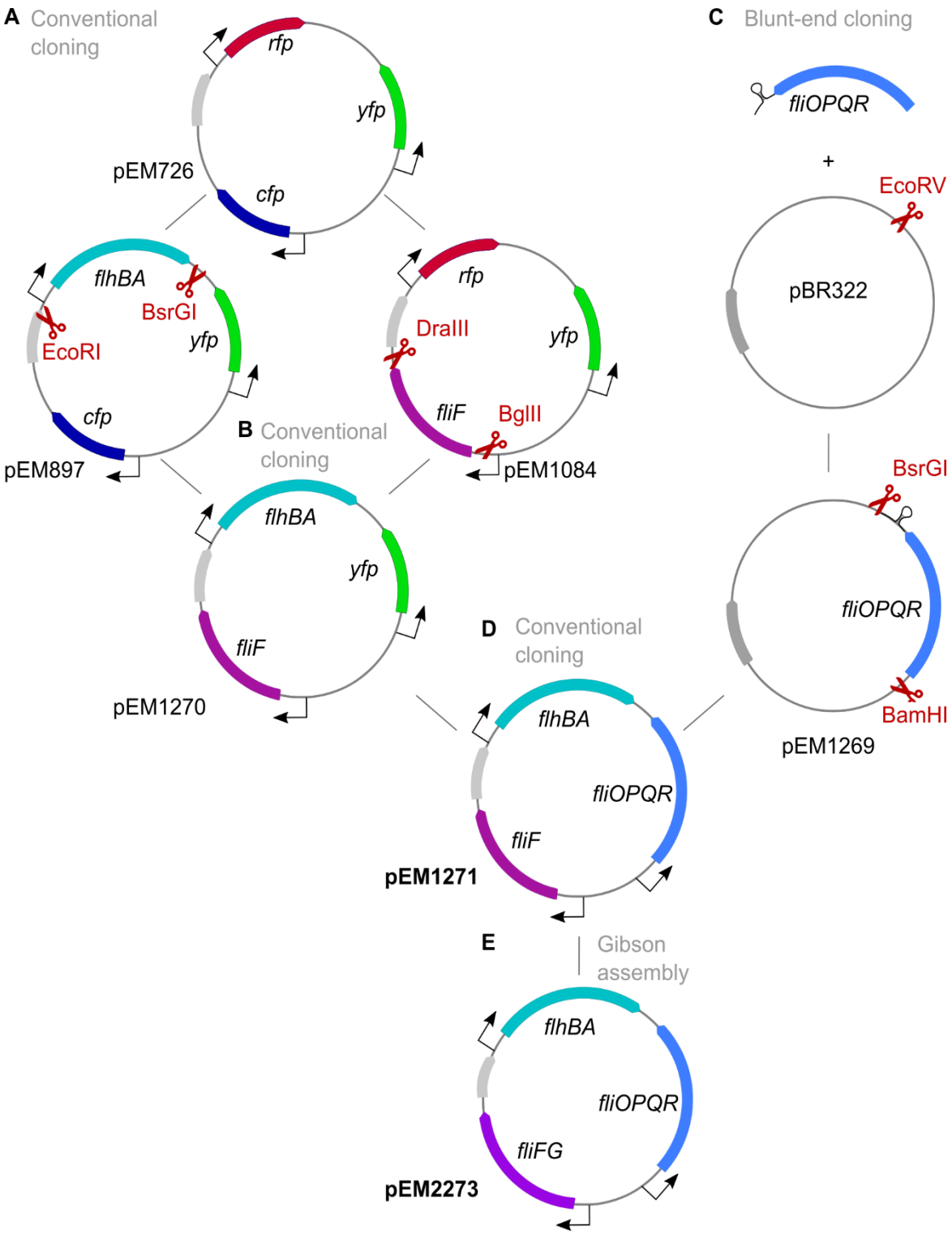

Figure 7: Construction of minimal T3SS plasmids. A) pEM897 and pEM1084, carrying *flhBA* and *fliF* respectively, were created by insertion of P*nahG-flhBA* and *fliF* fragments into pEM726. **B)** *fliF* was inserted into pEM897 **C)** *fliOPQR*, previously fused with the terminator region of pEM726, was inserted blunt-end into pBR322. **D)** *fliOPQR* was cut out and inserted into pEM1270 to create the *flhBA-fliF-fliOPQR* encoding plasmid pEM1271**. E)** pEM2273 was created by Gibson assembly®. The enzyme used for restriction are indicated in red.

The three operons were under the control of *tet*, *lac,* and *nah* promoters, which are either repressed by TetR and LacI or activated by NahR, respectively. However, *Salmonella* does not carry the genes coding for *tetR*, *lacI,* and *nahR*. We therefore built a plasmid harboring the three regulators by Gibson assembly® using pKG137 as backbone vector [97]. We then took advantage of the FRT site present on this plasmid to insert the regulators onto the chromosome at the P22 phage attachment site, in order to have a single chromosomal copy of each gene. With the presence of these regulators, *fliFG*, *flhBA* and *fliOPQR* expression could be induced by addition of anhydrotetracycline, sodium salicylate, and IPTG respectively (Figure 8).

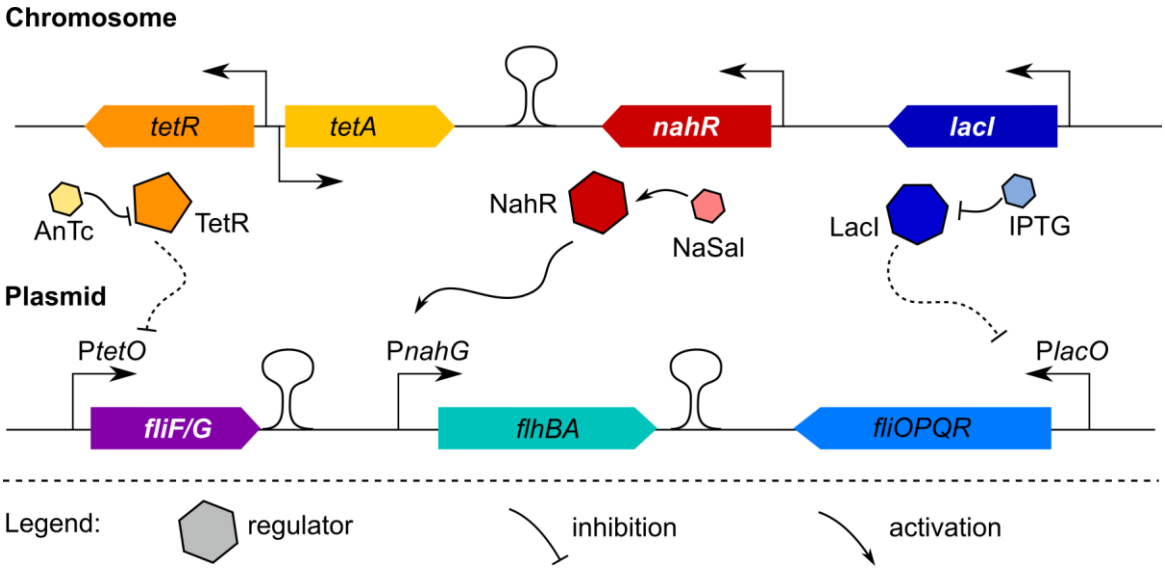

Figure 8: Flagellar operons induction on pEM1271 and pEM2273. In absence of induction, the *tetO* promoter is under repression of TetR, P*nahG* and P*lacO* are not activated. In presence of the inducers, *tetR* is repressed, hence, P*tetO* is turned on. NahR and LacI are produced and activate transcription of *flhBA* and *fliOPQR* respectively. *tetR*, *nahR* and *lacI* were inserted on the chromosome at the P22 attachment site. The flagellar operons are encoded on the plasmid.

2.1.3. The minimal T3SS complement single operon deletions

Before testing FlgE-Bla export, we validated the functionality of the *fliFG*, *flhBA,* and *fliOPQR* expressing plasmid and determined appropriate concentrations of inducer that complemented respective deletion mutants of the fT3SS operons. To assess the ability of pEM2273 to complement deletion of single operons when it was integrated on the chromosome, we monitored motility in soft agar in *ΔfliF*, *ΔflhBAE*::FRT and *ΔfliOPQR*::FRT strains, in presence of increasing concentrations of the appropriate inducer. When cultivated in soft agar, flagellated bacteria can swim and form a halo while bacteria that are unable to synthesize functional flagella only grow at the inoculation site. The results are depicted in (Figure 9). In the *ΔfliOPQR* background, motility was restored upon induction with 250 µM or higher concentration of IPTG, in presence of pEM2273 but not with the control plasmid. The *ΔfliF* and *ΔflhBAE* strains, however, remained unmotile, regardless of the presence of the plasmid. Increasing inducer concentration did not improve motility. Induction with 0.5 $\mu g \cdot ml^{-1}$ anhydrotetracycline even affected motility of the WT, probably due to a cytotoxic effect of the inducer itself. These results indicated that the plasmid was either nonfunctional or that the expression levels of *flhBA* and *fliF* were too low. This could not be improved by increasing inducer concentrations.

Hence, we performed the same complementation assay with pEM2273 present episomally (Figure 10). In a *ΔfliF* background, motility was restored to WT levels upon induction with 0.01 $\mu g \cdot ml^{-1}$ AnTc while the control strain remained non-motile (Figure 10 B). The strain lacking *fliOPQR* was also fully complemented in presence of 250 µM or higher concentration IPTG (Figure 10 C). Finally, induction with 2.5 µM NaSal was sufficient to rescue motility in *ΔflhBAE* (Figure 10 A). However, we observed that even without induction, motility was partially restored in presence of the plasmid in the *ΔflhBAE* strain and to a lesser extend in the *ΔfliF and ΔfliOPQR* backgrounds, suggesting that the optimal concentrations of inducer to reconstitute our minimal T3SS apparatus might be inferior to the tested values. These results not only proved that the plasmid, carried episomally, was functional and able to complement single deletions, but it also allowed us to determine that induction with 0.01 $\mu g \cdot ml^{-1}$ AnTc, 2.5 µM NaSal and 250 µM IPTG was sufficient to complement single deletions.

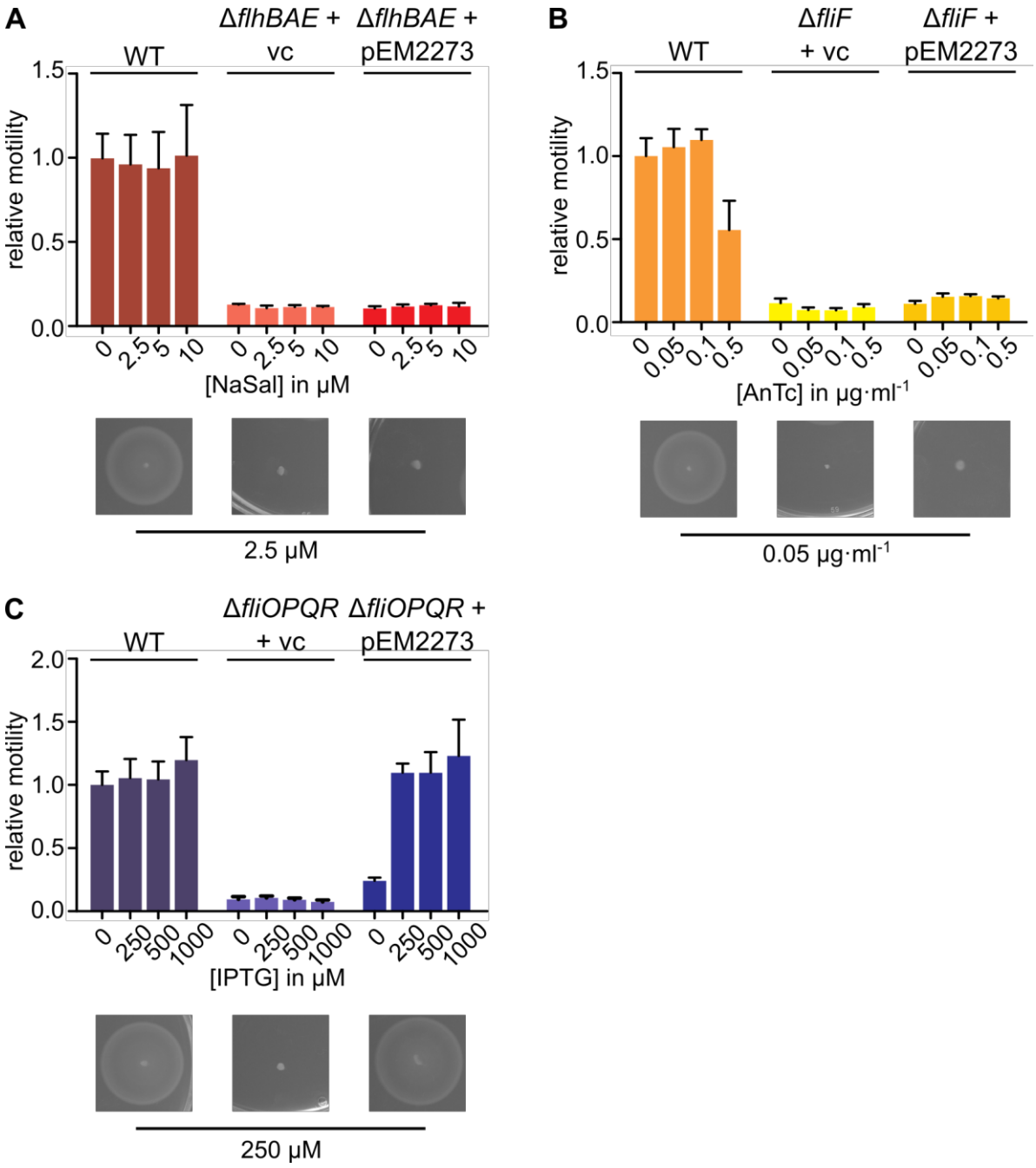

Figure 9: Chromosomally encoded pEM2273 failed to complement single operons deletions. Mutant lacking single flagellar operons and harboring pEM2273 (p*fliFG-flhBA-fliOPQR)* or pEM726 (vc) on the chromosome were inoculated in 0.3 % agar LB plate supplemented with increasing concentration of **(A)** NaSal, **(B)** AnTc and **(C)** IPTG. Cells were incubated at 37 °C for 4.5 h and the diameters of the swarms were measured for each strain using ImageJ. Motility is expressed relatively to the size of the WT in absence of inducer using at least four replicates. Error bars represent SD. Example of motility are shown under each graph.

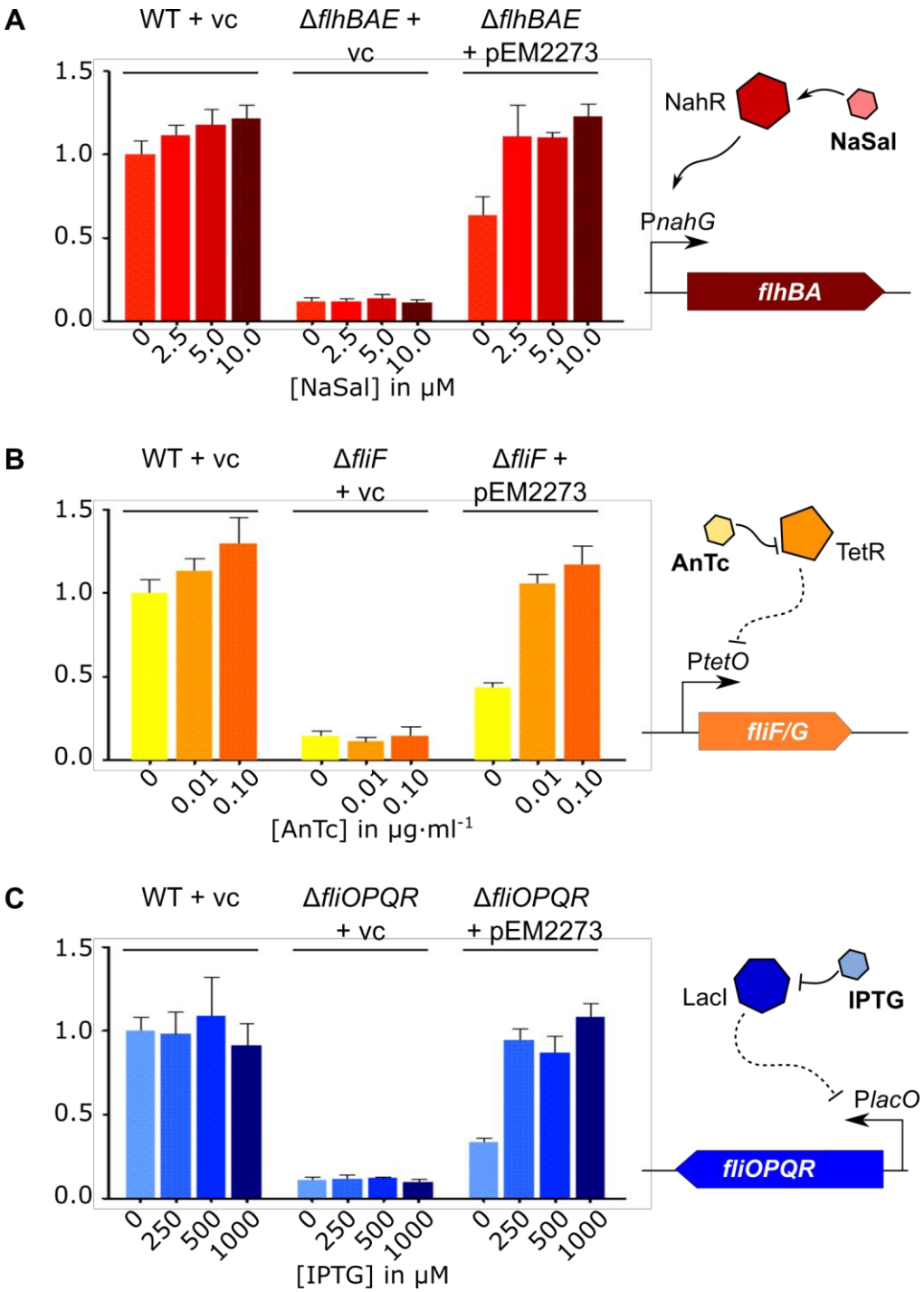

Figure 10: Episomally encoded pEM2273 complements single flagellar operon deletions. Mutant lacking single flagellar operons and harboring pEM2273 (p*fliFG-flhBA-fliOPQR)* or pEM726 (vc) were inoculated in 0.3 % agar LB plate supplemented with Cm and increasing concentration of **(A)** NaSal, **(B)** AnTc and **(C)** IPTG. Cells were incubated at 37 °C for 4.5 h and the diameters of the swarms were measured for each strain using ImageJ. Motility is expressed relatively to the size of the WT in absence of inducer. Error bars represent SD, n=6. For each panel, a schematic representation of the induction process is depicted on the right side.

2.1.4. Reconstitution of flagellar substrate export with minimal plasmids

To determine whether FliFG, FliOPQR and FlhBA were sufficient to assemble a functional export apparatus, a minimal inhibitory concentration assay (MIC) was performed in a strain expressing the hook-β-lactamase fusion as described above (Figure 5) and deleted for every other flagellar gene. Using this setup, strains were grown in increasing concentrations of ampicillin. In bacteria harboring a functional export apparatus, the FlgE-β-lactamase fusion is translocated via type III secretion in the periplasm, leading to an increase of survival. The strain background was also deleted for SPI-1 and SPI-2 genes, to prevent any possible export of the reporter protein fusion through the injectisome machinery. The expression of each operon was induced with the previously determined inducer concentrations. The results of the MIC assay are shown in Figure 11, the ampicillin concentration required to inhibit growth by half (IC_{50}) was calculated using a [R] script as described in the Material and Methods parts of this thesis. The calculated IC_{50} in the control strain was 0.31 $\mu g \cdot ml^{-1}$ ($\pm 1.3 \cdot 10^{-4}$) while it reached 0.39 $\mu g \cdot ml^{-1}$ ($\pm 9.7 \cdot 10^{-2}$) in presence of pEM2273. Although the IC_{50} moderately increased in presence of the plasmid, the difference was not significant, indicating that export remained abolished.

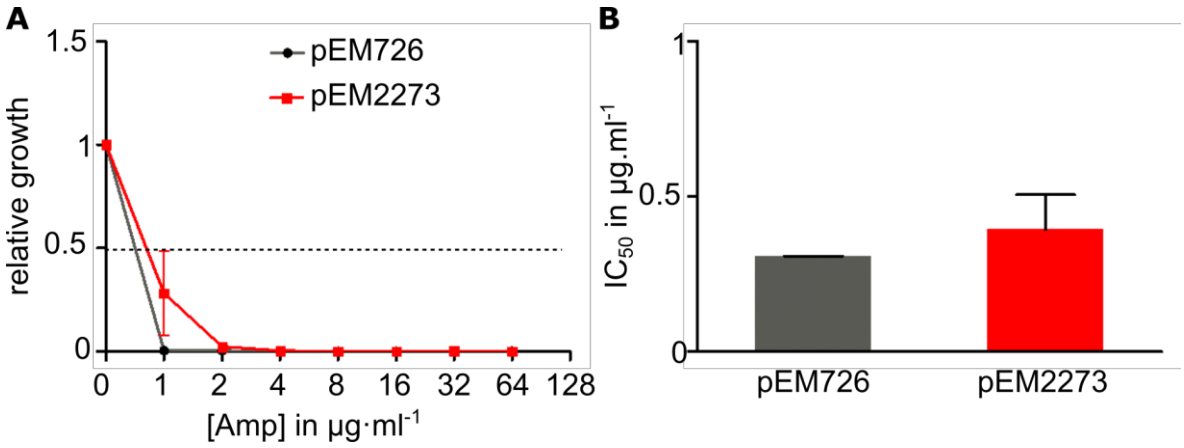

Figure 11: pEM2273 does not allow reconstitution of flagellar export. A) Example of MIC assay results. Synthesis of FlgE-Bla was induced with 0.1% arabinose and flagellar operons (*fliOPQR, flhBA, fliFG*) with 0.1 $\mu g \cdot ml^{-1}$ AnTc, 250 µM IPTG and 2.5 µM NaSal. Cultures were diluted 1:50 in 96 well plates and incubated at 37 °C under shacking. OD_{600} was measured after 5h. Bacterial growth is expressed relatively to the OD in absence of ampicillin. The assay was conducted with 4 replicates, error bars indicate the SD. The x axis displays the ampicillin concentration on a $\log_2$ scale. **B)** IC_{50} values of each strain were determined using a modified [R] package "stinepack" Error bars represent the SD.

We performed a Western blot against β-lactamase to exclude any problems with expression of the reporter fusion protein. The levels were similar in every strain (data not shown). We previously observed that an overproduction of FliF may be detrimental for growth (Erhardt et al, unpublished). This could be due to the formation of excess MS-ring like structures compromising the integrity of the IM. Since we also observed a slight growth defect in our export assay, we tried to reduce the concentration of AnTC as low as 0.005 $\mu g \cdot ml^{-1}$. Different concentrations of IPTG (50 - 100 μM) and NaSal (1 μM) were also tested since previous assays showed that motility was partially restored even without induction. Nevertheless, the MIC values did not increase under any of these conditions (data not shown). We therefore failed to reconstitute export with pEM2273, suggesting that other proteins might be required for the assembly of a minimal export apparatus or that our set up was not functional.

2.1.5. Construction of a chromosomally encoded minimal type III secretion apparatus

In vivo, the assembly of the flagellar T3SS is a complex process. The expression of the master regulator $FlhD_4C_2$, which activates transcription from Class 2 promoters, is modulated by multiple regulators to maintain the optimal protein levels necessary for assembly of the basal body [43–45]. In our minimal T3SS plasmid system, the absence of FlhDC and the fact that the operons were not under control of their native promoters could result in uncontrolled levels of flagellar proteins. This could explain why we failed to assemble a functional export apparatus.

To circumvent this issue, another approach was adopted. A series of strains chromosomally encoding the putative essential proteins at their native locations was created. To that end, every flagellar gene previously described as non-essential was sequentially deleted, using λ-red recombination and phage transduction of individual deletions. In those strains, *flhDC* remained at its original locus. The organization of the operons on the chromosome of *S.* Tm strain LT2 and the deleted loci are indicated in Figure 12. To assess the effects of FliO and FliG on export efficiency, were constructed strains encoding *flhBA, fliF, fliPQR,* with either *fliO* and *fliG*, only *fliO* or *fliG*, or none of them. These strains were constructed by deleting *fliHIJK* and *fliLMN* but conserving the region containing *fliK* terminator and *fliL* promoter as described in Figure 12. Finally, the FlgD-FlgE-β-lactamase fusion was introduced under control of the arabinose promoter to enable measurements of flagellar export.

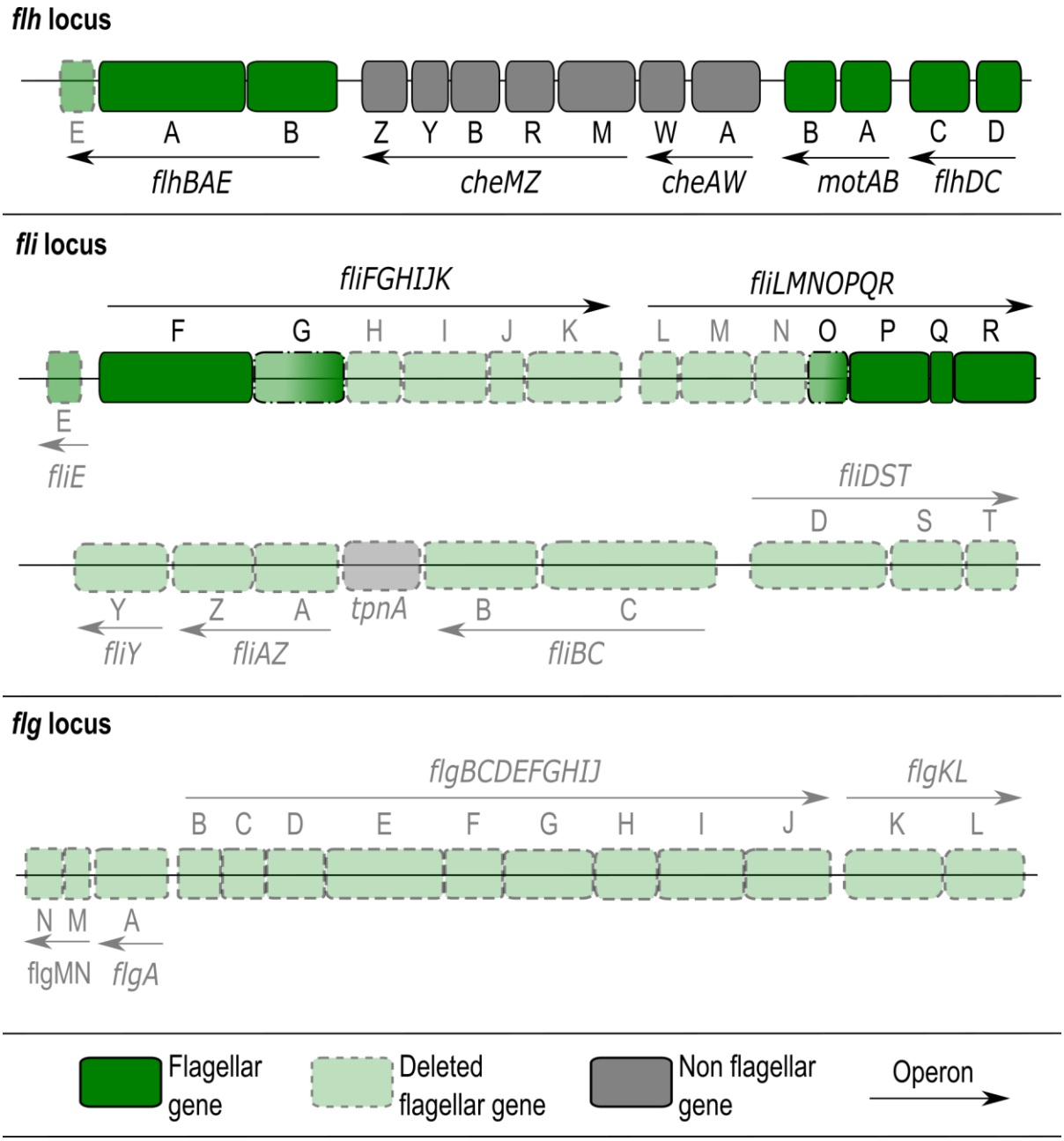

Figure 12: Organization of the flagellar operons at their native loci of *S. enterica* Typhimurium LT2. Each flagellar gene is represented by a green box and non-flagellar genes are depicted by a grey box. Operons are shown by an arrow. The genes deleted in the strains used in this study are represented in light green and with dashed outline. *fliO* and *fliG* were present in some strains and deleted in others (See EM4445 to EM4449 Table 6). All deletions were obtained by homologous recombination, as described in the Materials and Methods section.

2.1.6. Flagellar export reconstitution and definition of a minimal set of essential proteins

To assess the efficiency of flagellar export in the strains carrying *fliF(G), fli(O)PQR*, and *flhBA* and lacking all non-essential flagellar genes (EM4446 to EM4449 - see Table 6), an export assay was performed using the β-lactamase system described above (Figure 5). The curves representing bacterial growth in the presence of increasing concentration of ampicillin, as well as the calculated IC_{50} values of each strains, are shown in Figure 13. In presence of all putatively essential components (the MS- and C-ring proteins FliFG, and the export gate proteins FlhBA and FliOPQR. EM4446), the IC_{50} reached 240.6 ± 16.3 $\mu g \cdot ml^{-1}$. This was only one third of the WT IC_{50} (about 827.9 ± 36.5 $\mu g \cdot ml^{-1}$), but corresponded to a 36-fold increase compared to the strains lacking every flagellar gene (6.7 ± 0.3 $\mu g \cdot ml^{-1}$). This clearly indicated that these components, expressed from their native promoters, were sufficient to assemble a functional export apparatus. In absence of FliG (EM4447), the IC_{50} decreased to approximately 26.2 ± 1.7 $\mu g \cdot ml^{-1}$ of ampicillin, remaining four-fold higher than the negative control. In absence of FliO, however, and regardless of the presence of FliG (EM4448 and EM4449), this value dropped to the same level as in absence of all flagellar genes (7.8 ± 0.5 $\mu g \cdot ml^{-1}$). To rule out that these differences were due to different expression levels of FlgE-Bla or the other components, we performed a western blot against β-lactamase and FliG on the total extracts of every strains (Figure 14). No differences of expression were observed indicating that the results solely depended on the presence or absences of the different membrane components.

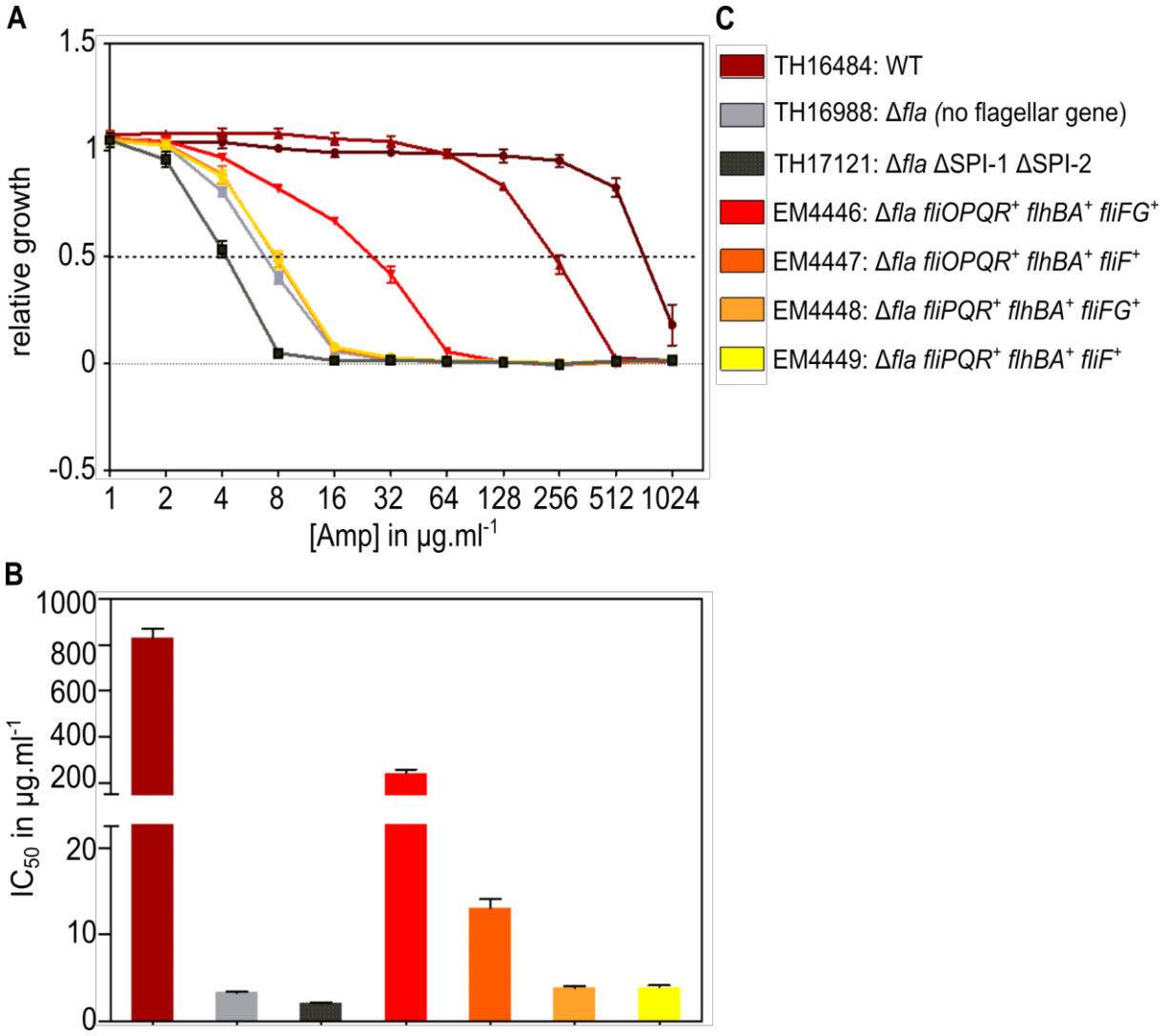

Figure 13: FliOPQR FlhBA and FliF are sufficient to restore flagellar export. A) Example of MIC assay performed with 5 replicates. Cells were grown for 4.5 h in LB supplemented with 0.1 % arabinose to induce FlgE-Bla. Cultures were diluted 1:50 in LB containing increasing concentration of ampicillin in a 96 well plates and incubated at 37 °C under shacking. OD_{600} was measured after 5h. Bacterial growth is expressed relatively to the OD in absence of Ampicillin. Error bars indicate the SD. The x axis displays the ampicillin concentration on a $\log_2$ scale. **B)** IC_{50} values of each strain were determined using a modified [R] package "stinepack" Error bars represent the SD. **C)** Relevant genotype of the strains used for this assay. All strains carry the Δ*araBAD*::*flgE-Bla* and the Δ*flgBC* mutations.

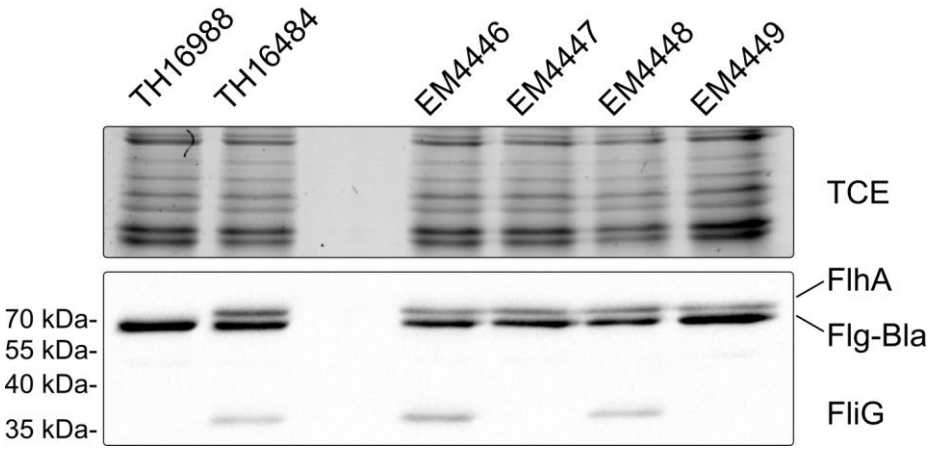

Figure 14: FlgE-Bla expression is similar in all strains. Western blot on whole cell extracts of strains expressing only essential flagellar genes (EM4446 to EM4449). After 4.5 h growth, 1 ml of culture was collected directly from the MIC test plate. Protein were precipitated with 10 % TCA, samples were loaded on a 15 % SDS-PAGE and analyzed by western blot. Anti-$FlhA_c$, Anti-FliG and Anti-β-lactamase antibodies were used to detect FlhA, FliG and FlgE-Bla respectively. TH16988 (Δ*fla*) and TH16484 (WT) were used as negative and positive control. All strains carry the Δ*araBAD*::*flgE-Bla* and the Δ*flgBC* mutations.

As mentioned above, Barker *et al*. isolated mutations in FliP that restored motility in Δ*fliO* [81], which suggested that FliO is involved in FliP expression. To determine whether export could occur independent of FliO, we transformed the strains lacking the non-essential flagellar genes (EM4447 to EM4449) with the pKG116 plasmid carrying *fliP* under control of a NaSal inducible promoter and repeated the MIC experiment in presence of 2.5 µM NaSal. In the strain encoding *fliFG fliPQR flhBA*, and lacking FliO and all non-essential flagellar genes (EM4447), the IC_{50} increased by four-fold upon overexpression of FliP compared to the strain carrying the empty vector, from 4 to 16 $\mu g \cdot ml^{-1}$. We also observed a two-fold increase in the strain only carrying *fliF fliPQR flhBA* (EM4449). In the strain encoding *fliF, fliOPQR,* and *flhBA* (EM4448) however, the IC_{50} values remained unchanged upon FliP overexpression. The same was observed in the WT (TH16484) and the strain lacking all flagellar genes (TH16988). These results indicated that FliO is not strictly required when FliP is present in excess. The fact that export did not occur in the strain lacking FliG but not the other essential components (FliF, FliOPQR, and FlhBA) indicated that this effect is specific for FliO, confirming the link between FliP expression and FliO function.

Altogether, these results showed that a minimal export gate composed only of FliF, FliOPQR and FlhBA is functional and that the absence of FliO is clearly detrimental under physiological conditions. On the other hand, although FliG dramatically improved the efficiency of the export complex by tenfold, its deletion did not completely abolish secretion, indicating that it not essential for flagellar assembly.

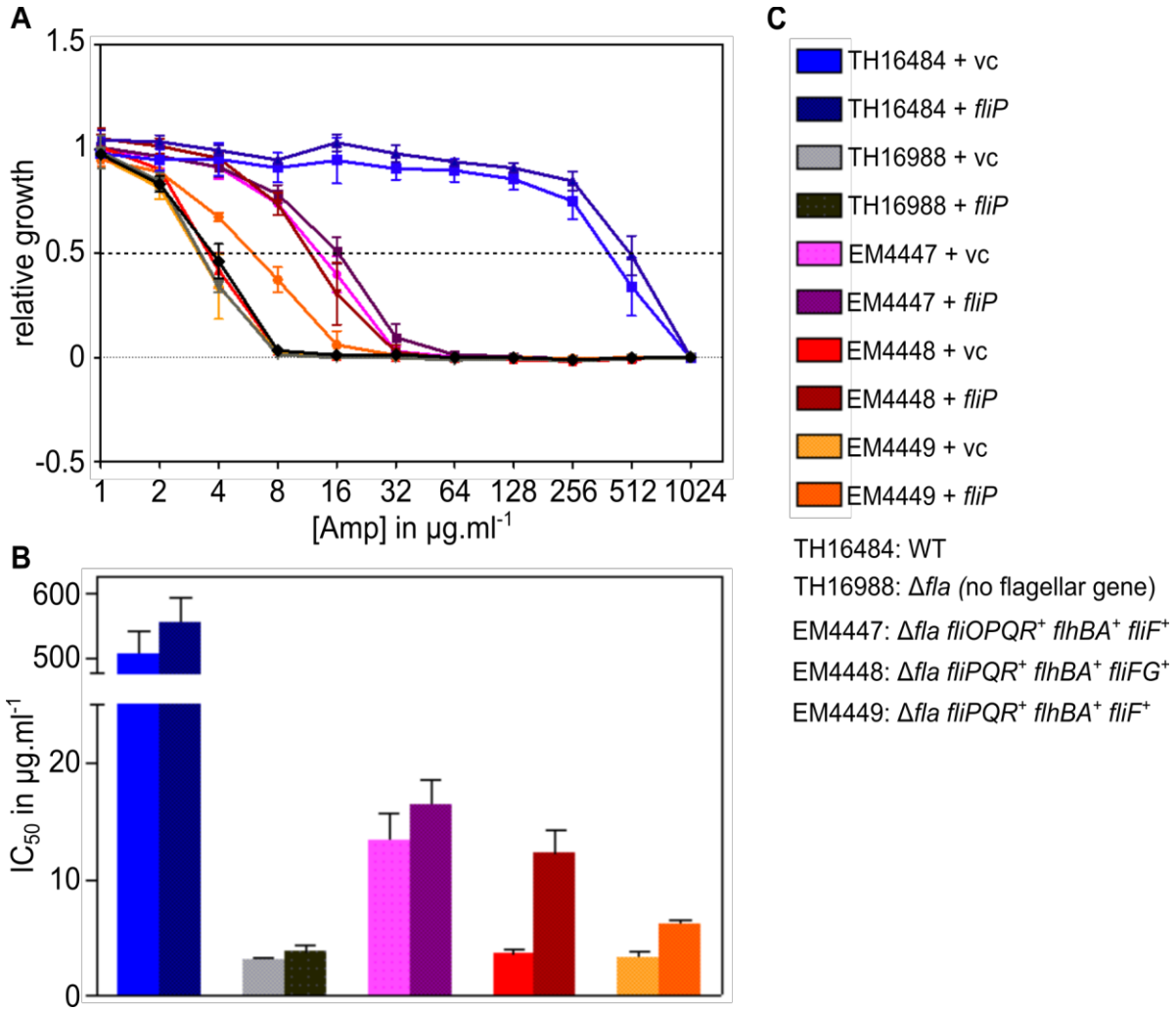

Figure 15: FliO is dispensable upon FliP overexpression. A) MIC assay in presence of pKG116-*fliP*. Cultures were grown in LB + Cm and *fliP* expression was induced with 2.5 µM of NaSal. Cultures were diluted 1:50 in a 96 well plates and incubated at 37 °C under shacking. OD_{600} was measured after 5h. Bacterial growth is expressed relatively to the OD in absence of ampicillin. The assay was performed with 4 replicates, error bars indicate the SD. The x axis displays the ampicillin concentration on a log_2 scale. **B)** IC_{50} values of each strain were determined using a modified [R] package "stinepack" Error bars represent the SD. **C)** Genotype of the strains used for this assay. All strains carry the Δ*araBAD*::*flgE-Bla* and the Δ*flgBC* mutations.

2.2. Unraveling the role of FliO

The flagellar and the virulence associated T3SS, and more especially their export gate exhibits many similarities. FliP, FliQ, FliR, FlhB and FlhA share a high degree of homology with their injectisome counterparts (Table 1) [62,98]. It is therefore surprising that FliO does not have a homolog in the vT3SS. Furthermore, while the other proteins of the export apparatus are strongly conserved among all flagellated bacteria, it is not the case of FliO, which is absent of the flagellum of some species, such as in the ancient bacterial species *Aquifex aeolicus* [99].

Little is known about FliO function, except that in its absence flagellar formation is affected [49]. In *Salmonella*, FliO is a 125 amino acid long, 13 kDa bitopic protein composed of a short N-terminal periplasmic part, a transmembrane domain and a large cytosolic C-terminal domain [55]. Due to the presence of a second translational start site 63 bp downstream of the first one, a shorter variant, lacking the periplasmic domain, is present in low amounts. Although the longest variant complements *fliO* deletion more efficiently, both species are functional, suggesting that the transmembrane and cytosolic domains are the functionally active parts [100]. Previous studies proposed that FliO is an integral part of the export apparatus located in the inner membrane [78,80] but this was never experimentally demonstrated. Although it was long thought to be essential for export, recent studies showed that it is not strictly required for export apparatus assembly [80]. Moreover, a FliOP fusion has been reported in *Buchnera aphidicola*, and Barker *et al.* characterized mutations in FliP that partially rescued motility in absence of FliO [55]. They also showed that FliO overexpression resulted in increased levels of FliP, strongly suggesting a functional link between these two proteins and they determined that a region between amino acid 22 and 95 is crucial for this interaction. FliP is a 25 kDa integral membrane protein, made of four transmembrane loops and a soluble 80-amino acid large periplasmic domain located between TM2 and TM3. It also harbors a cleavable N-terminal Sec signal peptide. FliP is one of the most conserved proteins of the export gate and is thought to be directly involved in flagellar export [78,80].

In this chapter, we investigated the function of FliO and its influence on FliP stability. We also observed the sub-cellular localization of FliO using super resolution microscopy. Finally, we studied the effects of FliO on FliP complex formation in flagellar assembly.

2.2.1. FliO function is related to FliP expression

FliP is essential for flagellar export, located in the inner membrane apparatus and conserved among the T3SSs as depicted in Figure 16. In the injectisome, SpaP is associated with SpaR in a $SpaP_5R_1$ complex forming a donut like structure which could be the translocation pore [102]. Consequently, FliP might have a central role in both assembly and secretion processes of the fT3SS. Several experimental results mentioned above hint towards a relationship between FliO function and FliP expression [55]. Therefore, we hypothesized that FliO facilitate production or stability of FliP.

To validate this idea, we carried out a complementation analysis, in which we expressed *fliP* from the NaSal inducible plasmid pKG116 in wild type (WT) and Δ*fliO* backgrounds (Figure 17 A). To that end, we determined whether flagellin secretion was restored by detection the presence of FliC in the supernatant after induction of FliP with increasing concentrations of sodium salicylate. We also monitored motility by measuring the size of the motility halo formed by the bacteria swimming in a 0.3% agar plate (Figure 17 B). In the WT background, overexpression of FliP did not increase motility compared to the empty vector control (vc). In the Δ*fliO* mutant, however, flagellin export and motility were partially restored upon *fliP* induction, thereby confirming that FliO is involved in FliP expression. We also looked at the motility of Δ*fliO* strains upon overproduction of the other export apparatus components (Figure 17 C). Excess of FliO and FliP complemented a *fliO* deletion, while in presence of excess FlhA, FlhB, FliQ and FliR, the bacteria remained nonmotile. This observation indicated that FliO function is specifically linked with FliP.

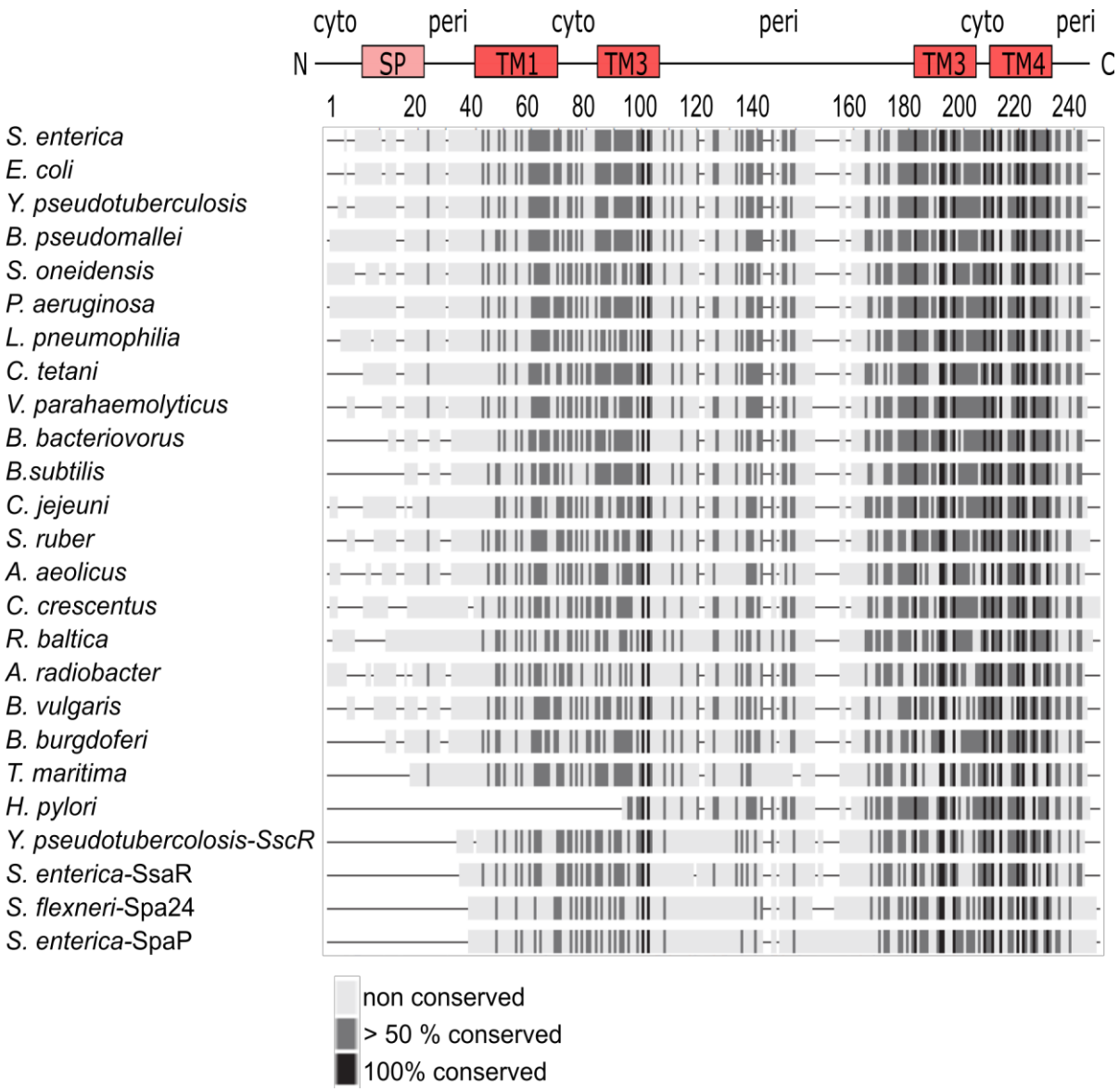

Figure 16: FliP is highly conserved among species. Fingerprint alignment of *S. enterica* FliP with homologues in other species as well as injectisome counterparts of different species. The color scale shows the degree of conservation. Sequence pre-processed with ClustalW and alignment was performed using the LaTeX package TeXshade [82]. Courtesy of Dr. Marc Erhardt.

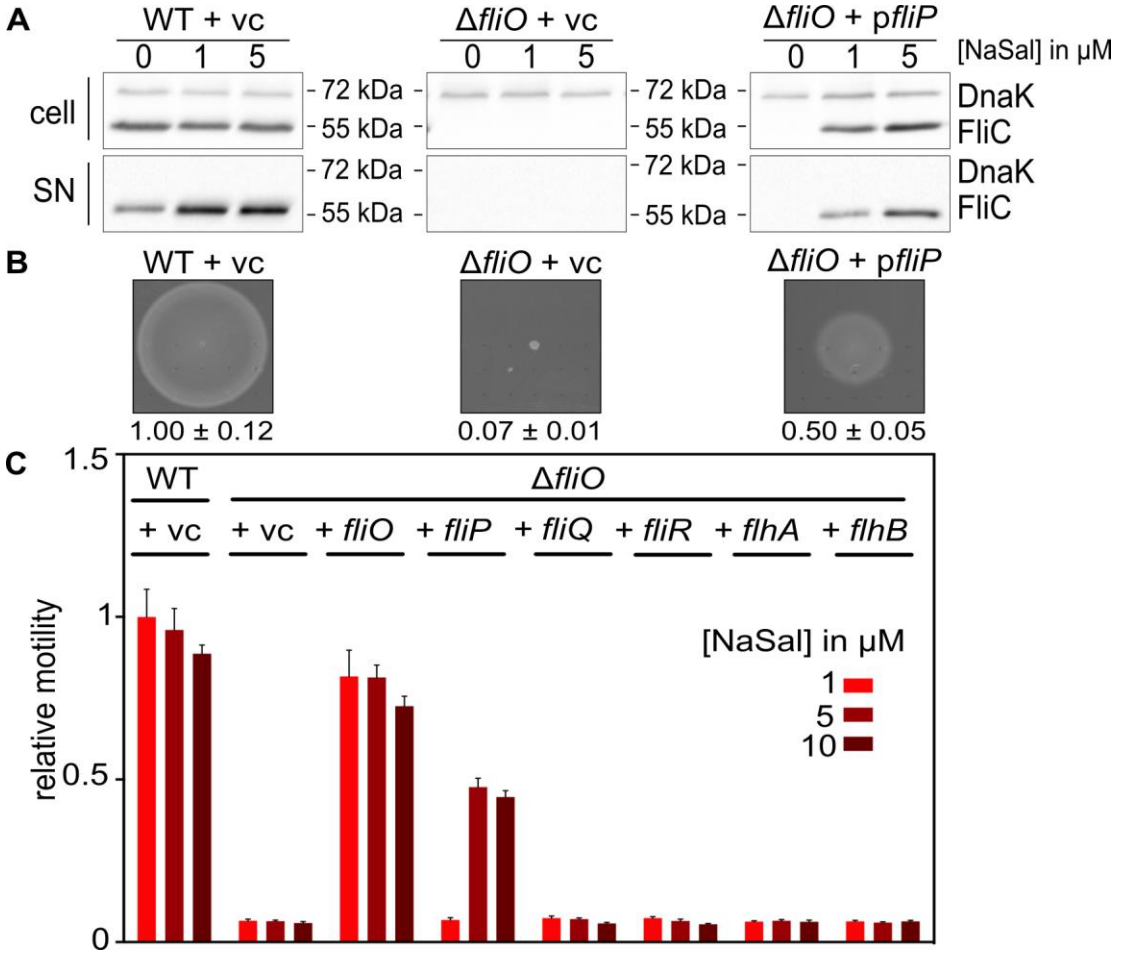

Figure 17: overexpression of FliP complements *fliO* deletion. A) Detection of flagellin FliC by western blot, in the supernatant and the whole cell extracts of WT cells, Δ*fliO* harboring an empty vector (vc), and Δ*fliO* harboring pKG116-*fliP*. DnaK was used as loading control. **B)** Example of motility after 5 h at 37 °C in 0.3 % agar plates, upon induction with 5 µM NaSal. Sizes of the halos, relative to the WT, and SD are indicated below. **C)** Motility of Δ*fliO* upon overexpression of other components of the export gate relative to WT. All proteins were expressed from pKG116 and induced with NaSal.

2.2.2. FliO protects FliP from proteolysis

There are several mechanisms by which FliO could increase FliP expression. Either it enhances FliP synthesis, by directly or indirectly increasing transcription or translation of *fliP*, or it decreases FliP decay. FliO does not exhibit any DNA or RNA binding domain. Hence, it seemed unlikely that it is involved in FliP synthesis. Thereupon, we speculated that FliO was involved in FliP stability. To test this hypothesis, we constructed chromosomally encoded $FliP_{G157}$-3xFLAG tag and $FliP_{Q22}$-3xHA tag mutants, and tracked FliP levels for 3 hours after inhibition of *de novo* protein synthesis by addition of chloramphenicol and spectinomycin, in presence or absence of FliO. To exclude any influence of the tag on FliP stability or function, we monitored motility of the newly generated strains. The strain synthesizing the FliP-FLAG tag construct remained motile, as

well as a FliP-HA FliO-FLAG tag strain, indicating that FliP function was not affected (Figure 18 B). As expected, all strains were non-motile in absence of *fliO* or *fliF*. To monitor FliP stability, protein levels were detected by Western blot analysis using anti-FLAG antibodies. Following synthesis arrest, the amount of $FliP_{G157}$-3xFLAG decreased in absence of FliO, while the protein remained stable in the WT after 3 hours (Fig. 17 A). These results indicated that FliO prevents FliP degradation.

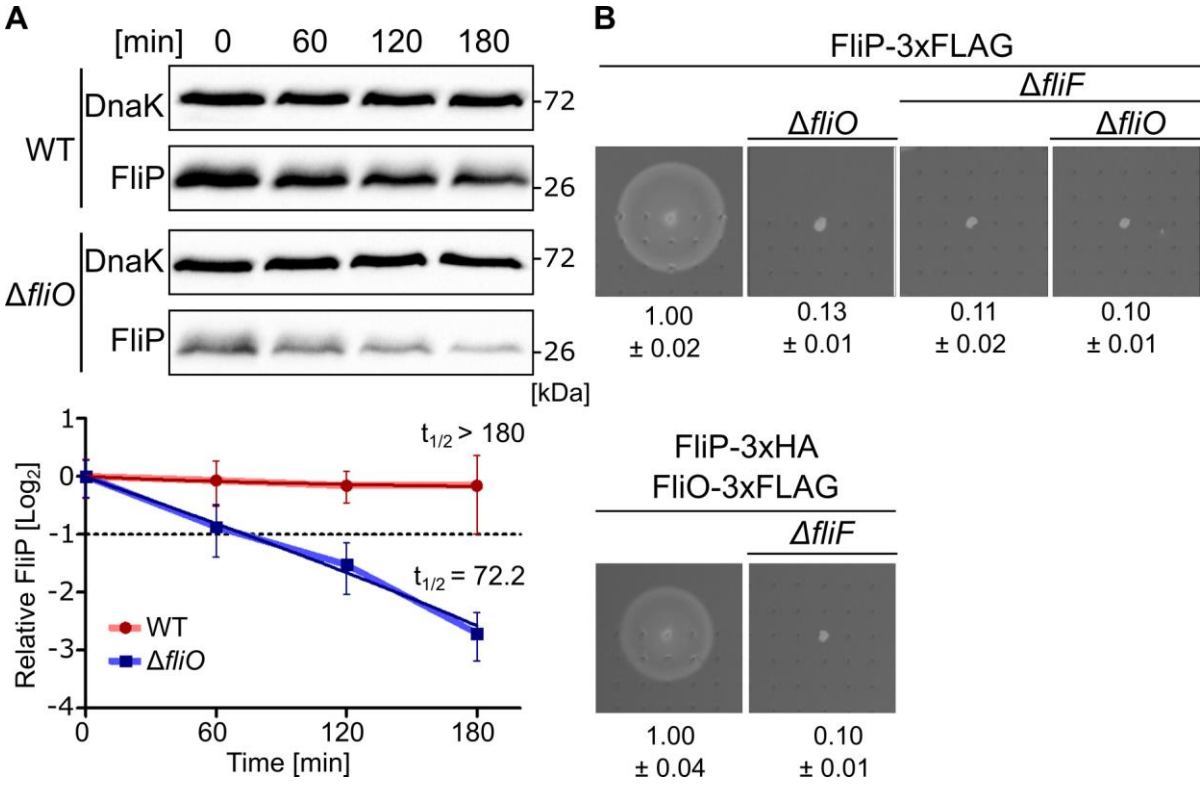

Figure 18: FliP is unstable in absence of FliO. A) Stability assays performed with chromosomally encoded FliP-3xFLAG. Synthesis was inhibited by addition of Spc and Cm, total protein extracts were collected and precipitated after 0, 60, 120, and 180 min. FliP was detected by western blot using anti-FLAG antibodies. DnaK was used as loading control. Quantification was made using data from six independent experiments. Data are represented as the relative FliP protein levels (FliP intensity/DnaK intensity relative to T_0) over time on a half-logarithmic scale. For each mutant, the thin straight line represents the non-linear exponential regression used to determined FliP half-life. The thick and light line links the experimental mean for each time point. Error bars indicate SD. **B)** Motility assay in soft agar after 4 h at 37 °C. The size of the swarms, relative to the WT, and the standard deviation (SD), from 9 replicates, are indicated below.

However, since *fliO* is located immediately upstream of *fliP*, its deletion could affect *fliP* mRNA stability and therefore protein levels. To rule out such a polar effect, we performed the same assay with an episomally encoded $FliP_{Q22}$-3xHA in Δ*fliOP* and Δ*fliP* backgrounds. To determine the optimal concentration of inducer, we checked motility upon induction with 0, 1 and 5 µM of NaSal (Figure 19). Induction with 1 µM NaSal was sufficient to restore motility in Δ*fliP* to the WT levels (Figure 19B). We thus used this condition for our

assay. As observed before, FliP was degraded in the absence of FliO and was stabilized otherwise (Figure 19 A). Therefore, we could exclude that a polar effect was responsible for FliP degradation, confirming that FliO acts on the protein level. Moreover, FliP was also degrading faster in three variants affecting functionality of the cytosolic domain (*fliO*$_{V72G}$, *fliO*$_{L92R}$, and *fliO*$_{L91\text{-}L94}$) than in the WT (Karen Freier's master's thesis), and the cytosolic domain of FliO has been shown to be crucial for FliO function. Altogether, these results clearly indicated that FliO acts on protein level by protecting FliP from proteolysis.

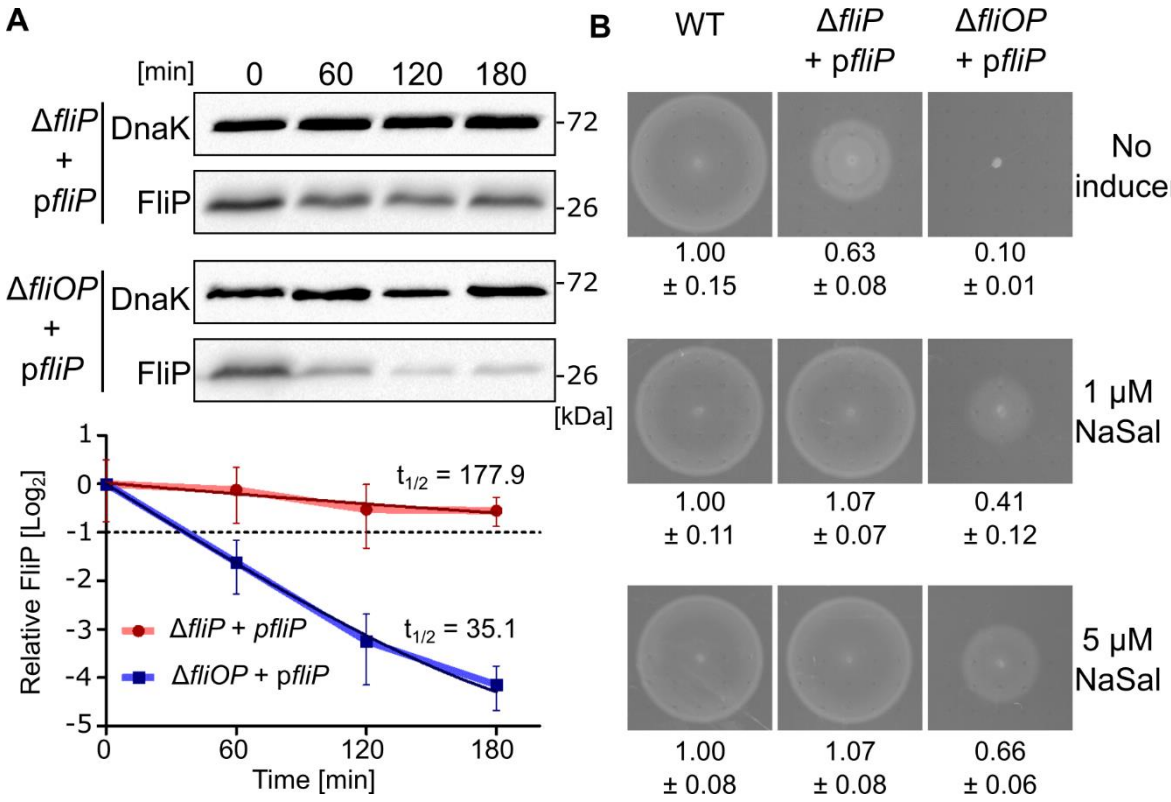

Figure 19: FliO acts on FliP stability at the protein level. A) Stability assay in presence of pKG116-*fliP-3xHA*. FliP expression was induced with 1 µM NaSal. *De novo* protein synthesis was inhibited by addition of Spc. Samples were collected after 0, 60, 120, and 180 min. FliP was detected by western blot using anti-HA antibodies. DnaK was used as loading control. Quantification was performed on three independent experiments. FliP was detected by western blot using anti-FLAG antibodies. DnaK was used as loading control. Data are represented as the relative FliP protein levels (FliP intensity/DnaK intensity relative to T_0) over time on a half-logarithmic scale. For each mutant, the thin straight line represents the non-linear exponential regression used to determined FliP half-life. The thick and light line links the experimental mean for each time point. Error bars indicate SD. **B)** Motility in soft agar after 4h at 37 °C. the average size of the swarms, relative to the WT, and the SD, from 9 replicates, are indicated below.

To investigate whether FliO had broader effects, we considered another component of the export apparatus, the large membrane protein FlhA. Interestingly, FlhA was as well destabilized in absence of FliO while it was stable in the WT (Figure 20). This degradation appeared to be slower than that of FliP, although the half-life could not be determined due to the instability of the protein used as control for this experiment. This indicated that FliO does not have only an effect on FliP but also on FlhA and might affect every protein of the export apparatus. This result was consistent with previous observation in *H. pylori* in which FliO is required for FlhA assembly and stability [104]. However, we could not determine whether this was a direct effect or indirectly through FliP. Since FlhA overexpression does not complement *fliO* deletion, and the degradation is slower than that of FliP, we can exclude that FlhA decay is responsible for FliP instability, but not *vice versa*.

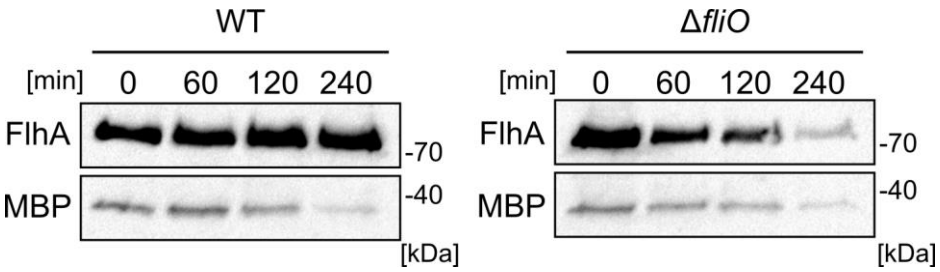

Figure 20: FliO is also involved in FlhA stability. A) Example of stability assay. Culture were grown until OD_{600} reached 0.6 and protein synthesis was inhibited by addition of Spc and Cm. Samples were collected 0, 60, 120 and 240 min after synthesis arrest, and analyzed by Western blot. FlhA was detected using anti-FlhA antibody. MBP was used as loading control.

2.2.3. FliP membrane integration is not influenced by FliO

Although our experiment demonstrated that FliO is involved in FliP stability, the underlying mechanisms remained unclear. As mentioned previously, FliP harbors a signal peptide important for membrane integration. We assumed that FliO could facilitate co-translational membrane integration and thus prevent proteolysis. To follow on this lead, crude membranes and cytoplasmic contents were collected in both WT and Δ*fliO* mutant strain. FliP levels, taken directly after synthesis arrest and 120 minutes later, were analyzed by Western blot (Figure 21 A). Expectedly, in the WT, the highly hydrophobic FliP was only detected in the membrane and was absent from the cytosol. Protein levels were stable over the course of the experiment. We did not observe any difference concerning FliP membrane integration in absence of FliO. Despite being present in the membrane, FliP was still degraded. To discriminate between properly integrated and aggregated proteins associated

to the membrane, membranes were washed with urea to eliminate aggregates. There again, no difference was seen between the WT and the mutant strain (Figure 21 B). These observations lead us to refute our hypothesis and conclude that FliO does not influence incorporation of FliP into the membrane.

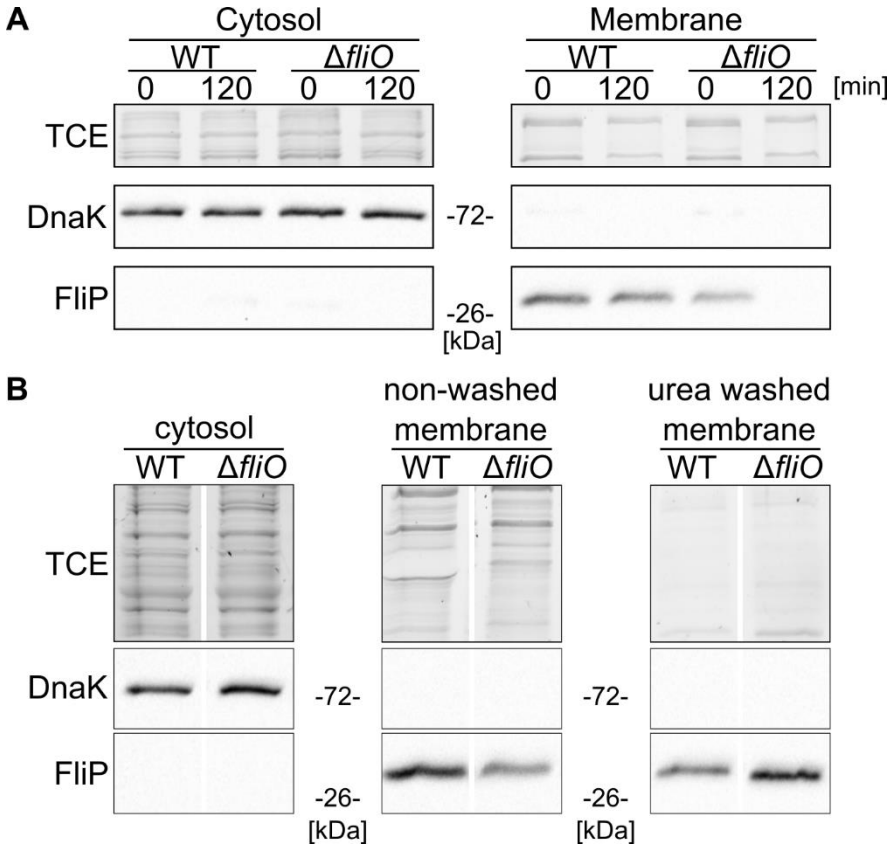

Figure 21: FliP membrane integration is independent on FliO. A) Time course cell fractionation and protein stability assay. Protein synthesis was blocked by addition of Cm and Spc, and samples were collected after 0 and 120 min. Cytosolic and membrane fractions were separated and analyzed by western blot using anti-FLAG antibodies. DnaK was used as loading control. **B)** Crude membranes were prepared from 10 OD units of culture and washed with a 8 M urea solution. Samples were analyzed by Western blot as described above. Total protein content was visualized by TCE staining.

2.2.4. Lon is responsible for FliP proteolysis

To gain further insight into the mechanisms of FliO-mediated stability of FliP, we next aimed to determine which protease is involved in FliP degradation. In bacteria, intracellular proteolysis is mostly dependent on four proteases: Clp, Lon, HslUV, and FtsH [84]. Since FliP is an integral membrane protein, FtsH was considered as a good candidate. Indeed, this essential AAA+ protease has the particularity of being anchored in the membrane. Besides, it is involved in quality control of improperly assembled membrane complexes, for instance the SecYEG translocase [74]. Since FtsH-dependent proteolysis is highly conserved between *E. coli* and *Salmonella* [106], FtsH is likely to be essential in *Salmonella*. Hence, we could not perform a stability assay in absence of FtsH. However, we measured FliP levels upon overexpression of STM1085, a homolog of YccA, an inhibitor of FtsH in *E. coli* [94]. As previously shown, FliP levels degraded overtime in Δ*fliO,* regardless of the presence of STM1085, (Figure 22 A) suggesting that FtsH is not involved in FliP degradation.

To assess the contribution of other proteases, we performed stability assays with the chromosomally encoded $FliP_{Q22}$-3xHA fusion in presence or absence of FliO in Δ*clpXP* and Δ*lon* backgrounds. In absence of ClpXP, FliP was stable in the WT background and degraded in the Δ*fliO* background*,* as in our previous experiments. In absence of Lon however, FliP was stabilized for more than three hours, even in absence of FliO. Altogether, these results indicate that FliP is targeted by the Lon protease for degradation.

This result was surprising since FliP is an integral membrane protein and Lon a cytosolic protease. Furthermore, we showed earlier that FliP was not detected in the cytosol (Figure 21). To explain these conflicting results, we hypothesized that in absence of FliO, FliP dissociates from the membrane and is transiently present in the cytosol where it is rapidly degraded by Lon. Therefore, in absence of Lon, FliP would accumulate in the cytosol. To test this hypothesis, we performed a new cell fractionation in a *Δlon* background, in presence or absence of FliO. There again, regardless of the presence of FliO, FliP was not detectable in the cytosol, even after 180 minutes (Figure 22). These results suggest that Lon degrades membrane bound FliP. This result was puzzling for a cytosolic protease. However, in *B. subtilis*, LonB is membrane bound and a Lon homolog in yeast has been shown to degrade membrane proteins [80], in accordance with our results.

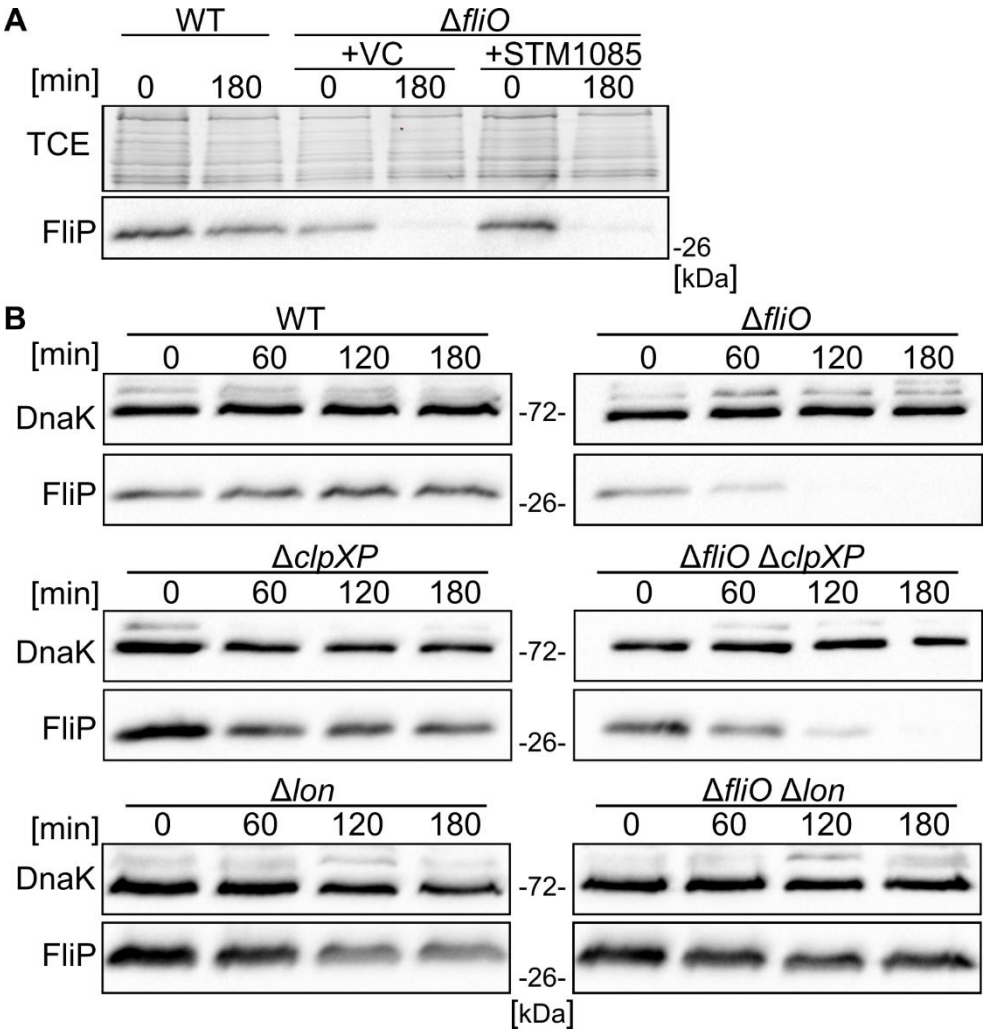

Figure 22: Lon is involved in FliP stability. A) Stability assay performed in presence of STM1085 on chromosomally encoded FliP-3xHA. Expression of STM1085 was induced with 1 mM IPTG from pTrc99-*stm1085* and protein synthesis was blocked by addition of Cm and Spc (vc = empty pTrc99). Samples were collected 0 and 180 minutes after protein synthesis arrest and Western blot was performed using anti-HA antibodies. **B)** FliP-3xHA stability assay in presence or absence of FliO in Δ*clpXP* and Δ*lon* backgrounds. Samples were taken at 0, 60 120 and 180 minutes after synthesis arrest. DnaK was used as loading control.

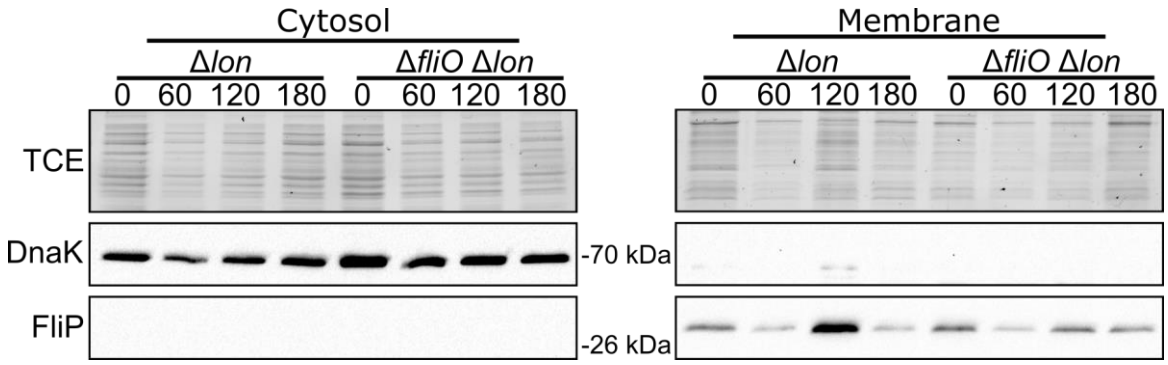

Figure 23: Lon dependent proteolysis occurs at the membrane. Cell fractionation assay in Δ*lon* vs Δ*fliO* Δ*lon*. Protein synthesis was inhibited in exponential growth phase by addition of Cm and Spc. Samples were collected after 0, 60, 120 and 180 min. Spheroplasts were prepared, membrane and cytosolic contents were separated by ultracentrifugation and samples were analyzed by western blot. $FliP_{Q22}$-3xHA was detected using anti-HA antibodies. DnaK was used as cytosolic loading control and was detected using anti-DnaK antibodies. Total proteins were imaged by TCE staining.

2.2.5. FliO is not localized in the export apparatus

The subcellular localization of a protein provides useful information regarding its function. In the case of the flagellar export apparatus, FliP, FliQ, and FliR are thought to be located within the flagellar basal body in the cytoplasmic membrane, are membrane bound and have homologs in the basal body of vT3SS [52]. Experimental evidence suggests that FliR and FliP are associated with the basal body [54]. However, the sub-cellular localization of FliO has not been observed, and a FLAG tagged fusion could not be detected in purified HBB [80]. It remains therefore unclear whether FliO is a structural component of the export apparatus. Consequently, we decided to observe FliO localization using super resolution microscopy (SRM). To that end, we fused the self labelling enzymes HaloTag and SNAP-tag to FliO and to protein of the flagellar basal body such as the C-ring proteins FliM and FliN, as controls, allowing localization of protein clusters *in vivo* using stochastic optical reconstruction microscopy (dSTORM) [109,110].

Prior to microscopy analysis, we tested whether the constructs were functional by assessing motility in soft agar plates (Figure 24 A). FliO fusions retained motility, indicating that the presence of the tags did not affect flagellar assembly. FliM and FliN fusions, however, were non-motile. As described above, FliM and FliN do not only play a role in flagellar substrate export, but also in filament rotation and directional switch. Hence, the loss of motility in these constructs does not necessarily correlate with a non-functional T3SS. We therefore checked extracellular flagellin secretion (Figure 24 B). To enable flagellin detection with α-FliC antibodies, we used strains in which the Hin invertase was deleted and where P*fljB*

was locked in *fljB*-OFF *fliC*-ON orientation. In this state, FljB is not synthetized and FljA-mediated inhibition of *fliC* is abolished, leading to FliC expression. In all constructs, FliC was secreted in comparable amounts to the WT, indicating that the export function of the C-ring was unaffected by the HaloTag fusions. Flagella observation by fluorescent microscopy confirmed that flagellar assembly occurred in presence of FliN fusions (Figure 24 C) and that theses strains harbored a similar number of flagella per cell, validating our experimental set up.

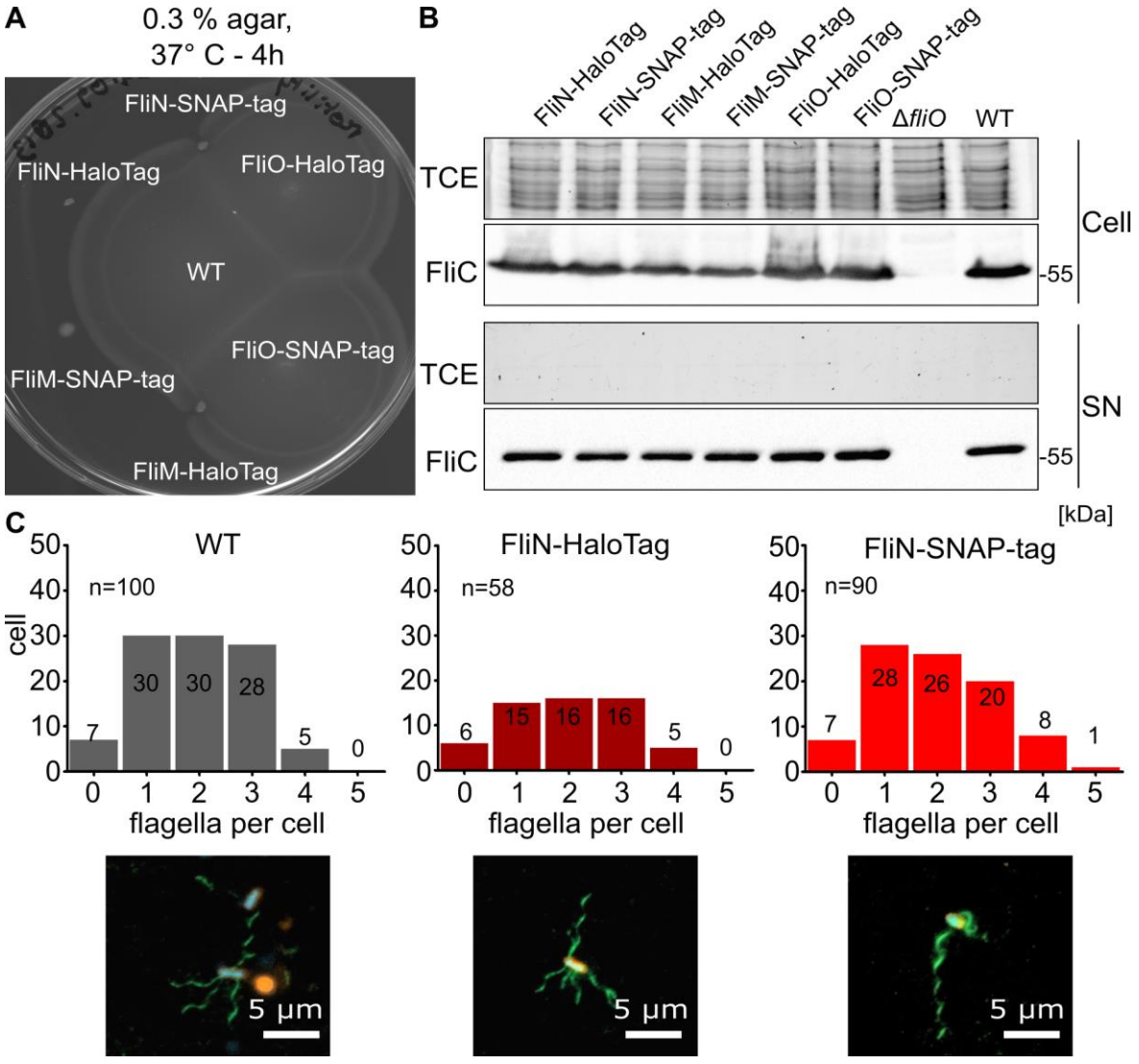

Figure 24: HaloTag and SNAP-tag fusion do not affect export and flagellar formation. A) Motility assay in soft agar plate after 4 h at 37 °C. **B)** Secretion assay in strains carrying the Halo/SNAP-tag fusion. Sample were collected when OD_{600} reached 0.6. Supernatant was separated from total cell extracts by centrifugation and samples were analyzed by western blot using anti-FliC antibodies. Total proteins were visualized by TCE staining. **C)** Examples of flagellar immunostaining on FliN Halo/SNAP-tag fusions. Flagella were stained using anti-FliC primary antibodies and Fluor488-coupled secondary antibodies (green). DNA was stained with DAPI (Blue) and membranes with FM 64 (red). The number of flagella per cell is displayed above. "n" indicates the number of bacterial cells analyzed.

Expectedly, the SRM observation revealed that FliM-HaloTag and FliN-HaloTag were localized in discrete clusters, most probably corresponding to the flagellar basal body. Surprisingly, this pattern was not observed for FliO-HaloTag. Instead of co-localizing with the C-ring proteins, FliO appeared evenly distributed in the cell envelope (Figure 25 A).

To verify these observations, we inserted a HA tag in a permissive site of the hook protein FlgE in a *fliO-HaloTag* positive strain, and performed immunostaining, to visualize FliO distribution and flagellar HBB complexes simultaneously (Figure 25 B). There again, while FlgE was restricted to 4 to 5 localized clusters per cell, FliO was more evenly distributed and mostly did not co-localize with the HBB. These observations clearly suggested that FliO is not part of the flagellar basal body.

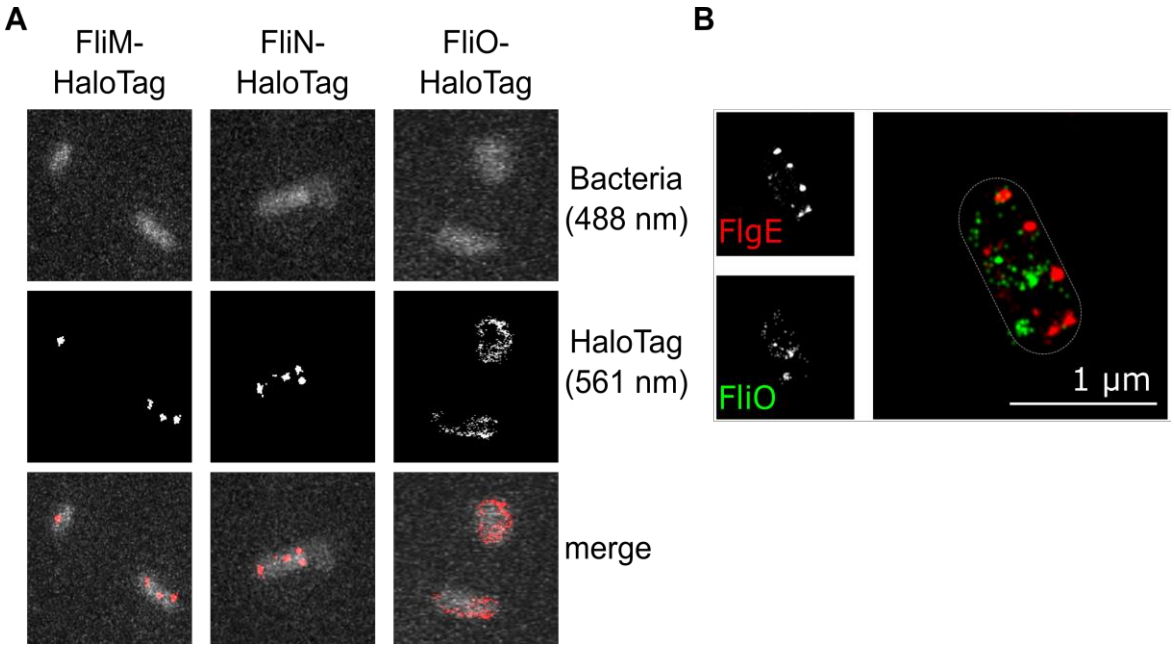

Figure 25: FliO does not co-localize with the basal bodies. A) dSTORM images of FliM, FliN and FliO-HaloTag strains. Strains were grown at 30 °C for 1.75 h and treated as described in the methods chapter. The 488nm signal corresponds to the whole cell fluorescence while the 561nm signal is specific for HaloTag. **B)** Fixed cell dual color labeling. FlgE-HA was detected by immunofluorescence using anti-HA antibodies and FliO-HaloTag visualized using fluorescent ligands as previously described**.** Microscopy was performed by Britta Peters.

It also appeared that two populations of FliO were present, one static population and one that could be mobile in the cell. To follow this idea, we performed single particle tracking of FliO compared to FliN (Figure 26). While FliN particles appeared to be static, with a diffusion coefficient of 0.03 $\mu m^2 \cdot s^{-1}$, FliO particles were clearly mobile, following long trajectories within the whole cell envelope. FliO diffusion coefficient was six-fold higher than that of FliN and reached 0.2 $\mu m^2 \cdot s^{-1}$, which is consistent with the values of other freely diffusing cytoplasmic membrane proteins, ranging from 0.02 to 0.2 $\mu m^2 \cdot s^{-1}$, reported in previous studies [89,90]. Taken together these results strongly suggest that FliO is not part of the completed export apparatus, but is freely moving in the inner membrane. We thus hypothesize that FliO acts as accessory protein during flagellar T3SS assembly.

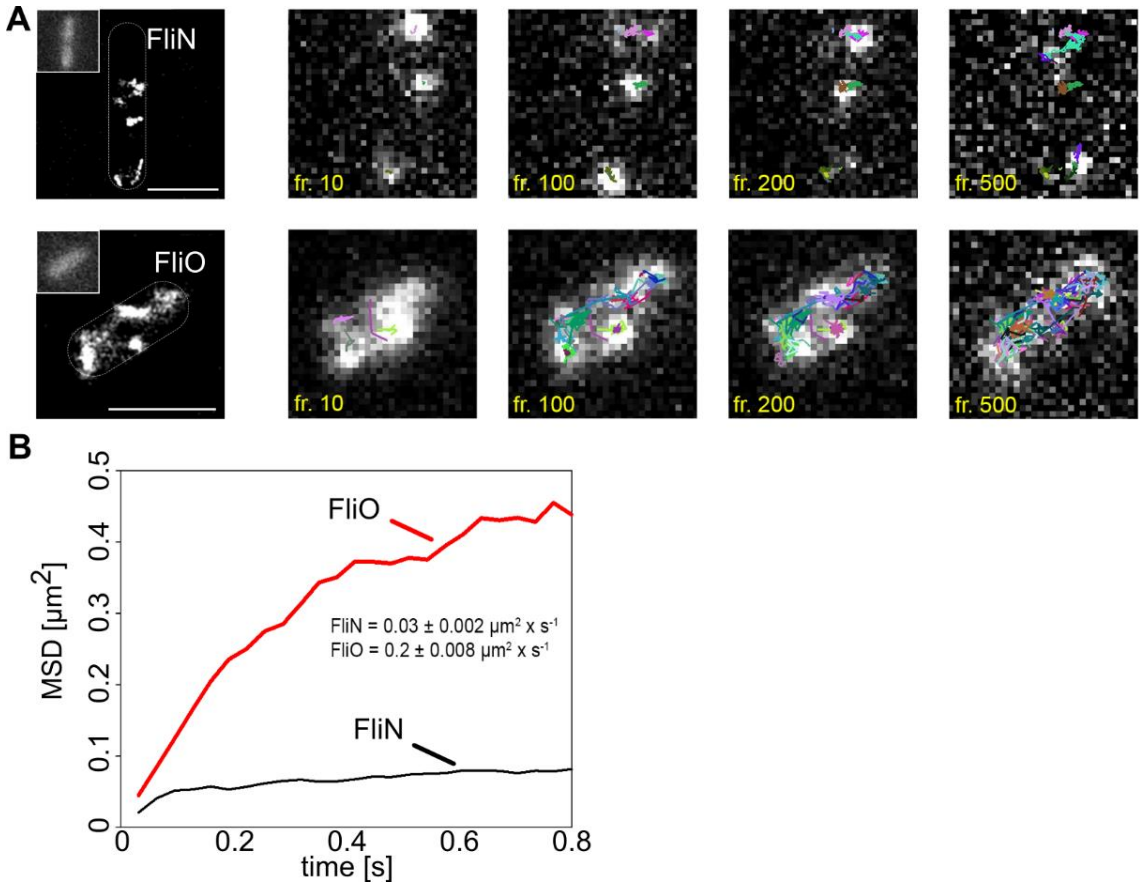

Figure 26: FliO is freely diffusing in the membrane. A) Example of single particle tracking of TMR ligand labeled FliN-HaloTag and FliO-HaloTag. Each image shows the same cells at different time frames over the course of the experiment. The trajectories of single molecules are displayed in colors. **B)** Mean square displacement (MSD) plots of FliO and FliN trajectories. The date of at least 25 bacteria recorded under the same conditions were pooled. The diffusion coefficient of each protein was calculated using Jaquaman algorithm and indicated on the graph. Microscopy was performed by Britta Peters.

2.2.6. FliO is required for FliP oligomer assembly in flagellar formation

To study the influence of FliO on flagellar export apparatus formation, we prepared and solubilized bacterial crude membranes in presence or absence of FliO and analyzed the presence of FliP complexes under native conditions using Blue Native PAGE. In the wild type background, we detected the presence of at least four different protein complexes containing FliP-3xFLAG (Figure 27 A). According to their apparent native masses, we assumed that the highest complex (i) was the completed hook basal body and that the lowest band (v) corresponded to FliP-3xFLAG monomers. We hypothesized that the intermediate complexes (iii and iv) were precursors of the export gate. To characterize these complexes, we excised them from the gel and performed mass spectrometry analysis. The mass spectrometry results indicated the presence of proteins of the hook, the export gate, and of the L, P, MS and C-rings, in the highest complex (i) (Figure 27 B) confirming that this was indeed the completed basal body. In accordance with the SRM analysis shown above, no FliO was detected in the HBB. Mass spectrometry data also showed the presence of FliO and FliP in complex (iii) and FliO and FliR in complex (iv). Although, FliP was not detected in the latter complex, the fact that (iv) was visible with FLAG antibody directly implies FliP presence. Moreover, the complex (iv) migrated in a similar fashion to the $SpaP_5R_1$ complex, an intermediate of needle complex assembly observed in the injectisome [44,81]. This strongly supports the hypothesis that the complex (iv) is a precursor of the flagellar export gate.

In absence of FliO however, we did not detect the completed HBB nor the intermediate precursors, indicating that FliO is required for the formation of FliP sub-complexes necessary for export gate and basal body assembly. Consistently, FliP monomers were strikingly more abundant in Δ*fliO*. We also observed the presence of a high molecular weight complex migrating slightly lower than the HBB. It contained FliP and other flagellar proteins, and could correspond to uncompleted or misassembled basal bodies, or aggregated FliP-protease complexes as suggested by the presence of FtsH. Interestingly, while completed basal bodies were absent, the intermediate FliP complexes were still present in the absence of the MS-ring protein FliF (Figure 27 C), indicating that FliP multimerization is not dependent of the MS ring. Consistently, no FliF peptide was detected in (iii) and (iv), in contrast to the HBB (i).

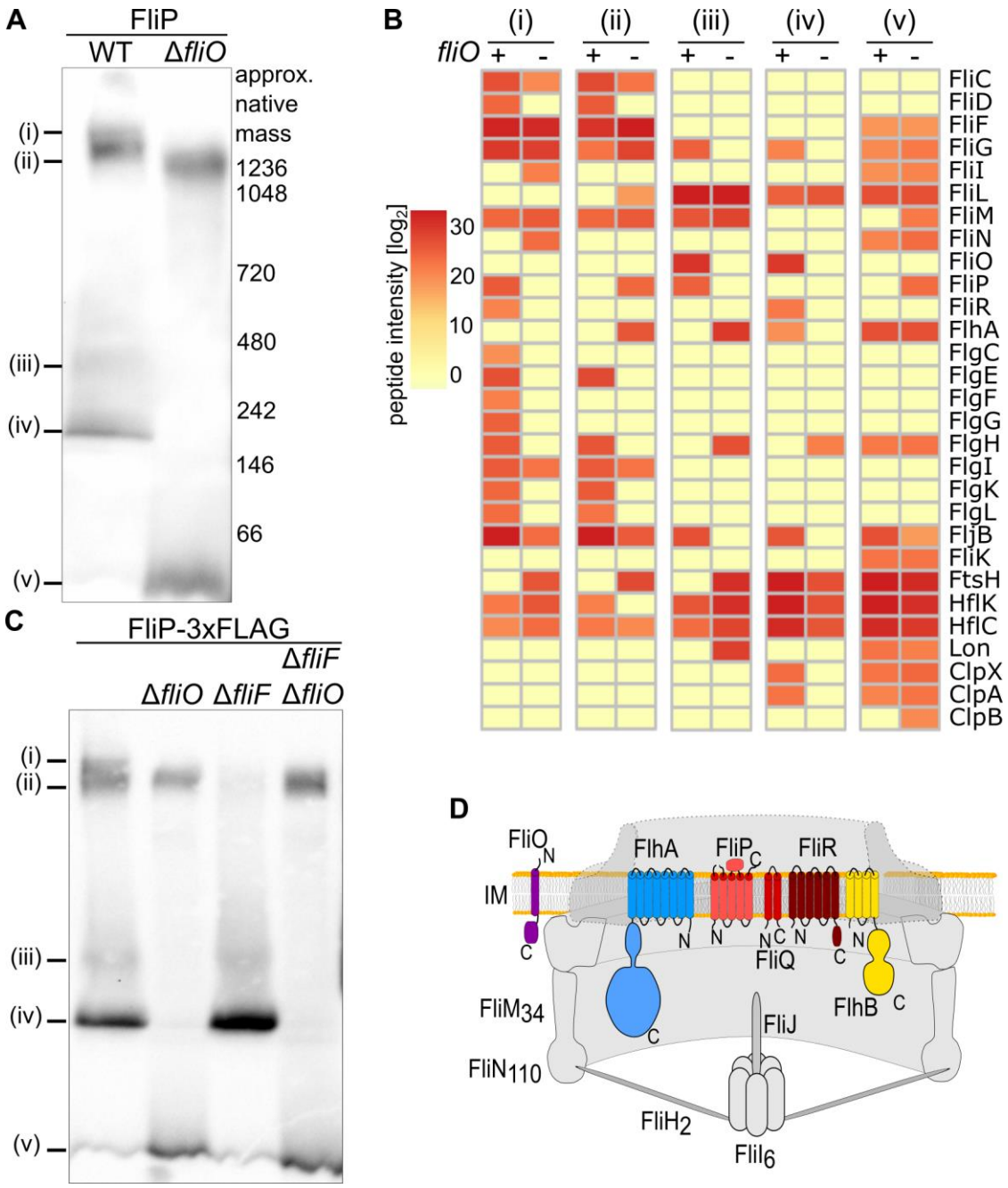

Figure 27: FliO is required for FliP complexes assembly. A) BN-PAGE using FliP-3xFLAG. Membranes were prepared from 1 l of culture and analyzed on BN-PAGE using anti-Flag antibodies. **B)** Bands containing FliP complexes were excised from the gel in both WT and Δ*fliO* and analyzed by LC-MS/MS. Heat map shows the $\log_2$ intensities of the relevant peptides detected in each complex. **C)** Example of BN-PAGE performed on crude membrane in absence or presence of FliF. **D)** Schematic representation of the components of the flagellar T3SS.

To gain a better insight into the composition of the FliP sub-complexes, and clearly determine interaction partners of FliP, we performed a pull-down of FLAG-tagged FliP using anti-FLAG resin under native conditions (Figure 28). To ensure accessibility of the tag from the periplasm, we deleted the rod proteins FlgBC. Moreover, to increase the yield, the negative FlhDC regulator YdiV, was also deleted.

Analysis of the eluate by BN-PAGE revealed the presence of seven complexes containing FliP (A to G). In the Δ*ydiV* Δ*flgBC* background (Figure 28), the number and size of flagellar complexes slightly differed in comparison to the wild type background (Figure 27). Due to the absence of FlgBC, the HBB complex identified in the wild type was completely missing in Δ*ydiV* Δ*flgBC*. The complex (A) and (B), appeared to migrate at slightly higher and lower than complex (ii), respectively. The approximative sizes of complexes (E) and (F) indicate that they might correspond to the intermediate complexes (iii) and (iv), while (C), (D) and (G) did not match any of the complexes previously observed. Complexes (A), (B), (F), and (G) were analyzed by mass spectrometry. Beside FliR and FliG, all flagellar proteins detected in (iv) were present in (F), namely FliL, FliO, FliP and FlhA (Figure 28). This confirms that it is either the completed export gate or one of its precursor. The presence of more complexes can easily be explained by the larger amount of material obtain with the purification in comparison to the crude membranes. The detection of an intense band at a lower molecular weight (G) was more puzzling, but could result from the dissociation of a protein from the (F) oligomer after elution. Indeed, previous studies on purified needle complexes reported that InvA, the SPI-1 homolog of FlhA, easily dissociates from the rest of the structure and that it assembles at last [44]. Therefore, the absence of FlhA signal could point towards an uncompleted export gate, missing the FlhA nonamer. Notably, FliO was present in every complex analyzed suggesting that FliO is physically associated with FliP.

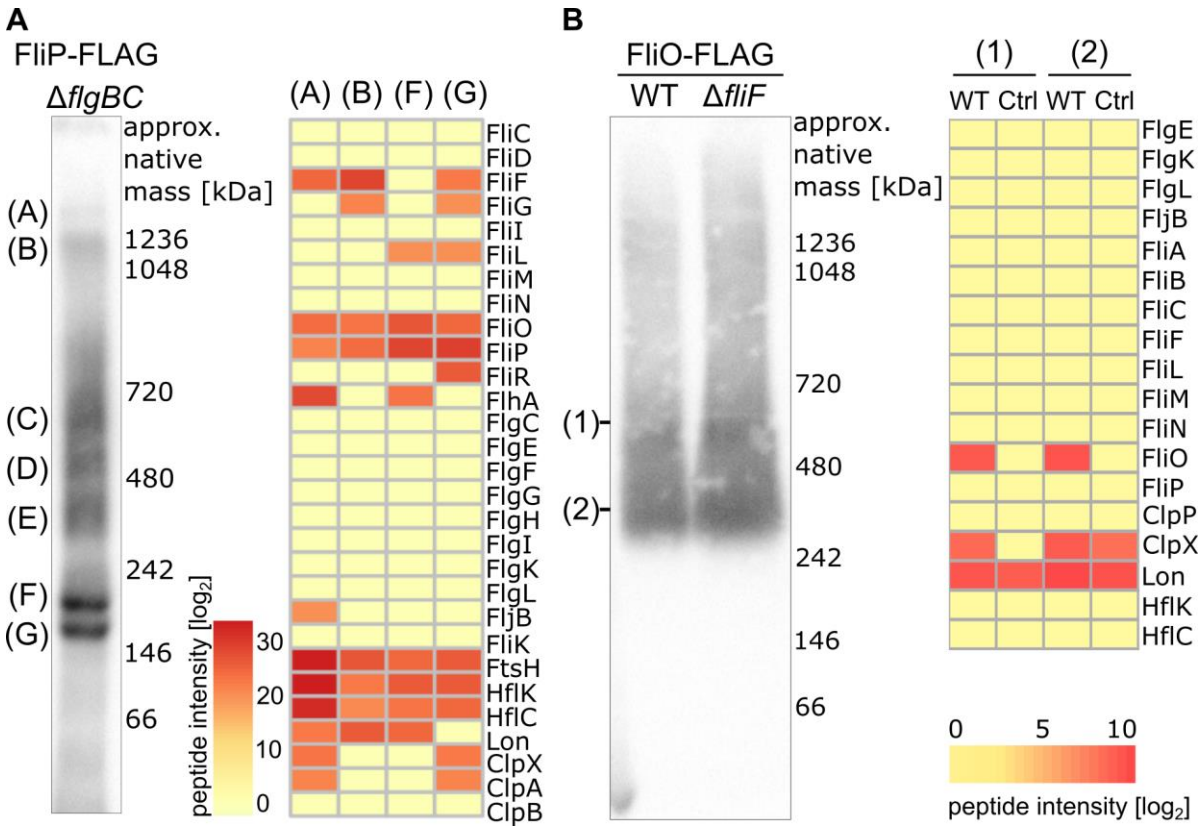

Figure 28: FliO physically interacts with FliP but is absent of the basal body. A) BN-Page after purification of FliP-FLAG from 1 l of culture under native condition, using anti-FLAG resin. The different FliP complexes are indicated by capital letters. Complexes A, B, F and G were excised and analyzed by mass spectrometry. **B)** Crude membranes were prepared from 10 ml of cultures of FliO-3xFLAG strains. BN-PAGE was followed by western blot using anti-FLAG antibodies. Complexes 1 and 2 were excised and analyzed by LC-MS/MS. Heat maps represent the $\log^2$ of the intensities of the detected peptides.

Finally, we were interested in the assembly of putative FliO complexes. Hence, we analyzed the crude membrane extract of cells chromosomally encoding a FliO-3xFLAG fusion (Figure 28 B). We observed smears in which two intense bands (1 and 2) were detected. Consistently with our previous observations, no specific FliO signal was detectable at the size of the completed basal bodies. Surprisingly, the two complexes did not co-migrate with the FliP sub-complexes observed in Figure 27 A, in contradiction with the detection of FliO peptides in the FliP intermediate. This could suggest that only a small fraction of the FliO pool is associated with FliP and most of it is present in these two FliO complexes. None of the other flagellar proteins beside FliO were detected by mass spectrometry in complexes (1) and (2), pointing towards FliO homo-oligomers or FliO complexes associated with proteins unrelated to flagellar biosynthesis.

2.3. The role of the N-terminal signal peptide of FliP

Although FliP, FliQ and FliR have highly conserved homologues in the vT3SS, FliP has a particular feature which is absent in its injectisome counterpart. FliP harbors a 22-amino acid signal peptide at its N-terminus and undergoes cleavage during maturation. Cleavable signal peptides are normally found in periplasmic or outer membrane proteins in prokaryotes, and facilitate translocation in the periplasm. Together with the absence of a FliO homolog, the presence of the FliP signal peptide is one of the major differences between fT3SS and vT3SS. Therefore, we were interested in the role of this unique feature of the flagellar export apparatus and we investigated whether it is linked with FliO-dependent stabilization. Previously, Ohnishi *et al*. demonstrated that motility decreases dramatically in a mutant expressing only mature FliP, lacking the 22 first amino acids, although motility was restored when mature FliP was overexpressed [78]. In a cleavage site mutant, however, the effect on motility was limited, suggesting that the signal peptide, but not cleavage of the signal peptide, might be required for FliP function. To obtain further insight into the role of the signal peptide cleavage, we created a series of cleavage site mutants affecting FliP maturation. We studied the effect of cleavage deficiency on motility, membrane integration, stability, topology, and flagellar formation. We also analyzed whether FliO had an influence on FliP signal peptide cleavage efficiency.

2.3.1. Construction of cleavage site mutants

Ohnishi *et al* proposed that the cleavage site of FliP is located before position Q_{22}. They created a $A_{21}D$ $Q_{22}P$ mutant preventing signal peptide cleavage and observed a limited effect on motility. However, both the mature and the precursor form of FliP were detected by Western blot, indicating that cleavage still occurred although with a greatly reduced efficiency. Hence, the strain could retain a motile phenotype solely because of the remaining mature FliP and the abolished cleavage could be more detrimental than previously stated.

In proteins secreted through Sec-dependent pathway, signal peptide cleavage is dependent on signal peptidase 1 [113,114]. In *E. coli,* the signal peptidase 1 cleaves after a Ala-X-Ala sequence, following the so-called "-3, -1" rule. The five to six amino acid preceding the cleavage site also play a role [114]. Furthermore, the presence of a proline directly after the cleavage site (position +1) prevents peptidase activity [115]. To assess the importance of the cleavage process, the sequence preceding the cleavage site was more dramatically altered than in the previous study. In addition to the FliP$_{A21D/Q22P}$ mutation tested by Ohnishi *et al.*, we constructed two other cleavage site mutants. In the second variant, the original PAAAAQ sequence site was substituted by PADADQ (FliP$_{PADADQ}$). The glutamine residue at position +1 was retained, but the -1 and -3 alanine residues, which are small hydrophobic and neutral, were replaced by two larger, negatively charged aspartate residues. In the third cleavage site mutant (FliP$_{GSGSGP}$), the sequence was dramatically modified by introducing flexibility at the beginning with the P$_{17}$G substitution while replacing alanine residues by glycine and serine and adding a proline at position +1. Finally, a FliP variant mimicking the mature form (FliP$_{\Delta 2\text{-}22}$), missing amino acids 2 to 22, was created. All mutants are depicted in Figure 29. To enable detection by Western blot, the *fliP* variants carried a 3xFLAG tag at position G$_{157}$. All mutants were introduced by λ-Red homolog recombination at the native chromosomal location of *fliP* and were also made in a Δ*fliO* background.

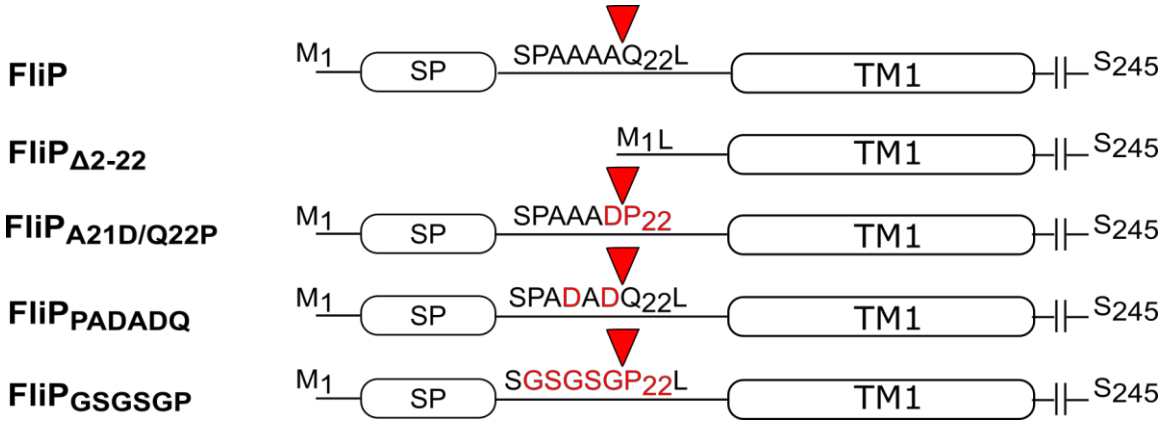

Figure 29: Schematic view of the cleavage site mutants used in this study. The cleavage site is indicated by the arrow and the substituted amino acids in red. The signal peptide (SP) and the first transmembrane domain (TM1) are indicated by boxes, all domains after TM1 are not shown here.

2.3.2. Cleavage is crucial for motility

We were interested in the effect of cleavage on motility. To that end, we first detected FliP by Western blot on total cell extract, to observed the effect of each mutation on cleavage efficiency and FliP expression (Figure 29 A). As expected, only the mature form was observed in the WT, Δ*fliO* and in the $FliP_{\Delta 2\text{-}22}$ mutant. For the $FliP_{A21D/Q22P}$ mutant, we observed equivalent amounts of cleaved and non-cleaved FliP. However, this effect was not as dramatic as described by Ohnishi *et al*. Cleavage efficiency was more affected in presence of the $FliP_{PAAAQ}$ variant, and almost abolished in the $FliP_{GSGSGP}$ mutant. The absence of FliO did not seem to have any effect on cleavage efficiency although the levels of the precursor protein were slightly lower than in the WT background. Remarkably, expression of FliP was somewhat decreased in absence of the signal peptide and this effect was slightly more pronounced in absence of FliO. This indicated that the signal peptide is important for FliP expression.

We then monitored motility of all the constructs in 0.3 % agar plates after 4.5 h at 37 °C (Figure 29. B). In accordance to the results of Ohnishi *et al.*, the absence of signal peptide led to a decrease in motility, consistent with the decrease in FliP expression (Figure 30 A), but the $FliP_{\Delta 2\text{-}22}$ mutant still retained about 55 % motility compared to the WT (Figure 30 B). Interestingly, the decrease in motility was correlated with a decrease in cleavage efficiency. The $A_{21}D\ Q_{22}P$ strain, exhibited a decrease in motility (about 85 % of the WT), consistent with previous reports [78]. While motility decreased to 42 % in the $FliP_{PAAAQ}$ expressing strain, and the $FliP_{GSGSGP}$ mutant was almost non-motile (17 %). Expectedly, in absence of FliO, motility further decreased in all strains. These results demonstrate that FliP cleavage is essential for motility, unlike previously suggested. Besides, we showed that FliO has no influence on cleavage efficiency. Finally, these results confirmed that the presence of the signal peptide enhances FliP expression and motility, but is not strictly required.

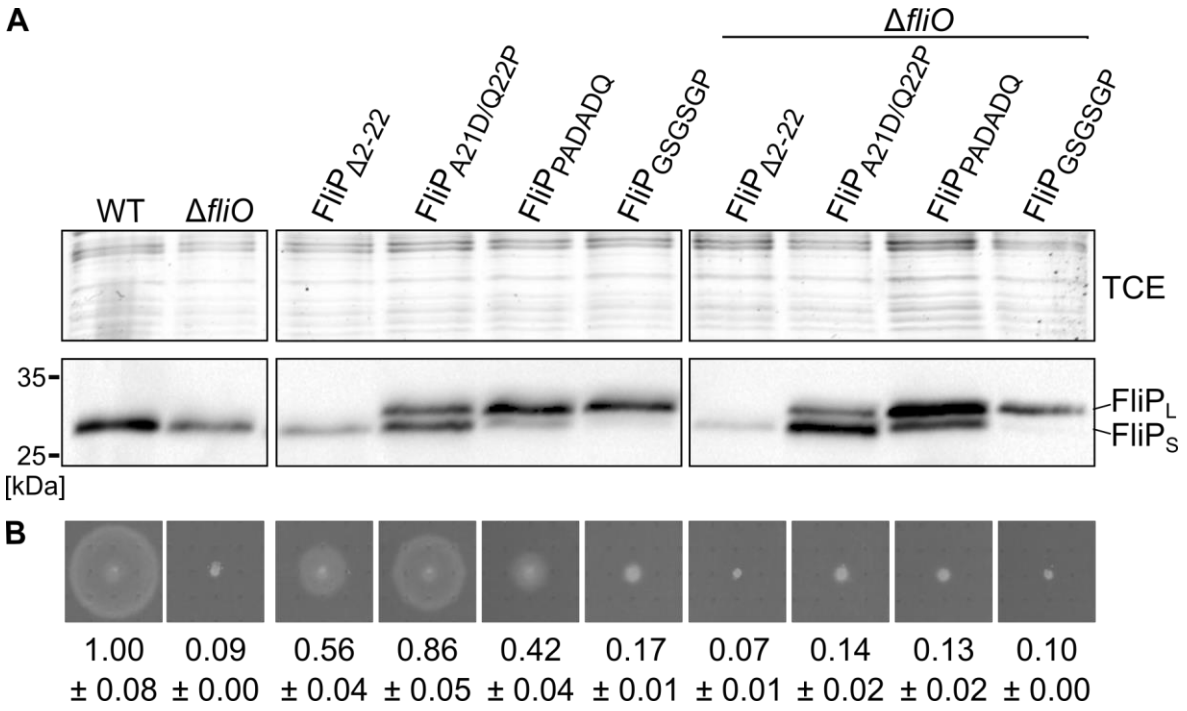

Figure 30: Signal peptide cleavage is crucial for motility. A) Detection of FliP variants by western blot. Cells were grown at 37 °C in LB under shaking, bacteria were collected when OD_{600} reached 0.6 and protein were precipitated with TCA. Samples were separated on a 15 % SDS-PAGE and analyzed by western blot using anti-FLAG antibodies. Total proteins were visualized using TCE staining and served as loading control. **B)** Example of motility in soft agar. Strains were inoculated in 0.3 % LB agar plates and grown for 4.5 h at 37 C. the diameters of the swarms were measured using ImageJ. The average size of the swarm, relative to the WT and the SD are indicated below.

2.3.3. Both cleavage and the presence of the signal peptide are important for FliP stability

We observed that the deletion of the 21 N-terminal amino acids affected FliP expression levels. One explanation could be that the absence of signal peptide influences protein stability. To verify this hypothesis, we monitored FliP levels over time after inhibition of protein synthesis as performed above. We also observed FliP levels in the cleavage deficient mutants to see of if cleavage increases stability. In a WT strain, FliP levels were completely stable over the course of the experiment (Figure 31), suggesting that neither the signal peptide nor the cleavage affected protein stability. We previously showed that FliO stabilizes FliP, and observed that the precursor form of FliP is slightly less abundant in absence of FliO (Figure 30). To test whether FliO specifically stabilized the FliP precursor protein. We also monitored the stability each variant in absence of FliO. In the three strains harboring a FliP variant with a mutated cleavage site, both the mature and the precursor FliP species were unstable (Figure 31). Nevertheless, while the levels of mature FliP ($FliP_S$)

decreased in a similar fashion as previously observed for the WT variant in a Δ*fliO* background, the precursor form ($FliP_L$) degraded strikingly faster (Figure 31). This suggested that the cleavage process increases stability and that FliO prevents degradation of both species. Interestingly, in absence of FliO, the $FliP_{\Delta 2\text{-}22}$ variant, missing the signal peptide, displayed lower steady-state protein levels than the WT variant and was undetectable after 120 minutes. This clearly demonstrates that the presence of the signal peptide stabilizes FliP, probably by facilitating membrane integration directly after translation.

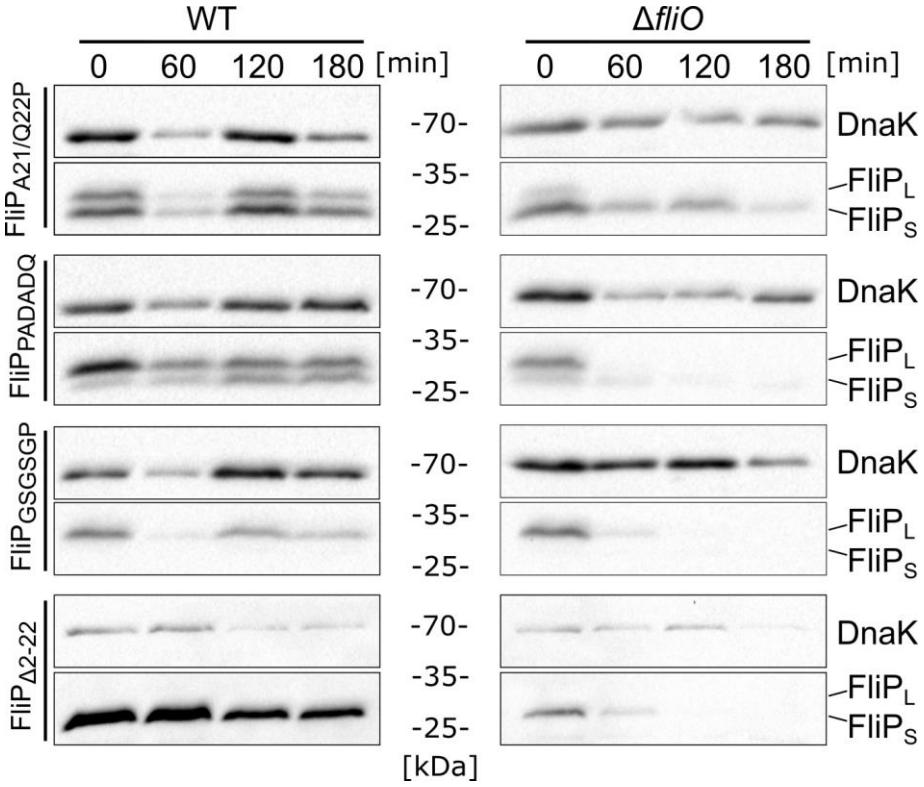

Figure 31: The presence of the signal peptide and cleavage efficiency influence FliP stability. Representative examples of stability assays in the different FliP mutants in presence or absence of FliO. Cells were grown in LB at 37 °C until OD_{600} reached 0.6. and protein synthesis was stopped by addition of Cm and Spc. Samples were collected after 0, 60, 120 and 180 minutes, precipitated, separated by SDS-PAGE and analyzed by western blot. FliP and DnaK were detected using anti-Flag and anti-DnaK antibodies respectively. DnaK was used as loading control.

2.3.4. The signal peptide facilitates membrane integration

The function of the signal peptide of FliP remains unclear, especially because it is absent in *B. subtilis* [91] and in its injectisome counterpart SpaP [81]. Furthermore, strains lacking the signal peptide are still motile, suggesting that it is not required for membrane integration. To verify if cleavage deficiency or the absence of the signal peptide affect FliP integration into the membrane, we performed a cell fractionation assay as described above. We isolated crude membrane extracts and washed them with urea to remove aggregated proteins. In all cleavage site mutants, both the precursor ($FliP_L$) and the mature ($FliP_S$) forms were integrated in the membrane. After urea washing, the amount of total protein was lower, but the ratio between both species remained unchanged (Figure 32). This suggested that the cleavage of the signal peptide has no influence on the membrane integration process. The construct lacking the signal peptide was also present in both washed and non-washed fractions. Nevertheless, the amount of integrated $FliP_{\Delta 2\text{-}22}$ appeared to be decreased in comparison to the other constructs, while the difference was not as obvious in the unwashed fraction. These results confirmed that the signal peptide is important but not essential for membrane integration and that cleavage does not influence insertion.

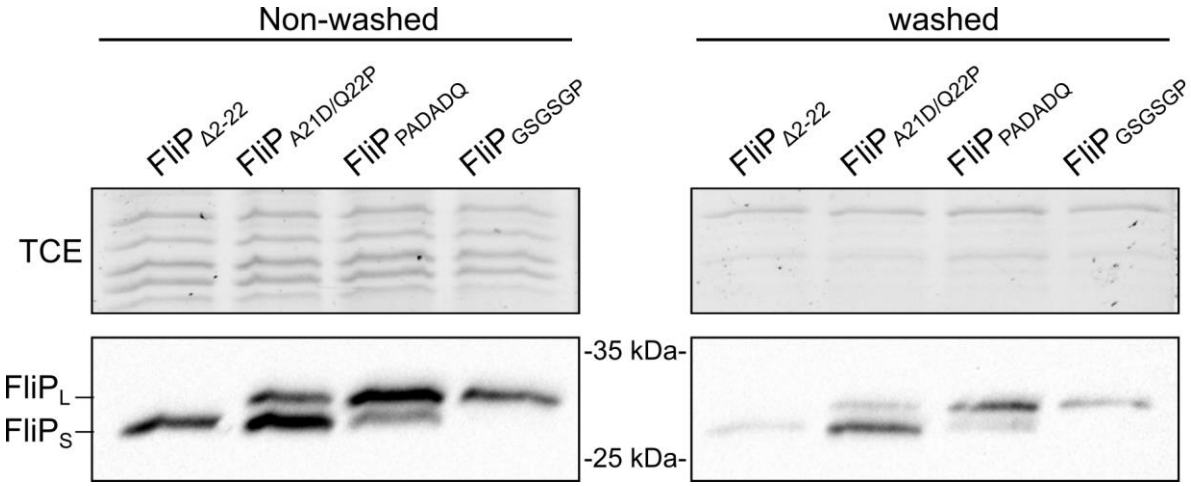

Figure 32: The signal peptide influences membrane insertion. Representative example of cell fractionation assay. Cells were grown until OD_{600} reached 0.6 and crude membrane fractions were collected by ultracentrifugation. Half of the material was washed with 8 M Urea to eliminate aggregated proteins associate with the membrane and samples were analyzed by western blot. FliP was detected using anti-FLAG antibody. Total proteins were visualized by TCE staining and served as loading control.

2.3.5. Cleavage might be involved in the folding process

We demonstrated that cleavage of the signal peptide did not influence membrane integration and that the uncleaved / precursor species ($FliP_L$) was more unstable in absence of FliO. We hypothesized that the cleavage process could be important for correct folding, and that improperly folded FliP is rapidly degraded by the protein quality control system. To verify the FliP folding state, we analyzed FliP topology of both species by performing single cysteine labeling, also known as substituted-cysteine accessibility method (SCAM). This assay enables to determine the sub-cellular localization of a residue based on the binding of PEG-maleimide to cysteine. A single amino acid is replaced by a cysteine, the outer membrane is permeabilized, the peptidoglycan layer is degraded, and spheroplasts are incubated with PEG-maleimide. Cysteines located in the periplasm are accessible and PEG-maleimide can bind. Upon binding, the molecular weight of the protein increases and a shift can be observed after SDS-PAGE. Cysteines buried in the membrane or located in the cytosol are inaccessible for PEG-maleimide and the protein is not modified. In this experimental setup, the amino acids A_{32} or S_{117} were substituted by a cysteine in the $FliP_{A21D/Q22P}$ mutant. Both residues are located in the periplasm according to the topology prediction and previous single cysteine labeling results from our lab (Renault *et al.* unpublished). The advantage of using the $FliP_{A21D/Q22P}$ mutant is that the precursor ($FliP_L$) and the mature ($FliP_S$) forms of FliP are present in similar amount allowing the study of both species in the same strain.

With the $FliP_{A32C}$ variant, a shift of the mature species ($FliP_s$) but not of the uncleaved precursor ($FliP_L$), was observed. As expected, the positive control treated with SDS exhibited a shift for both bands (Figure 32). The absence of the highest shift indicated that the cysteine was not accessible in the precursor. This suggests that the topology of the non-cleaved precursor differs from that of the mature FliP. Hence, the precursor might be unproperly folded. To analyze a putative role of FliO in folding of FliP, we also performed the experiment in absence of FliO. The presence of FliO did not affect these results (Figure 33).

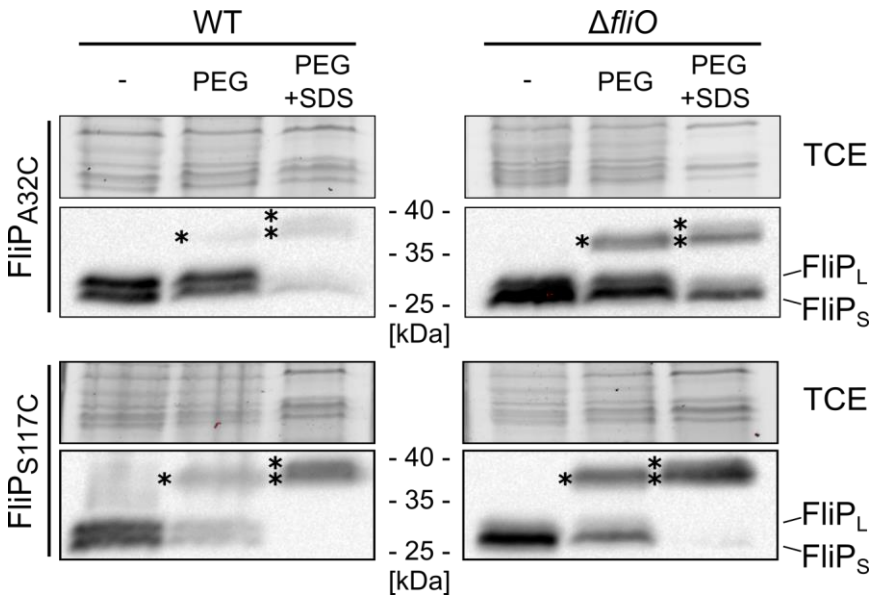

Figure 33: Signal peptide cleavage influences the FliP topology. Single cysteine labeling of $FliP_{A21D/Q22P}$. A single amino acid was substituted with a cysteine at position 32 or 117 in a $FliP_{A21D/Q22P}$-3xFLAG construct. Spheroplasts were prepared from culture in exponential growth phase. Spheroplasts were either left untreated (-), incubated with PEG-maleimide or incubated with PEG-maleimide + SDS, as positive control. Samples were separated by SDS-PAGE and analyzed by western blot. FliP was detected using anti-FLAG antibody. Total proteins were visualized by TCE staining and served as loading control. The PEG-bound FliP are indicated by and asterisk (*).

In the $FliP_{S117C}$ variant, we could also visualize a shift of the mature form but not of the precursor. There again, the absence of FliO had no effect. Although these results are preliminary and must be repeated for confirmation, they suggest that the cleavage process is essential for proper folding of FliP. They also show that FliO has no influence on FliP folding.

2.3.6. Cleavage is essential for proper assembly of the basal body

Our results showed that signal sequence cleavage was crucial for motility and might be necessary for correct folding of FliP. Therefore, we analyzed FliP complex formation by BN-PAGE to determine whether mutations in the signal peptide cleavage also influenced basal body assembly. The experiment was performed, as previously (see 2.2.6), with the $FliP_{GSGSGP}$ construct, in which cleavage is virtually abolished, with the variant lacking the signal sequence ($FliP_{\Delta 2\text{-}22}$), and with WT FliP. In the wild type background five complexes (i-v) (Figure 34) could be identified as observed above (see 2.2.6). These complexes were also found in the $FliP_{\Delta 2\text{-}22}$ strain, although with a weaker signal, suggesting that assembly was not affected but the amount of FliP was reduced. This was consistent with our previous results (chapter 2.3.3). In presence of the cleavage deficient FliP, however, the assembly process was dramatically affected (Figure 34). Completed basal bodies (i) were not detectable and most of FliP was aggregated (ii). An intense band was also detected at about the size of FliP sub-complex (iii), and complex (iv) was only present in extremely low amounts, suggesting that the cleavage of the signal peptide is required for the formation of this FliP oligomer. The remaining signal could be due to the presence of residual cleaved FliP. Other lower molecular weight complexes were present and could correspond to degradation products. The composition of these complexes was not determined. The fact that complex (iv), but not complex (iii), was affected could suggest that complex (iii) forms before FliP cleavage. However, the presence of this complex in presence of the $FliP_{\Delta 2\text{-}22}$ mutant contradicts this interpretation. Nevertheless, since complex (iii) appears to migrate slightly higher in the cleavage deficient mutant, it could be the same complex formed with non-cleaved FliP. The quasi absence of the complex previously identified as a FliP/FliR oligomer (iv) in presence of $FliP_{GSGSGP}$, suggests that this complex is formed after cleavage. Together, these results indicate that FliP needs to be cleaved to properly assemble with its interaction partners and form a functional export gate.

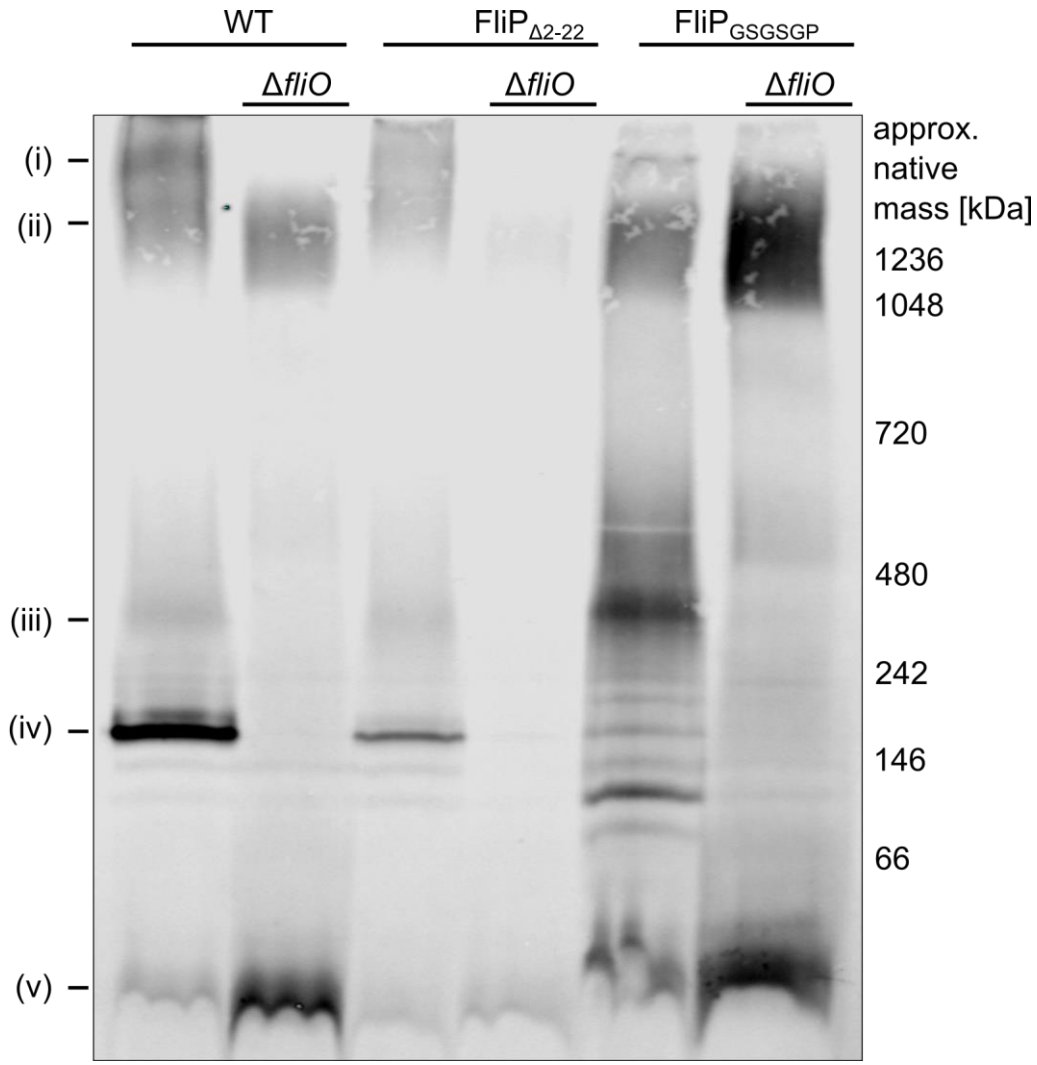

Figure 34: Cleavage is crucial for FliP complexes formation. BN-PAGE on crude membranes of FliP mutants in presence or absence of FliO. Crude membrane extracts were prepared by ultracentrifugation from 10 ml of exponential phase culture. Membranes were solubilized in DDM and samples were separated on a 3-12% Native-PA gel and analyzed by western blot using anti-FLAG antibodies to detect FliP.

3. Discussion

3.1. FliF, FlhBA and FliOPQR are sufficient to assemble a functional T3SS export apparatus

To get a better understanding of the complex mechanism underlying flagellar export and establish a simplify model of fT3SS, we intended to determine the most crucial components for secretion and aimed at reconstituting a minimal export apparatus. Among the proteins originally classified as essential (including FliFG, FliHIJ, FliGMN, FliOPQR and FlhBA), FliHIJ and FliMN had already been shown to be dispensable [86,88,92,93]. Previous experiments conducted in our group using the FlgE-βlactamase reporter system, under physiological conditions and upon overexpression of FlhDC, provided us with more information. Under physiological conditions, secretion was abolished in all tested mutants. Upon overexpression of FlhDC, however, export was restored in Δ*fliHIJ* and Δ*fliMN*, but also to a lesser extent in Δ*fliO* and Δ*fliG*. In every case, FliF, FliPQR and FlhBA were necessary (Erhardt *et al.* unpublished). This was expected since these proteins are highly conserved in flagellated bacteria and in the injectisome systems [117]. FliF and FlhA are most likely to be essential due to their importance as scaffold and for fueling export, respectively [79,118]. Furthermore, the probable formation of the translocation port by FliP, FliR and possibly FliQ, as in the injectisome, strongly suggested that they are crucial as well [102]. We therefore focused on FliF, FliPQR and FlhBA and tested the effect of the presence or absence of FliG and/or FliO on the secretion efficiency.

Our first approach was to build a single plasmid encoding the three different operons placed under the control of inducible promoters. The advantage of this system resided in the possibility to not only determine the essential components, but also to recreate a minimal T3SS apparatus in any given system supporting this plasmid. The underlying idea would be to create a simplified minimal T3SS for structural and functional analysis. Unfortunately, although expression of the flagellar genes from the plasmid complemented single operons deletions, we failed to restore export of flagellar substrate in strains deleted of all non-essential flagellum related genes. These observations lead us to conclude that some crucial components were lacking in our set-up. However, the results we obtained using a chromosomal-based approach clearly contradicted this conclusion. Instead, it appears more

likely that the plasmid-based T3SS is functional but that the expression of each T3SS component must be precisely regulated. In this work, we did not find the optimal conditions required to assemble a functional export apparatus. Our unsuccessful attempt to reconstitute export based on this minimal T3SS plasmid led us to revise our set up. We deleted every flagellar gene considered as non-essential to only keep the crucial genes at their native position on the chromosome. Under these conditions, we could reconstitute export and show that FliG greatly improves export efficiency while remaining dispensable. Although observations of export in Δ*fliO* in excess of FlhDC suggested that FliO was also dispensable (Erhardt *et al.* unpublished), our experiments demonstrated that it is essential for flagellar substrate secretion under normal conditions and was only dispensable when FliP was present in excess.

Altogether, we concluded that the assembly of a minimal T3SS apparatus requires an accurate expression of each essential operons which, in our case, could only be achieved by retaining the genes coding for the essential T3SS components in their native loci. We also determined that FliG is not crucial for export, while the membrane components FliF, FlhBA and FliPQR are strictly required. The fact that FliG has no structural homolog in the injectisome, and is structurally related to the cytosolic N-terminal domain of the magnesium transporter MgtE [68], could suggest that FliG had been possibly acquired by horizontal gene transfer. Considering this, and that is not essential for export, we can speculate that FliG might have been absent in the archaic flagellum, and that its acquisition sensibly enhanced flagellar export. FliO on the other hand appeared to be essential and was only dispensable upon FliP overexpression. This last observation confirmed the results of an earlier study suggesting that FliO function is linked to FliP expression [81].

Although our attempt to create a plasmid based minimal T3SS did not yield the expected results, we determined a limited subset of proteins required and sufficient for secretion. This new insight contributes to a better understanding most crucial actors involved in type III mediated secretion of flagellar substrates.

3.2. FliO act as a flagellum-specific chaperone facilitating the assembly of the export gate

As mention above, the T3SS is the cornerstone of two complex nanomachine whose role is crucial in the infection process. However, little is known about assembly of the core export apparatus and especially about one of the most notable difference between both systems: the flagellar protein FliO. Beside the functional link with FliP suggested by Barker *et al.* and older studies showing FliO implication in flagellar synthesis [81], nothing was known about its function. In the present work, we demonstrated that FliO affects FliP expression by protecting it from degradation and showed that Lon was the protease primary responsible for this proteolysis. In contraction with previous studies – suggesting that it was part of the export gate – our super-resolution microscopy observations showed that FliO does not co-localize with the basal bodies but is mobile in the cell envelope. In addition to the important information regarding its sub-cellular location, this finding was crucial because it implies that FliO is not directly involved in the export process and does not have a structural role in the completed apparatus. This led us to hypothesize that FliO could rather have a role during flagellar assembly. This hypothesis was confirmed by our analysis of FliP complexes by BN-PAGE. Indeed, not only we could show that completion of the hook basal body complex required FliO, but also that several FliP oligomers, corresponding to different intermediates of the export gate, were formed only in presence of FliO. We also showed that FliO interacted with FliP intermediary oligomers but was not found in the completed basal body. The formation of theses FliP precursor was unaffected by the absence of FliF, indicating that the export gate assembles independently of the MS ring.

In regard to all these observations, we propose that FliO acts as a flagellum-specific chaperone facilitating the oligomerization of FliP. Based on previous stoichiometry predictions and data from the injectisome, this oligomer could be composed of 5 FliP and 1 FliR [78,102,119]. However, Fukumura *et al.* (unpublished) observed the formation of a trimer of dimers of FliP in the fT3SS, which suggests an organization of the export gate on a base-3 symmetry, matching the FlhA nonamer. We therefore propose a model in which the FliP hexamer, forming the protein-conducting export channel, would serve as a starting point for export gate assembly, by subsequent association of FliR, FliQ and probably FlhB (Figure 35). The MS-ring would then assemble around this FliPQR-FlhB complex. Like in the injectisome, the FlhA nonameric ring would form at a later stage around the

channel in the inner side of the MS-ring, completing the assembly of the inner membrane export apparatus. Since we demonstrated that the formation of the export gate precursors does not require the presence of the MS ring, in contradiction with the assembly mechanism previously suggested [47,120], we propose that FliO serves as scaffold or assembly platform for the central channel. This hypothesis is also consistent with Fukumura *et al.*, who observed ring-like structures formed by FliO in association with the FliP ring (unpublished). In the later stage of assembly, FliO would dissociates from the structure after completion of the export gate.

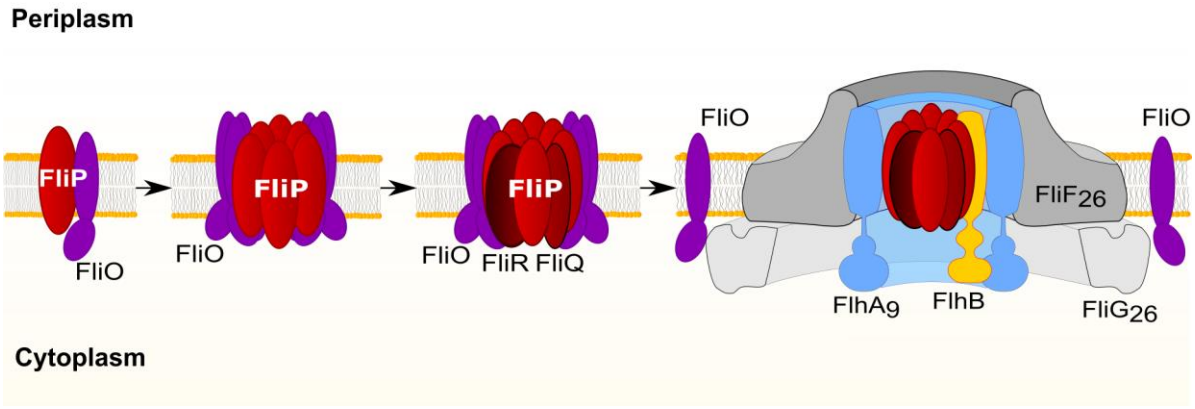

Figure 35: FliO facilitates FliP assembly within the IMEA complex. At the initial step of assembly, FliO protects FliP monomer from proteolysis and enable a FliP to polymerize, possibly as a hexamer, and associate with FliR and most likely FliQ. After dissociation of FliO, we propose that the central channel associates with FlhB at the center of the MS-ring. Finally, FlhA forms a nonameric complex between the central channel and the MS-ring.

Ultimately, this study provided us with crucial information relative to the location and the function of FliO during flagellar assembly. This newly acquired knowledge will participate to unravel the yet poorly understood mechanisms underlying type III secretion.

3.3. Signal peptide enhances FliP membrane insertion and must be cleaved for flagellum assembly

The presence of a cleavable N-terminal signal peptide in FliP, while SpaP and the other injectisome homologs lack such a feature, raise the question of the role of this striking difference between otherwise very conserved proteins. The only other report, which studied FliP cleavage-site mutants concluded that the presence of a signal peptide was important for motility. The same authors also reported that its cleavage was not essential for motility or flagellar synthesis [78].

In the present study, we confirmed that the signal peptide contributes to motility by facilitating membrane insertion. We also showed that the presence of the signal peptide is not essential for flagellar assembly. In particular, our results suggest that cleavage of the signal peptide is crucial for flagellar body assembly and thus for motility. The presence of an additional transmembrane domain at the N-terminal extremity of the mature FliP appears to affect the protein folding dynamics and accordingly, affects formation of a FliP oligomeric complex, which is essential for export gate assembly.

The signal peptide is therefore important during the early stage of flagellar assembly by facilitating FliP membrane integration, but presumably must be removed to ensure a proper association between FliP and the other protein of the export gate.

3.4. FliO and the signal peptide probably got lost during injectisome evolution

In the last two parts (2.2 and 2.3), we took an interest in two of the most striking differences between the flagellar and virulence associated T3SS systems. Interestingly, the signal peptide and FliO play similar role in the T3SS. Indeed, both greatly enhance the efficiency of basal body assembly but are not strictly required. Considering this, why are such beneficial features absent of the injectisome?

At that point, we can only speculate. Regarding the signal peptide, a few species, such as *Bacillus* subspecies, do not possess a signal peptide. A phylogenetic analysis of FliP homologs using the eggNOG database shows that the signal peptide is widespread and is only absent in a few clades suggesting an early appearance. Although FliO is widespread among flagellar systems, some species, such as *Aquifex aeolicus,* have been reported to be lacking any FliO homolog [99]. This hyperthermophilic bacterium belongs to the family of the Aquificaceae which is one of the earliest branching among eubacteria [121,122]. This could advocate for the idea that FliO arose during flagellar evolution after the separation from other bacterial families. Nonetheless, a phylogenic study based on the distribution of flagellar genes proposed that *Aquifex* flagellum diverged from proteobacteria later than *Clostridium* or *Bacillus*, and defined seven clades having a flagellated common ancestor [68]. Furthermore, homologs of FliO are found in multiple phyla remote from proteobacteria, including in the Aquifexales *T. takaii* (Table 2). Finally, Abby and Rocha proposed that the vT3SS derived from the fT3SS of proteobacteria after the divergence of Thermotogae and Spirochetes, where FliO homologs and the FliP signal peptides are present [41]. This suggests that FliO was present in the common ancestor. We can thus assume, that both FliO and the signal peptide were lost in the injectisome.

Phylum		**Species**	**Gene**
Aquifexales		*Thermosulfidibacter takaii*	TST_0643
Firmicutes		*Bacillus subtilis*	BSU16340
		Clostridium botulinum	NPD7_433
Spirochetes		*Borrelia. burgdorferi*	BB_0276
		Treponema socranskii	HMPREF1325_1176
Thermotogales		*Thermotoga maritima*	TM_0699
		Pseudothermotoga thermarum	Theth_0695
Proteobacteria	**α**	*Caulobacter crescentus*	CCNA_01003
		Rhodobacter sp.	D516_1436
	β	*Burkholderia cepacia*	DM41_1317
		Bordetella pertussis	BP1392
	γ	*Salmonella enterica* Typhimurium	STM1978
		Escherichia. coli	b1947
		Yersinia. pseudotuberculosis	ERS008566_00308
		Pseudomonas. aeruginosa	PA1445
		Vibrio. cholerae	VC_2124
	δ	*Geobacter sulfurreducens*	RW64_11365
		Desulfobacterium autotrophicum	HRM2_37170
	ε	*Helicobacter pylori*	HP_0583
		Campylobacter jejuni	Cj0352
Planctomycetales		*Pirellula sp.*	VN12_23805
		Planctomyces sp.	VT03_26965
Actinobacteria		*Leifsonia aquatica*	N136_04749

Table 2: Examples of FliO homologs in multiple phyla of the bacterial domain. Several proteins are annotated as FliZ but are homolog of *S.* Typhimurium FliO. HP0583 and Cj0352 have been previously identified as FliO homologs [99,104]

One hypothesis explaining their absence in the injectisome could be that mutational events lead to a better expression of FliP and made FliO and the signal sequence obsolete. Transcriptomic data from Kröger *et al.* provide interesting information in this regard. Indeed, SpaP expression ranges between 134 to 689 transcripts per million (TPM), but is expressed only under specific conditions, while FliP is expressed under almost every tested conditions but never reaches more than 170 TPM [123]. Synthetizing permanently a large amount of proteins would be energy consuming. The presence of FliO ensures efficient FliP assembly within the core fT3SS and correct flagellar formation with lower amount of FliP and reduces therefore energy consumption. The same conclusions can apply for the signal peptide. In case of the injectisome, SpaP expression is turned off most of the time. Synthetizing a large amount of SpaP when needed is less detrimental because limited to certain conditions. Since the loss of both FliO and the signal peptide can be compensated by FliP overexpression, these features were probably not required for the highly-expressed homolog SpaP and were not conserved during injectisome evolution.

4. Conclusions

In this work, we identified the most crucial components of the T3SS. This could help to create an artificial T3SS export system, composed only of FliF, FlhBA and FliOPQR, used for *in vitro* analysis. More importantly, we revealed the role of FliO in export gate assembly and highlighted its functional relationship with FliP. The existence of a FliP specific partner further supports the idea that FliP plays a major role in secretion. Altogether, these results provide a better understanding of both flagellar and virulence associated T3SS. Such virulence factors play a crucial role in the pathogenesis of most gram-negative bacteria. These pathogens increasingly exhibit resistances to several classical antibiotics. All antibiotics currently available are either bacteriocidal, i.e. killing susceptible bacteria, or bacteriostatic, i.e. preventing bacterial growth. Such antibiotics affect not only equally commensals and pathogens, but they also dramatically increase selective pressure, leading to the selection of the strains carrying resistance genes. A good knowledge of both T3SS and their specificity could pave the way to the development of more specific anti-microbial drugs which would neutralize bacterial pathogenicity without selecting for resistance [124,125].

Finally, our work provides a more detail understanding of a crucial part of the flagellum and the injectisome, the export apparatus. Beyond the putative applications, our findings contribute to advance our general knowledge of the molecular basis of protein secretion and macromolecular structure assembly.

5. Materials and Methods

5.1 Material, buffers and chemicals

Chemicals, enzymes, kits and equipment were purchased from Ambion, Amersham Biosciences, Applichem, BD Biosciences, Beckman Coulter, Bioline, Biometra, Bio-Rad, Biozym, Difco, Edmund Bühler, Fermmentas, Fisher Scientific, Fluka, G. Heinemann, GE healthcare, Gibco, Greiner, Invtirogen, J.T. Baker, Kern & Sohn, Kimtech Science, Life Technologies, Marchery-Nagel, Merck, MP Biomedicals, Milli-Q, New Brunswick Scientific, New England Biolabs Inc. (NEB), PerkinElmer, Pierce, Promega, QIAGEN, Roche, ROTH, SARSTEDT, Sartorius, Scientific industries, Serva, Sigma-Aldrich, Starlab, Stratagene, TECAN, Thermo Scientific. Special chemicals or equipment are stated in the text. Culture additives and other media are listed in Table 3 and Table 3 respectively.

Table 3: list of antibiotics and other additives

ADDITIVES	STOCK CONCENTRATION	FINAL CONCENTRATION
Ampicillin (Amp)	20 $\mu g \cdot ml^{-1}$ in H_2O	0.1 $\mu g \cdot ml^{-1}$
Chloramphenicol (Cm)	2.5 $\mu g \cdot ml^{-1}$ in ethanol	12.5 $\mu g \cdot ml^{-1}$
Tetracycline (Tc)	3 $\mu g \cdot ml^{-1}$ in H_2O	15 $\mu g \cdot ml^{-1}$
Kanamycin (Km)	10 $\mu g \cdot ml^{-1}$ in H_2O	50 $\mu g \cdot ml^{-1}$
Anhydrotetracycline (AnTc)	0.2 $\mu g \cdot ml^{-1}$ in H_2O	1 $\mu g \cdot ml^{-1}$
Spectinomycin (Spc)	50 $\mu g \cdot ml^{-1}$ in H_2O	0.5 $\mu g \cdot ml^{-1}$
Arabinose (Ara)	20 % in H_2O	0.1 %
IPTG	100 mM	250 µM
Sodium Salicylate (NaSal)	1 mM	2.5 µM

Table 4: List of media and buffers

SOLUTION	COMPOSITION	
LB medium	- Bacto Tryptone	10 $mg \cdot ml^{-1}$
	- NaCl	5 $mg \cdot ml^{-1}$
	- Yeast Extract	5 $mg \cdot ml^{-1}$
		In H_2O
LB agar plates	- Bacto Agar	18 $mg \cdot ml^{-1}$
		In LB medium
Green plates	- Bacto Tryptone	7.9 $mg \cdot ml^{-1}$
	- NaCl	4.9 $mg \cdot ml^{-1}$
	- Yeast Extract	1 $mg \cdot ml^{-1}$
	- D-Glucose	7.4 $mg \cdot ml^{-1}$
	- Bacto Agar	12 $mg \cdot ml^{-1}$
	- Methyl blue	65 $\mu g \cdot ml^{-1}$
	- Alizarin Yellow G	0.6 $mg \cdot ml^{-1}$
		In H_2O
Fusaric acid plates	- Bacto tryptone	5 $mg \cdot ml^{-1}$
	- Yeast Extract	5 $mg \cdot ml^{-1}$
	- NaCl	10 $mg \cdot ml^{-1}$
	- NaH_2PO_4 x H_2O	10 $mg \cdot ml^{-1}$
	- Bacto Agar	12 $mg \cdot ml^{-1}$
	- Fusaric Acid	2.4 $mg \cdot ml^{-1}$
	- AnTc	0.1 $\mu g \cdot ml^{-1}$
		In H_2O
Motility agar plates	- Bacto Tryptone	10 $mg \cdot ml^{-1}$
	- NaCl	5 $mg \cdot ml^{-1}$
	- Bacto Agar	3 $mg \cdot ml^{-1}$
		In H_2O
PBS (1 x)	- NaCl	115 mM
	- Na_2HPO_4 _ $2H_2O$	16 mM
	- KH_2PO_4	4 mM
		In H_2O
TBS	- Trizma HCl	2.423 $g \cdot ml^{-1}$
	- NaCl	8.006 $g \cdot ml^{-1}$
		pH 7.6
		In H_2O
TBST	- Tween 20	0.1% (v/v)
		In TBS
P22 broth	- E-salts (50 x)	1 x
	- D-Glucose	0.2 % (v/v)
	- P22 HT int φTH3708	10^8 $pfu.ml^{-1}$
		In LB medium
H5 phage broth		
TAE buffer (50 x)	- Tris Base	242 $mg \cdot ml^{-1}$

	- 0.5 M EDTA (pH 8)		10 % (v/v)
	- Glacial Acetic Acid		5.71 % (v/v)
		In H_2O	
DNA loading dye (6 x)	- Glycerol		30 % (v/v)
	- Bromophenol Blue		2.5 mg·ml^{-1}
		In H_2O	
Ethidium bromide	- Ethidium bromide		0.1 % (v/v)
		In H_2O	
TFB1 buffer	- KAc		30 mM
	- $CaCl_2$		10 mM
	- $MnCl_2$		100 mM
	- RbCl		15 % (v/v)
	- glycerol		pH 5.8
		In H_2O	
TFB2 buffer	- PIPES		10 mM
	- $CaCl_2$		75 mM
	- RbCl		10mM
	- Glycerol		15 % (v/v)
			pH 6.5
		In H_2O	
Buffer K	- Triethanolamine (TEA)		50 mM
	- Sucrose		250 mM
	- EDTA		2 mM
	- Lysozyme		10 µg·ml^{-1}
	- DNase		10 µg·ml^{-1}
	- $MgCl_2$		1 mM
	- cOmplete™ Protease Inhibitor Cocktail		
		In H_2O	
Buffer L	- TEA		50 mM
	- Sucrose		250 mM
	- pH 7.5	In H_2O	
Buffer M	- TEA		50 mM
	- EDTA		1 mM
	- pH 7.5	In H_2O	
Urea solution	- Urea		8 M
	- TAE		50 mM
	- EDTA		1 mM
	- pH 7.5	In H_2O	
Spheroplast buffer	- Sucrose		20 %
	- EDTA		5 mM
	- Lysozyme		0.6 mg·ml^{-1}
		In H_2O	
Native loading dye (10 x)	- Glycerol		50 % (v/v)

	- Aminocaproic acid		250mM
	- Coomassie Blue G		5 % (v/v)
		In H_2O	
SDS sample buffer (2 x)	- Tris HCl pH 6.8		200mM
	- SDS		4 % (v/v)
	- Glycerol		20 % (v/v)
	- EDTA		25mM
	- Bromophenol Blue		0.04 % (v/v)
	- β-Mercaptoethanol		2 % (v/v)
		In H_2O	
SDS running buffer	- Tris-HCl		25 mM
	- Glycine		192 mM
	- SDS		0.1 % (v/v)
	- pH 8.3	In H_2O	
Anode buffer (10 x)	- Bis-Tris		500 mM
		In H_2O	
Cathode buffer I (10 x)	- Tricin		500 mM
	- Bis-Tris		150 mM
	- Coomassie Blue G		2 $mg \cdot ml^{-1}$
		In H_2O	
Cathode buffer II (10 x)	- Tricin		500 mM
	- Bis-Tris		150 mM
		In H_2O	
Transfer buffer	- Tris-HCl		25 mM
	- Glycine		192 mM
	- Methanol		20 % (v/v)
	- pH 8.3	In H_2O	
Stripping buffer	- Tris-HCl		62.5 mM
	- β-Mercaptoethanol		100 mM
	- SDS		2 %
	- pH 6.7	In H_2O	

5.2 Antibodies

Antibodies used in this study are listed in Table 5. They were diluted in 5 % milk in TBS-T and stored at – 20 °C except α-FLAG® M2 which was stored at 4 °C after dilution

Table 5: List of antibodies used in this study

ANTIBODY	HOST	CONCENTRATION	COMPANY
Primary antibodies			
α-DnaK	Mouse	1: 10,000	abcam
α-FlhAc	Rabbit	1: 10,000	T. Minamino [73]
α-FliG	Rabbit	1: 5000	T. Minamino [73]
α-HA	Mouse	1: 2000	Enogen
α-FLAG® M2	Mouse	1: 5000	Sigma Aldrich
α-FliC	Rabbit	1: 5000 (WB)	Becton Dickinson
		1: 1000 (IF microscopy)	& Company
α-β-Lactamase	Mouse		
Secondary antibodies			
α-mouse-HRP (goat)	Goat	1: 20,000	Bio-Rad
α-rabbit-HRP (goat)	Goat	1: 20,000	Bio-Rad

5.3 Bacterial strains, plasmids and media

Bacterial strains used in this study are listed in Table 4. Cells were grown in LB medium at 37 °C with appropriate additives if needed.

5.4 Strain constructions

Chromosomal fusions or clean deletions of genes were created using λ-red recombination either by *tetRA* cassette replacement using pKD46 plasmid [126] or by *aph-I-sceI* cassette replacement using pWRG730 [127]. One step gene inactivation was performed as described by Datsenko and Wanner [128] Mutations, fusions and deletions were transferred between strains using P22 phage transduction. Plasmids were constructed by restriction/ligation cloning or Gibson assembly. Inserts were generated by proof reading PCR except when stated otherwise.

Table 6: List of strains used for this study

NAME	GENOTYPE	SOURCE
TH437	WT LT2	Hughes KT
TH3708	DEL1103(*tct-zfg*-3516::*Tn10dTc-fljB*5001::*mudJ*) DEL1131(*fliA*5059::*Tn10dTc-fliO*5097:: *mudJ*) DEL1133(*flhAB*5056::*Tn10dTc-flhC*5213:: *mudJ*)(Δ*flhD*) DEL1137(*flgN*5220:: *mudJ -flgL*566::*Tn10*)-No flagellar genes	Hughes KT
TH10605	*fliO*1087$_{L91R}$ *fljB*enx vh2	
TH10607	*fliO*1089$_{V72G}$ *fljB*enx vh2	
TH10608	*fliO*1432 *fljB*enx vh2	
TH12219	CC118 *pir*+	
TH16484	Δ*araBAD*1077::*flgD-flgE-bla* Δ*flgBC*6557	Hughes KT
TH16988	Δ*araBAD*1077::*flgD-flgE-bla* DEL1103[*tct-fljB*] DEL1131[*fliA-fliR*] DEL1133[*flhB-flhD*] DEL1137[*flgN-flgL*]	Hughes KT
TH17121	Δ*sseA-ssaV*::FRT Δ*invH-sprB*::FRT Δ*araBAD*1014::*flgE-bla* DEL1103[*tct-fljB*] DEL1131[*fliA-fliR*] DEL1133[*flhB-flhD*] DEL1137[*flgN-flgL*]	Hughes KT
TH17448	pKG116- *fliP*::Q_{22}-3xHA /Δ*fliP6709*	Hughes KT
EM897	CC118 *pir*+/ pTB23-*att*λ-P*nahG-flhBA* (CmR)	Hughes KT
EM902	DH10beta	Dersch P
EM919	MST4718=LT2 pir+ (link to purA) Δ*fliF*7339::tetRA	this study
EM1077	*fliO*22315::HaloTag	this study
EM1081	*fliN*22319::HaloTag	[57]
EM1084	CC118 *pir*+/ pTB23-*att*λ-*fliF* (CmR)	this study
EM1139	MST4718=LT2 *pir*+ / pEM726	this study
EM1214	*fliO*22315::HaloTag *flgE*7742::3xHA	this study
EM1269	cc18 *pir*+/pBR322-*fliOPQR*-terminators (from pEM726) (AmpR)	this study
EM1270	cc18 *pir*+/pTB23-*att*λ- P*nahG-flhBA-fliF* (CmR)	this study
EM1271	cc18 *pir*+/pTB23-*att*λ- P*nahG-flhBA-fliF-fliOPQR* (CmR)	this study
EM1274	Δ*fliO*22334 *fliP*8004::Q_{22}-3xHA	this study
EM1326	*fliO*22315::HaloTag Δ*hin*-5717::FCF	this study
EM1330	*fliN*22319::HaloTag Δ*hin*-5717::FCF	[57]
EM1609	Δ*fliOP*6856 / pKG116	this study
EM1610	Δ*fliOP*6856 / pKG116- *fliP*::Q_{22}-3xHA	this study
EM2072	CC118 *pir*+/pKG137-*lacIq-nahR-tetR* (pEM2072)	this study
EM2073	LT2 - *att*λ::pEM1271 (integrated)	this study
EM2225	*fliP*22354::G157-3xFLAG	Lab stock

EM2269	*fliO*22348::3xFLAG *fliP*8004::Q_{22}-3xHA	this study
EM2270	MST4718=LT2 *pir*+ Δ*fliOPQR*7499::FRT	this study
EM2271	MST4718=LT2 *pir*+ Δ*flhBAE*7669::FRT	this study
EM2273	CC118 pir+/pTB23-*attλ*- P*nahG-flhBA-fliFG-fliOPQR* (CmR)	this study
EM2320	Δ*hin*-5717::FRT/pKG116	this study
EM2321	Δ*hin*-5717::FRT /pKG116-*fliP*	this study
EM2322	Δ*hin*-5717::FRT /pKG116-*fliO*	this study
EM2323	Δ*fliO*6708 Δ*hin*-5717::FRT /pKG116	this study
EM2324	Δ*fliO*6708 Δ*hin*-5717::FRT /pKG116-*fliP*	this study
EM2325	Δ*fliO*6708 Δ*hin*-5717::FRT /pKG116-*fliO*	this study
EM2496	*att*P22::pEM2072 (pKG137-*lacIq-nahR-tetR*)	this study
EM2687	*attλ*::pEM2273	this study
EM2716	*fliP*22354::G_{157}-3xFLAG *flgE*6569::bla Δ*flgBC*6557 Δ*ydiV*	this study
EM2742	*fliO*1087 *fljB*enx vh2 *fliP*8004::Q_{22}-3xHA	this study
EM2743	*fliO*1089 *fljB*enx vh2 *fliP*8004::Q_{22}-3xHA	this study
EM2744	*fliO*1431 *fljB*enx vh2 *fliP*8004::Q_{22}-3xHA	this study
EM2869	Δ*flhBAE*7669::FKF *att*P22::*tetRA nahR lacI*	this study
EM2870	Δ*fliOPQR*7499::FKF *att*P22::*tetRA nahR lacI*	this study
EM2871	Δ*fliF*7355 *att*P22::*tetRA nahR lacI attλ*::pEM726	this study
EM2872	Δ*fliF*7355 *att*P22::*tetRA nahR lacI attλ*::pEM2273	this study
EM2873	Δ*fliG*7356 *att*P22::*tetRA nahR lacI attλ*::pEM726	this study
EM2874	Δ*fliG*7356 *att*P22::*tetRA nahR lacI attλ*::pEM2273	this study
EM2875	Δ*flhBAE*7669::FKF *att*P22::*tetRA nahR lacI attλ*::pEM2273	this study
EM2876	Δ*fliOPQR*7499::FKF *att*P22::*tetRA nahR lacI attλ*::pEM726	this study
EM2877	Δ*fliOPQR*7499::FKF *att*P22::*tetRA nahR lacI attλ*::pEM2273	this study
EM2885	*fliP*22749::$\Delta_{2\text{-}22}$ G_{157}-3xFLAG	this study
EM2886	*fliP*22750::A_{21}D Q_{22}P G_{157}-3xFLAG	this study
EM2887	*fliP*22751::PADADQ$_{17\text{-}22}$ G_{157}-3xFLAG	this study
EM2888	*fliP*22752::GSGSGP$_{17\text{-}22}$ G_{157}-3xFLAG	this study
EM3188	Δ*sseA-ssaV*::FRT Δ*invH-sprB*::FRT Δ*araBAD*1014::*flgE-bla* DEL1103[*tct-fljB*] DEL1131[*fliA-fliR*] DEL1133[*flhB-flhD*] DEL1137[*flgN-flgL*]*att*P22::tetRA nahR lacI pir+/pEM726	this study
EM3189	Δ*sseA-ssaV*::FRT Δ*invH-sprB*::FRT Δ*araBAD*1014::*flgE-bla* DEL1103[*tct-fljB*] DEL1131[*fliA-fliR*] DEL1133[*flhB-flhD*] DEL1137[*flgN-flgL*]*att*P22::tetRA nahR lacI pir+ / pEM2273	this study
EM3192	Δ*fliO*22334 *fliP*8004::Q_{22}-3xHA / pTrc99a	this study
EM3193	Δ*fliO*22334 *fliP*8004::Q_{22}-3xHA / pTrc99ffa-STM1085	this study

EM3201	Δ*fliO*22770 *fliP*22354::G_{157}-3xFLAG	this study
EM3910	Δ*fliF*7355 *fliO*22348::3xFLAG *fliP*8004::Q_{22}-3xHA	this study
EM4009	Δ*fliO*22770 *fliP*22806::A_{21}D Q_{22}P G_{157}-3xFLAG	this study
EM4010	Δ*fliO*22770 *fliP*22807::PADADQ$_{17\text{-}22}$ G_{157}-3xFLAG	this study
EM4011	Δ*fliO*22770 *fliP*22808::GSGSGP$_{17\text{-}22}$ G_{157}-3xFLAG	this study
EM4018	*fliP*8004::Q_{22}-3xHA Δ*clpXP*::FRT	this study
EM4019	Δ*fliO*22334 *fliP*8004::Q_{22}-3xHA Δ*clpXP*::FRT	this study
EM4437	*fliP*22806::A_{21}D Q_{22}P S_{117}C G_{157}-3xFLAG	this study
EM4438	Δ*fliO*22894 *fliP*22806::A_{21}D Q_{22}P S_{117}C G_{157}-3xFLAG	this study
EM4439	*fliP*22806::A_{21}D Q_{22}P A_{32}C G_{157}-3xFLAG	this study
EM4440	Δ*fliO*22895 *fliP*22806::A_{21}D Q_{22}P A_{32}C G_{157}-3xFLAG	this study
EM4441	*fliP*22808::GSGSGP$_{17\text{-}22}$ S_{117}C G_{157}-3xFLAG	this study
EM4442	*fliP*22808::GSGSGP$_{17\text{-}22}$ A_{32}C G_{157}-3xFLAG	this study
EM4443	Δ*fliO*22896 *fliP*22402:: S_{117}C G_{157}-3xFLAG	this study
EM4444	Δ*fliO*22897 *fliP*22409:: A_{32}C G_{157}-3xFLAG	this study
EM4445	Δ*fliO*22898 *fliP*22749::$\Delta_{2\text{-}22}$ G157::3xFLAG	this study
EM4446	Δ*flgN-L*7840 Δ*flhE*7404 Δ*fliY-T*7843 Δ*fliH-N*22818 (Δ*fliH-K* Δ*fliL-N*) Δ*araBAD*1077::*flgD-flgE-bla*	this study
EM4447	Δ*flgN-L*7840 Δ*flhE*7404 Δ*fliY-T*7843 Δ*fliG-N*22819 (Δ*fliG-K* Δ*fliL-N*) Δ*araBAD*1077::*flgD-flgE-bla*	this study
EM4448	Δ*flgN-L*7840 Δ*flhE*7404 Δ*fliY-T*7843 Δ*fliH-O*22820 (Δ*fliH-K* Δ*fliL-O*) Δ*araBAD*1077::*flgD-flgE-bla*	this study
EM4449	Δ*flgN-L*7840 Δ*flhE*7404 Δ*fliY-T*7843 Δ*fliG-O*22821 (Δ*fliG-K* Δ*fliL-O*) Δ*araBAD*1077::*flgD-flgE-bla*	this study
EM4478	*fliO*22348::3xFLAG *fliP*8004::Q_{22}-3xHA Δ*lon*	this study
EM4479	Δ*fliO*22334 *fliP*8004::Q_{22}-3xHA Δ*lon*	this study
EM4480	Δ*fliO*22899 *fliP*22808::GSGSGP$_{17\text{-}22}$ S_{117}C G_{157}-3xFLAG	this study
EM4481	Δ*fliO*22900 *fliP*22808::GSGSGP$_{17\text{-}22}$ A_{32}C G_{157}-3xFLAG	this study
EM4482	*fliP*22749::$\Delta_{2\text{-}22}$ S_{117}C G_{157}-3xFLAG	this study
EM4483	Δ*fliO*22901 *FliP*22749::$\Delta_{2\text{-}22}$ S_{117}C G_{157}-3xFLAG	this study
EM4484	*fliP*22749::$\Delta_{2\text{-}22}$ A_{32}C G_{157}-3xFLAG	this study
EM4485	Δ*fliO*22902 *FliP*22749::$\Delta_{2\text{-}22}$ A_{32}C G_{157}-3xFLAG	this study
EM4486	*fliP*22354::G_{157}-3xFLAG / pKG116-*fliO*	this study
EM4487	Δ*fliO*22770 *fliP*22354:: G_{157}-3xFLAG / pKG116-*fliO*	this study
EM4488	*fliP*22749::$\Delta_{2\text{-}22}$ G_{157}-3xFLAG / pKG116-*fliO*	this study
EM4489	*fliP*22750::A_{21}D Q_{22}P G_{157}-3xFLAG / pKG116-*fliO*	this study
EM4490	*fliP*22751::PADADQ$_{17\text{-}22}$ G_{157}-3xFLAG / pKG116-*fliO*	this study

EM4491	*fliP*22752::GSGSGP$_{17\text{-}22}$ G$_{157}$-3xFLAG / pKG116-*fliO*	this study
EM4492	Δ*fliO*22898 *fliP*22749::Δ$_{2\text{-}22}$ G$_{157}$-3xFLAG / pKG116-*fliO*	this study
EM4493	Δ*fliO*22770 *fliP*22806::A$_{21}$D Q$_{22}$P G$_{157}$-3xFLAG / pKG116-*fliO*	this study
EM4494	Δ*fliO*22770 *fliP*22807::PADADQ$_{17\text{-}22}$ G$_{157}$-3xFLAG / pKG116-*fliO*	this study
EM4495	Δ*fliO*22770 *fliP*22808::GSGSGP$_{17\text{-}22}$ G$_{157}$-3xFLAG / pKG116-*fliO*	this study
EM4774	*fliP*22402:: S$_{117}$C G$_{157}$-3xFLAG Δ*flgBC*6143::t*etRA flgM*6427::*bla*	this study
EM4775	Δ*fliO*22896 *fliP*22402:: S$_{117}$C G$_{157}$-3xFLAG S117C Δ*flgBC*6143::t*etRA*	this study
EM4776	*fliP*22409:: A$_{32}$C G$_{157}$-3xFLAG Δ*flgBC*6143::t*etRA*	this study
EM4777	Δ*fliO*22897 *fliP*22409:: A$_{32}$C G$_{157}$-3xFLAG Δ*flgBC*6143::t*etRA*	this study
EM4778	*fliP*22806::A$_{21}$D Q$_{22}$P S$_{117}$C G$_{157}$-3xFLAG Δ*flgBC*6143::t*etRA*	this study
EM4779	Δ*fliO*22895 *fliP*22806::A$_{21}$D Q$_{22}$P S$_{117}$C G$_{157}$-3xFLAG Δ*flgBC*6143::t*etRA*	this study
EM4780	*fliP*22806::A$_{21}$D Q$_{22}$P A$_{32}$C G$_{157}$-3xFLAG Δ*flgBC*6143::t*etRA*	this study
EM4781	ΔfliO22894 fliP22806::A$_{21}$D Q$_{22}$P A$_{32}$C G$_{157}$-3xFLAG Δ*flgBC*6143::*tetRA*	this study
EM4782	*fliP*22808::GSGSGP$_{17\text{-}22}$ S$_{117}$C G$_{157}$-3xFLAG Δ*flgBC*6143::t*etRA flgM*6427::*bla*	this study
EM4783	Δ*fliO*22899 *fliP*22808::GSGSGP$_{17\text{-}22}$ S$_{117}$C G$_{157}$-3xFLAG Δ*flgBC*6143::t*etRA flgM*6427::*bla*	this study
EM4784	*fliP*22808::GSGSGP$_{17\text{-}22}$ A$_{32}$C G$_{157}$-3xFLAG Δ*flgBC*6143::t*etRA flgM*6427::*bla*	this study
EM4785	Δ*fliO*22900 *fliP*22808::GSGSGP$_{17\text{-}22}$ A$_{32}$C G$_{157}$-3xFLAG Δ*flgBC*6143::t*etRA flgM*6427::*bla*	this study
EM4786	*fliP*22749::Δ$_{2\text{-}22}$ S$_{117}$C G$_{157}$-3xFLAG Δ*flgBC*6143::t*etRA flgM*6427::*bla*	this study
EM4787	Δ*fliO*22901 *fliP*22749::Δ$_{2\text{-}22}$ S$_{117}$C G$_{157}$-3xFLAG Δ*flgBC*6143::t*etRA flgM*6427::*bla*	this study
EM4788	*fliP* 22749::Δ$_{2\text{-}22}$ A$_{32}$C G$_{157}$-3xFLAG Δ*flgBC*6143::t*etRA flgM*6427::*bla*	this study
EM4789	Δ*fliO*22902 *fliP* 22749::Δ$_{2\text{-}22}$ A$_{32}$C G$_{157}$-3xFLAG Δ*flgBC*6143::t*etRA flgM*6427::*bla*	this study
EM4909	Δ*fliF*5629::FKF *fliP*22354::G$_{157}$-3x FLAG	this study
EM4910	Δ*fliF*5629::FKF Δ*fliO*22770 *fliP*22354:: G$_{157}$-3x FLAG	this study
EM4915	*fliO*22348::3xFLAG *fliP*8004:: Q$_{22}$-3xHA Δ*hflK*	this study
EM4916	Δ*fliO*22334 *fliP*8004:: Q$_{22}$-3xHA Δ*hflK*	this study
EM5223	Δ*araBAD*1077::*flgD-flgE-bla* Δ*flgBC*6557 / pKG116	this study

EM5224	Δ*araBAD*1077::*flgD-flgE-bla* Δ*flgBC*6557 / pKG116-*fliP*::Q_{22}-3xHA	this study
EM5225	Δ*araBAD*1077::*flgD-flgE-bla* DEL1103[*tct-fljB*] DEL1131[*fliA-fliR*] DEL1133[*flhB-flhD*] DEL1137[*flgN-flgL*] / pKG116	this study
EM5226	Δ*araBAD*1077::*flgD-flgE-bla* DEL1103[*tct-fljB*] DEL1131[*fliA-fliR*] DEL1133[*flhB-flhD*] DEL1137[*flgN-flgL*] / pKG116-*fliP*::Q_{22}-3xHA	this study
EM5227	Δ*flgN-L*7840 Δ*flhE*7404 Δ*fliY-T*7843 Δ*fliG-N*22819 (Δ*fliG-K* Δ*fliL-N*) Δ*araBAD*1077::*flgD-flgE-bla* / pKG116	this study
EM5228	Δ*flgN-L*7840 Δ*flhE*7404 Δ*fliY-T*7843 Δ*fliG-N*22819 (Δ*fliG-K* Δ*fliL-N*) Δ*araBAD*1077::*flgD-flgE-bla* / pKG116-*fliP*::Q_{22}-3xHA	this study
EM5229	Δ*flgN-L*7840 Δ*flhE*7404 Δ*fliY-T*7843 Δ*fliH-O*22820 (Δ*fliH-K* Δ*fliL-O*) Δ*araBAD*1077::*flgD-flgE-bla* / pKG116	this study
EM5230	Δ*flgN-L*7840 Δ*flhE*7404 Δ*fliY-T*7843 Δ*fliH-O*22820 (Δ*fliH-K* Δ*fliL-O*) Δ*araBAD*1077::*flgD-flgE-bla* / pKG116-*fliP*::Q_{22}-3xHA	this study
EM5231	Δ*flgN-L*7840 Δ*flhE*7404 Δ*fliY-T*7843 Δ*fliG-O*22821 (Δ*fliG-K* Δ*fliL-O*) Δ*araBAD*1077::*flgD-flgE-bla* / pKG116	this study
EM5232	Δ*flgN-L*7840 Δ*flhE*7404 Δ*fliY-T*7843 Δ*fliG-O*22821 (Δ*fliG-K* Δ*fliL-O*) Δ*araBAD*1077::*flgD-flgE-bla* / pKG116-*fliP*::Q_{22}-3xHA	this study

Table 7: List of plasmids used in this study

NAME	DESCRIPTION	RESISTANCE
pBR322	Cloning vector	Tet/Amp
pCP20	Flp recombinase encoding plasmid	Cm/Amp (Ts)
pEM726	pTB23- attλ CRIM plasmid	Cm
pEM897	pTB23- attλ-P*nahG*::*flhBA*	Cm
pEM1084	pTB23- attλ-*fliF*	Cm
pEM1269	pTB23- attλ-*fliOPQR*	Cm
pEM1270	pTB23- attλ-P*nahG*::*flhBA-fliF*	Cm
pEM1271	pTB23- attλ-P*nahG*::*flhBA-fliF-fliOPQR*	Cm
pEM2273	pTB23- attλ-P*nahG*::*flhBA-fliFG-fliOPQR*	Cm
pINT-ts	λ-integrase CRIM helper plasmid	Amp (Ts)
pKD46	λ-red recombinase encoding plasmid	Amp (Ts)
pKG116	NaSal-inducible expression vector	Cm
pKG116-*fliO*	*fliO* expression vector	Cm
pKG116-*fliP*	*fliP* expression vector	Cm
pKG116-*fliQ*	*fliQ* expression vector	Cm
pKG116-*fliR*	*fliR* expression vector	Cm
pKG116-*flhA*	*flhA* expression vector	Cm
pKG116-*flhB*	*flhB* expression vector	Cm
pKG116-*fliP*-HA	$fliP_{Q22}$::3xHA expression vector	Cm
pTrc99ffa	*IPTG inducible expression vector*	Amp
pTrc99ffa-*stm1085*	*stm1085 expression vector*	Amp

Table 8: List of primers used for plasmids and strains construction in this study

PRIMER NUMBER	NAME	SEQUENCE
482	5'-EcoRI-PNahG-flhBA_fw	GATCGAATTCTGGGTTATTGCTGGTGCCCG
483	3'-BsrGI-flhA_rv	GATCTGTACATTATTATTATTTTCCTCCAATGGTCGCCG
484	5'-BamHI-fliO_fw	cgcgggatcccggtgcagaaaataaggaggaaaaaaaaATGAAGACAGAAGCCACGG
525	5'-BglII-fliF1_fw	tgagcacatcagcaggacgcactgaccgaaGATCTTCCTGGAGAAAATAAGGAGGAAAAAAAAATGAGTGCGACTGCATCG
530	3'-DraIII-fliF3_rv	gccagcagccgttacaaattccagcagcaccatttaTTATTACTCATGATCGTTACTCATCCACTG
664	HALO/SNAP-fliO-Cter_fw	ggcggatttccagaacatgatgaagagcttactcaagcgttccgggagatccATCGGCTCTGCGGCGTCTGC
665	HALO-fliO-Cter_rv	agagaaaggaataacaaacggcgcatcaggatctcccggaCTAACCGGAAATCTCCAGAG
666	SNAP-fliO-Cter_rv	agagaaaggaataacaaacggcgcatcaggatctcccggaCTAACCCAGCCCAGGCTTGC
667	HALO/Snap-fliM-Cter_fw	agaacatttgatcaacccaattttgaattcgctgaatgaggaacagcccaaaATCGGCTCTGCGGCGTCTGC
668	HALO-fliM-Cter-rv	tcatcggacggattattcatgtcactcatttgggctgttcCTAACCGGAAATCTCCAGAG
669	SNAP-fliM-Cter-rv	tcatcggacggattattcatgtcactcatttgggctgttcCTAACCCAGCCCAGGCTTGC
670	HALO/Snap-fliN-Cter_fw	tattattacgccatccgagcgtatgcgtcgtttgagtcgtATCGGCTCTGCGGCGTCTGC

671	*HALO-fliN-Cter-rv*	*gcggtgggctgagaaaccgtggcttctgtcttcatcattaC TAACCGGAAATCTCCAGAG*
672	SNAP-fliN-Cter-rv	gcggtgggctgagaaaccgtggcttctgtcttcatcattaCT AACCCAGCCCAGGCTTGC
673	tetRA-FliN-Cter_fw	tattattacgccatccgagcgtatgcgtcgtttgagtcgtTT AAGACCCACTTTCACATT
674	tetRA-FliN-Cter_rv	gcggtgggctgagaaaccgtggcttctgtcttcatcattaCT AAGCACTTGTCTCCTG
905	pTB-OPQR - fw	ggccattatgacgctgaagt
932	FliR-KpnI-TR-17-fw	AGCGAGATGCCGATAAATAATAACC CATAAggtacctgcaggtcgtctcggatcga
933	FliR-KpnI-TR-17-rv	tcgatccgagacgacctgcaggtaccTTATGGGTT ATTATTTATCGGCATCTCGCT
936	ΔFliO/OP::tetRA-fw	gtatgcgtcgtttgagtcgttaatgatgaagacagaagccT TAAGACCCACTTTCACATT
937	ΔFliO::tetRA-rv	agagaaaggaataacaaacggcgcatcaggatctcccgga CTAAGCACTTGTCTCCTG
938	ΔFliOP::tetRA-rv	cggattcaggagtcattttgcgcctctaactgtaaaagctCT AAGCACTTGTCTCCTG
939	ΔFliO clean-rv	agagaaaggaataacaaacggcgcatcaggatctcccgga ggcttctgtcttcatcatta
940	ΔFliOP clean-rv	cggattcaggagtcattttgcgcctctaactgtaaaagcttaat gatgaagacagaagcc
1232	3´-lacIq-gibson-rv	GTCACGCAGTTCCATattcaccaccctgaaTC ACTGCCCGCTTTCCAGTC
1233	5´-nahR-gibson-fw	GAAAGCGGGCAGTGAttcagggtggtgaatA TGGAACTGCGTGACCTGGA
1234	3´-nahR-gibson-rv	GAAAGTGGGTCTTAAattcaccaccctgaaT CAATTCTCTCTATCCTGCG
1235	5´-tetR-gibson-fw	GATAGAGAGAATTGAttcagggtggtgaatT TAAGACCCACTTTCACATT

1243	*5´pKG137-gibson-fw*	*taatctagacatcattaattcctaattttGAAGTCGCTTAAGCAATCAA*
1244	3´pKG137-gibson-rv	ccgtcagggcgcgtcagcgggtgttggcggGGTCATAGCTGTTTCCTGTG
1245	5´lacIq-gibson-pKG137-fw	aacaatttcacacaggaaacagctatgaccCCGCCAACACCCGCTGACGC
1246	3´tetR-gibson-pKG137-rv	gcatccgacattgattgcttaagcgacttcAAAAATTAGGAATTAATGAT
1292	FliP_G157-3xFLAG_rv	cgtaaaaccgatctgaaacgcc
1712	5´-DN22-FliP_fw	tgatgaagagcttactcaagcgttccgggagatcctgatgCTGCCGGGGCTTATCAGCCA
1713	5´-A21D Q22P-FliP_fw	tctctggcgggtctgtggctttttagtcccgccgccgctgaccaCTGCCGGGGCTTATCAGCCA
1714	5´-PADADQ-FliP_fw	ttcctttctctggcgggtctgtggctttttagtcccgccgacgctgaccaaCTGCCGGGGCTTATCAGCCA
1715	5´-GSGSGP-FliP_fw	tttgttattcctttctctggcgggtctgtggctttttagtggtagcggtagtggcccaCTGCCGGGGCTTATCAGCCA
1918	5'-ndeI-STM1085(Δ5-12)-fw	acgtcatatggatcgtatcTCGCTACTGAGTACGCACAA
1919	3'-BamHI-STM1085-rv	acgtggatccTTAGTCGCGGCTGGCGAAGC
2194	5'_fliG-Cter-fw	TTACGCGAGAAGTTCCTGCG
2195	3'_fliO-Nter-rv	GGCCAAGCGAGGCGCTGGCT
2196	5'_DfliG-L-fw	gctggtcattcgccagtggatgagtaacgatcatgagtaaTACCTATGTCTAACGCCAGA
2212	5'_Dlon::tetRA_fw	ggacactaaactaagagagagctctatgaatcctgagcgtTTAAGACCCACTTTCACATT
2213	3'_Dlon::tetRA_rv	tattagcgctatttgcgcgaggtcactattttgcggttacCTAAGCACTTGTCTCCTG
2214	5'_Dlon_fw	ggacactaaactaagagagagctctatgaatcctgagcgtGTAACCGCAAAATAGTGACC

2215	*3'_Dlon_rv*	*TATCGCACCTGAATCCTTC*
2216	3'_DfllPq22::tetRA	cagctttggcctccgccgcataatggttggctgataagCT
	A32C_rv	AAGCACTTGTCTCCTG
2217	3'_DfliO FliP(Dn1-22)_rv	ggcctccgcccgctaatggttggctgataagccccggcag
		CATCAGGATCTCCCGGAGGC
2551	gBlock DfliH-K DfliL-N	TTACGCGAGAAGTTCCTGCGCAATAT
		GTCCCAGCGCGCCGCCGATATCCTGC
		GCGACGACCTTGCCAACCGTGGCCC
		GGTTCGTCTGTCTCAGGTGGAAAACG
		AGCAGAAAGCGATTCTGCTTATTGTG
		CGTCGTCTGGCGGAAACCGGCGAAA
		TGGTGATTGGCAGCGGCGAGGATAC
		CTATGTCTAAcgccagaggtagcatgattatccgc
		gtcttttccacgctttgtcgtggacaggacacgggataatcag
		ccaataagcagtaccgaaacaggaagcccgtatcagCGT
		TTGAGTCGTTAAtgATGAAGACAGAA
		GCCACGGTTTCTCAGCCCACCGCGCC
		AGCCGGATCGCCGCTCATGCAGGTG
		AGCGGCGCATTAATTGGCATTATTGC
		GCTCATTCTGGCGGCGGCCTGGGTGA
		TTAAGCGTATGGGATTCGCGCCAAA
		AGGAAATAGCGTCCGGGGACTGAAG
		GTGTCAGCCAGCGCCTCGCTTGGCC

5.4.1 Proof reading amplification

Inserts were generated by PCR using Phusion® High-Fidelity DNA Polymerase (NEB) as described below in 50 µl reaction

Table 9: PCR amplification with proof reading polymerase

	Stock concentration	Final volume (µl)
Phusion® HF buffer	5 X	10
dNTPs	20 mM	2
Primer (each)	10 µM	2.5
Phusion® polymerase	5 units/µl	0.5
Template (gDNA, plasmid)	1-10 ng/µl	1
Total		**50**

PCR was performed as follows: Denaturation 3 min at 98 °C, 30 s annealing, 30 s/kb elongation time at 72 °C, for 35 cycles and 5 min final elongation. PCR products were then cleaned using NucleoSpin® Gel and PCR Clean-up Kit (Macherey-Nagel) and eluted in 30 µl elution buffer.

5.4.2 Amplification with Go-Taq® polymerase

Non-proof reading amplifications were performed using GoTaq® polymerase (Promega) as described below.

Table 10: PCR amplification with Go-Taq polymerase

	Stock concentration	Final volume (µl)
Green GoTaq® flexi buffer	5 X	10
$MgCl_2$	25 mM	3
dNTPs	20 mM	2
Primer (each)	10 µM	2.5
GoTaq® polymerase	5 units/µl	0.5
Template (gDNA, plasmid)	1-10 ng/µl	1
Total		**50**

Reaction was performed as follows: Initial denaturation 3 min at 95 °C, denaturation 10 s at 95 °C, 30 s annealing, 1 min/kb elongation time at 72 °C, for 35 cycles and 5 min final elongation. PCR products were then cleaned using NucleoSpin® Gel and PCR Clean-up Kit (Macherey-Nagel) and eluted in 30 µl elution buffer.

5.4.3 Colony PCR

Single colonies were used as template for colony PCR. Amplification was performed using Go-Taq DNA polymerase as described below for 35 cycles (denaturation 95 °C, 30 s annealing, 1 min/kb elongation time at 72 °C) and 5 min final elongation. Results were checked by electrophoresis on 1 % agarose gel in TEA buffer.

Table 11: PCR amplification with Go-Taq polymerase

	Stock concentration	Final volume (µl)
Green GoTaq® flexi buffer	5 X	4
$MgCl_2$	25 mM	1.2
dNTPs	20 mM	0.8
Primer (each)	10 µM	1
GoTaq® polymerase	5 units/µl	0.5
Template (colony)	1-10 ng/µl	1
Total		**20**

5.4.4 Plasmid purifications

The donor strain was grown overnight at 37 °C in 15 ml LB supplemented with the appropriate antibiotic. Cells were harvested in two 15 ml Flacon tubes containing 7.5 ml of overnight culture. Purification was performed using NucleoSpin® Plasmid columns and buffer kits (Macherey-Nagel). Each pellet was resuspended in 250 µl A1 buffer, lysed by addition of 250 µl A2 buffer for 5 minutes and neutralized with 350 µl A3 buffer. After 10 min centrifugation at 11,000 x g, the lysates of both tubes were loaded on the same column and treated as described in the user manual.

5.4.5 Enzymatic restriction digest

Purified vectors and inserts were digested in 50 µl reaction containing 1µl of each enzyme, 5 µl of appropriate 10 X Buffer and 30 µl or 43 µl of purified DNA for insert and vector respectively in sterile MQ water. Digestion was performed at 37 °C for 2.5 h.

5.4.6 Vector dephosphorylation

To prevent relegation of empty plasmids, backbone vectors were dephosphorylated after enzymatic restrictions for 30 min at 37 °C using Antarctic phosphatase (NEB) as described below.

Table 12: dephosphorylation

	Concentration	Volume
Digested vector	30-100 ng/µl	40 µl
Antarctic phosphatase buffer	10 X	4.6 µl
Antarctic phosphatase	5 units/µl	1 µl
Total		**46 µl**

5.4.7 Insert phosphorylation.

To allow blunt end ligation, PCR generated inserts were phosphorylated to allow ligation with the backbone vector pBR322, previously digested with EcoRV. The insert was phosphorylated for 30 min at 37 ºC using T4 kinase (fermentas) as described below.

Table 13: phosphorylation

	Concentration	Volume
DNA	30-100 ng/µl	30 µl
T4 DNA ligase buffer	10 X	5 µl
T4 Kinase	10 units/µl	1 µl
Total		**50 µl**

5.4.8 Agarose gel electrophoresis

PCR products and digested plasmids were checked by agarose gel electrophoresis. 1 % agarose was melted and solubilized in TAE buffer, and poured in RunOne™ Agarose Gel Casting System. Samples previously amplified in Go-Taq buffer of Phusion HF buffer were directly loaded on the gel. Digested or purified DNA fragments were mixed with 6x loading dye. Electrophoresis was performed in TEA buffer at 130 V for 20 min in a Wide Mini-Sub Cell GT Cell (BioRad). Fisher BioReagents™ exACTGene™ 1kb Plus DNA Ladder was used as marker. After electrophoresis gels were stained with an ethidium bromide solution for 1-3 minutes and imaged by UV transillumination using a Gel Doc™ XR+ system (BioRad).

5.4.9 Gel extraction

After digestion, sample were run on a 1 % agarose gel, incubated 2-5 min in ethidium bromide, and DNA was detected using BioRad ChemiDoc™ XRS+ System (BioRad), EtBr protocol. Digested fragments were then cut out of the gel using a clean scalpel and purified using NucleoSpin® Gel and PCR Clean-up Kit (Macherey-Nagel) according to the manufacturer´s protocol. DNA was eluted in 20 µl elution buffer.

5.4.10 DNA concentration measurement

Purified DNA concentration was measured via determination of the absorbance at 260 nm in a photometer (NanoDrop, PEQLAB).

5.4.11 Ligation

Ligation was performed using 1 µl T4 DNA ligase (Fermentas) in 1 x T4 DNA ligase buffer (Fermentas) and 100ng of vector with a 1:3 vector: insert molar ratio in 20 µl at 22 °C for 1 h. For blunt end, ligation was performed overnight at 4 °C.

5.4.12 Chemically competent cells preparation

Recipient strains were diluted 1:100 in 100ml LB supplemented with 20 mM of $MgSO_4$ and grown at 37 °C until OD_{600} reaches 0.6. Cells were harvested by centrifugation at 10,000 g for 5 min at 4 °C. Supernatant was discarded, cells were resuspended in 40 ml of TFB1 buffer and incubated for 10 min on ice. Cells were then centrifuged at 10,000 x g for 5 min, resuspended in 4 ml TFB2 buffer and incubated for 15 to 60 min on ice. Competent cells were then aliquoted and kept at -80 °C until further use.

5.4.13 Electro-competent cells preparation

Overnight cultures of recipient strains were diluted 1:100 into 25 ml fresh LB supplemented with appropriate additives, and grown at 37 °C, or 30 °C for thermosensitive plasmids, until OD_{600} reached 0.6. Cells were then transferred into 50 ml Falcon tubes and spun at 10,000 x g for 5 min at 4 °C. Supernatants were discarded and pellets were resuspended in 25 ml of ice-cold sterile MQ water. This operation was repeated three times and cells were finally resuspended in 250 – 350 µl ice-cold water and kept on ice before transformation.

5.4.14 Electroporation

5µl of ligation product were added to 50 µl competent cells and transferred into a 1ml electroporation cuvette (Brand). Electroporation was performed in an Eppendorf Eporator®, 1 ml fresh LB was added and cells were grown for 1 h at 37 °C, or 30 °C for thermosensitive plasmids, at 700 rpm in a thermoblock. Samples were centrifuged at 10,000 x g for 1 minute, to remove most of the supernatant, and plated on appropriate selective agar plates.

5.4.15 PCR based fusion

The *fliOPQR*-terminators DNA fragments was constructed using PCR based fusion as previously described [129]. *fliOPQR* and the terminator regions were first amplified by proof-reading PCR with primers #484 + #933 and #932 + #905 respectively to create a 55 bp overlap between both fragments. After gel extraction and purification, a PCR without primer but both PCR fragment at 1.1 molar ratio was performed with Phusion® polymerase, with only 11 cycles and an annealing temperature of 54 °C. 3µl of the resulting product were then used as template for a second proof reading PCR as usual, using primers #484 + #905 and an annealing temperature of 60 °C. The resulting product was gel purified and used for cloning into pBR322.

5.4.16 Gibson assembly®

pEM2273 and the regulators cassette were built using the Gibson assembly® master mix as instructed in the user protocol and as described below. Each fragment was previously yielded by proof reading PCR. Gibson assembly reaction was performed for 1 h at 50 °C with a molar ratio vector: insert of 1:3.

Table 14: Gibson assembly® reaction

	2 - 3 fragments	**4 - 6 fragments**
Total amount of fragments	0.02 - 0.5 pmols	0.2 - 1 pmols
Vector	50 - 100 ng	50 - 100 ng
Gibson Assembly® master mix	10 µl	10 µl
Total	**20 µl**	**20 µl**

5 µl of reaction product were mixed with 50µl chemically competent TH12219. The mix was left 30 min on ice, heat shocked at 42 °C in a thermoblock for 30 s and incubated for 2 min on ice. 950 µl of SOC medium (Thermo Fisher scientific) were added to the cells and phenotypic expression was performed at 37 °C for 1h. Samples were then centrifuged at 10,000 x g for 1 min, 800 µl of the supernatant was discarded and the cells were resuspended in the rest of the medium. 100 µl of the cells were finally plated on selective plates and incubated overnight at 37 °C. Resulting clones were tested by PCR and sequenced.

5.4.17 Chromosomal integration of CRIM plasmids

Integration of the minimal T3SS plasmid on the chromosome was performed as described by Haldimann and Wanner [95]. Overnight culture of EM565, carrying the helper plasmid pINT-ts encoding the phage λ integrase, was diluted 1:100 in 25 ml LB + ampicillin at 30 °C until OD_{600} reached 0.6. Cells were made electro-competent and the T3SS plasmid was electroporated as described above. After 1h of phenotypic expression at 37 °C, cells were spread on LB agar + Cm plates. The following days, transformants were first streaked on non-selective media. The presence of integrant was checked by PCR.

5.4.18 FRT recombination

Cm and Km resistance cassette flanked by Flp recombinase target (FRT) sites, termed FCF and FKF cassettes respectively, were inserted by λ-Red recombination and excised in presence of Flp recombinase as described by Cherepanov and Wackernagel [130]. To excise the cassette, the temperature sensitive pCP20, carrying the Flp recombinase, was introduced by electroporation. Expression of the Flp recombinase lead to homologous recombination of the flanking FRT sites, removing therefore the resistance gene. After overnight incubation at 42 °C, strains were cured from the plasmid, preventing from reverse recombination, leaving only a FRT scare on the chromosome.

5.4.19 λ-red recombination for *tetRA* insertion

Recipient strains were first transformed by electroporation with pKD46, plated on LB agar plates + Amp (0.1 mg/ml) and incubated overnight at 30 °C. Resulting strains were streaked on LB + Amp plates, and a single colony was inoculated in 1 ml LB + Amp (0.1 mg/ml) and grown at 30 °C overnight. Cultures were then diluted 1:100 into 25 ml fresh in LB + Amp (0.1 mg/ml) + 0.2 % arabinose and grown until OD_{600} reached 0.6. Cells were made

electro-competent as described above. 5µl (300-500ng) of previously amplified *tetRA* cassette, harboring 40 bp homology flanking region, were transformed into 50 µl competent cells. 1 ml of LB was added after electroporation. After phenotypic expression, 100 µl of 10^{-1} dilution were plated on LB agar + Tc (15 µg/ml) and incubated overnight at 37 °C.

5.4.20 λ-red recombination for *tetRA* replacement

Recipient strains carrying *tetRA* cassette insertion and pKD46 were grown and made electro-competent as described above. 5 µl of PCR products, harboring 40bp homology, were electroporated in 50 µl competent. 1 ml of LB was added and 1 h phenotypic expression was performed at 37 °C. After 30 min, AnTc was added for *tetRA* induction. 100 µl of 10^{-1} and 10^{-3} dilutions were plated on *tetRA* sensitive plates and incubated at 42 °C for 48 h. The presence of the insert was check by colony PCR.

5.4.21 P22 transduction

Phage lysates were prepared from 1 ml culture in LB grown overnight at 37 °C. 4 ml of P22 broth were added to the culture and grown for 8-16 hours at 37 °C at 200 rpm. Samples were then centrifuged at 3,000 x g for 10 minutes at 4 °C, supernatant was collected into a fresh tube and 500 µl of $CHCl_3$ were added to the lysate. Tubes were thoroughly vortexed and stored at 4 °C. Recipient strains were grown overnight in 1 ml LB at 37 °C. 100 µl of recipient strain were mixed with 100 µl of 10^{-1} and 10^{-2} phage lysate dilution in PBS or 100 µl PBS as negative control. For phages carrying Amp, Cm and Kan resistance cassettes, 1 h phenotypic expression was performed at 37 °C and samples were spread on appropriate selection plates. For Tc cassette resistance carrying phages, samples were directly plated on LB + Tc plates, without phenotypic expression. For phages conferring Tc sensitivity, 100 µl of recipient were mixed with 100 µl 1:5 and 10^{-1} dilution and phenotypically expressed at 37 °C for 1 h. Samples were then diluted 10^{-1} and 10^{-2} in PBS and 100µl were plated on fusaric acid plates, incubated at 37 °C for 48 h.

After transduction, single colonies were streaked on green plates, to exclude phage infected cells, which turn dark blue and select the light green phage free cells. Some of the light green colonies might be stable lysogens and cannot be reinfected with P22 phage. To only discriminate phage free cells from lysogens, colonies were cross-streaked against H5 phage on green plates. Colonies that were sensitive to H5 phage were selected and streaked again on non-selective plates before being checked by PCR.

5.4.22 DNA-sequencing

The sequencing of PCR-products was performed by the Department of Genome Analysis at the Helmholtz-Centre for infection research, Germany.

5.5 Motility assay

Bacterial motility was assessed using soft agar motility plates. 0.3 % agar LB plates supplemented with appropriate additives were inoculated with a pin-tool previously dipped in overnight culture. Plates were incubated at 37 °C and scanned after 4 h to 7 h. The sizes of the halos were measured with ImageJ version 1,47v (for Windows).

5.6 Flagella staining – Immunofluorescence

Overnight cultures were diluted 1:100 in fresh LB and grown until OD600 = 0.5. Coverslips were incubated for 15 min in 0.1 % poly-L-lysine. A well was formed by placing a layer of double sided adhesive tape between the glass slides and the coverslips. 20 µl of the mid-log phase culture was pipetted into the well and the slides were incubated up-side down in a wet chamber. This operation was repeated three times. Cells were fixed by incubation for 10 min in 2 % formaldehyde + 0.2 % glutaraldehyde in PBS, rinsed slowly with 20 µl of PBS and blocked by addition of 10 % BSA. Cells were incubated in rabbit α-FliC primary antibodies diluted 1:1,000 in 2 % BSA overnight at 4˚C. After incubation, samples were washed with PBS and blocked with 10 % BSA. Subsequently, slides were incubated for 30 min in α -rabbit Alexa Fluor488 coupled secondary antibody diluted 1: 1,000 in PBS. After two washes with PBS, 5 µg/ml FM-64 was added in Fluoroshield mounting medium with DAPI (0.0002 %) (abcam). Samples were observed and images were collected using an AxioObserver fluorescent microscope (Zeiss). Data were analyzed using ImageJ version 1.47v (for Windows).

5.7 Minimal Inhibitory Concentration assay

Export of flagellar substrate was performed in strains lacking the rod proteins (*ΔflgBC*) and encoding the FlgE-β-lactamase fusion under control of the inducible *araBAD* promoter (Δ*araBAD*1077::*flgD-flgE-bla*). Overnight cultures were inoculated with single colony in 200 µl of LB, supplemented with the appropriate antibiotic and inducer when necessary, in a 96 well plate, and grown at 37 °C and under shaking at 180 rpm. The following day, ON cultures were first diluted in 1:5 in LB (dilution 1) supplemented with 0.1 % of arabinose

and the appropriate antibiotic and diluted again 1:10 (dilution 2: 1:50 of the ON culture) in the same medium. In the case of the mini T3SS plasmid, the different inducers were also added at this step. Cells were then grown at 37 °C for 2.5 h at 180 rpm. Afterwards, cells were diluted 1:10 into 300 µl of fresh LB medium supplemented with 0.1% arabinose and appropriate antibiotics and inducer (dilution 3). 20 µl of the dilution 3 were finally dispensed, using a multichannel pipette (Eppendorf explorer), in each well of 180 µl LB medium, supplemented as previously, containing increasing concentration of ampicillin. These wells were prepared by cascade dilution as described below.

Table 15: Ampicillin dilutions for MIC assay

Well number	[Amp] in µg/mL before addition of 20µl of dilution 3 (1.1 x Amp)	[Amp] in µg/mL in the test plate (1 x Amp)
1	0	0
2	1	1
3	2	2
4	4	4
5	9	8
6	18	16
7	35	32
8	70	64
9	141	128
10	282	256
11	563	512
12	**1226**	**1024**

Cells were then grown for 4 to 6 hours at 37 °C under shaking. Finally, OD_{600} was measured using a TECAN sunrise™ microplate reader with the TACAN Magellan™ software. IC50 values were calculated with the [R] package 'stinepack', using a Stineman interpolation for non-linear fit of the data, modified by Dr. Marc Erhardt.

5.8 Secretion assay

Cells were grown in LB at 37 °C until OD_{600} reached 0.8 - 0.9 and 1.9 ml of culture were harvested and cooled down on ice. Cells and supernatant were separated by 3 times 3 min centrifugation at 18,000 x g at 4 °C. The pellet and 1.5 ml supernatant of each strain were precipitated with 10 % TCA as described below. After normalization to the OD_{600}, samples were loaded on a 15 % SDS-PAGE and analyzed by Western blot.

5.9 Protein stability assay

Overnight cultures were diluted 1:100 into 25 ml of fresh LB and grown at 37 °C under shaking until OD_{600} reached 0.6. Protein synthesis was inhibited by addition of 0.5 $mg \cdot ml^{-1}$ Spectinomycin and 12.5 $\mu g \cdot ml^{-1}$ chloramphenicol. The equivalent of 1 ml at OD_{600} = 0.6 was collected at 0, 30, 60, 90, 120, and 180 min after synthesis inhibition in a 1,5 ml microcentrifuge tube. Samples were precipitated with 10 % TCA as described below. After precipitation, pellets were air dried and resuspensded in 2 x SDS-sample buffer Samples were run on 15 % SDS-PAGE, analyzed by Western blot and membranes were probed with antibodies against FLAG or HA tags for FliP detection and DnaK as loading control. Total proteins were image with TCE. For the stability assay in presence of STM1085, induction was performed with 1 mM IPTG.

For plasmid-encoded FliP stability assay, cultures were grown in LB supplemented with 12.5 $\mu g \cdot ml^{-1}$ chloramphenicol to maintain pKG116 and FliP expression was induced with 1 mM of NaSal.to ensure sufficient FliP expression without complementation effect. Because of the Cm resistance conferred by pKG116, protein synthesis was inhibited only with Spectinomycin. The rest of the experiment was performed as described above.

5.10 TCA precipitation

Total protein and cytosolic fractions were precipitated addition of TCA to a final volume of 10 %. Samples were incubated on ice for 30 min before centrifugation at 20,000 x g for 30 min. Supernatant was discarded and pellet was washed in 1ml ice-cold acetone, vortexed and spun down at 20,000 x g for 30 min. this washing step was repeated twice and acetone was removed. Pellets were then air dried overnight before resuspension in 2 x SDS loading buffer.

5.11 Cell fractionation assay

Overnight cultures were diluted 1:50 into fresh LB until OD_{600} reached 0.7 – 0.8. The equivalent of 8 OD_{600} units were harvested at 8,000 x g for 10 minutes, re-suspended in 750 µl Buffer K and incubated for 30 min at 4 °C. Cells were transferred in 1.5 ml screw cap tubes previously filled with 425-600 µm glass beads (Sigma) and lysates were spun at 10,000 x g for 10 min to eliminate unlyzed cells. Supernatants were then spun down at 150,000 x g at 4 °C for 50 min. 900 µl of supernatant were collected and precipitated with 10 % TCA, washed and resuspended in 2 x SDS loading buffer (Cytosolic fraction). Pellets

were resuspended in 100 µl cold PBS. Half of the suspension was directly mixed with 50 µl 2 x SDS-loading buffer (unwashed membranes). The rest of the membrane was washed with 1 ml of 8 M solution of urea in buffer M, for 1 h at room temperature, and centrifuged at 120,000 x g for 1.5 h at 23 °C. The supernatant was discarded and the pellet was resuspended in 100 µl of 1 x SDS loading buffer. Both fractions were run on SDS-PAGE and analyzed by Western blots.

5.12 SDS polyacrylamide gel

In order to discriminate protein according to their molecular weight under denaturating conditions, samples were loaded on sodium dodecyl sulfate polyacrylamide gel (SDS-PAGE). The electrophoresis was performed with BioRad Mini-PROTEAN tetra cell system. 15 % SDS-PAGE were prepared as described in Table 16. Samples were previously mixed with 2 x SDS loading buffer, and run at 150 V for 1.5 h in 1 x SDS running buffer. Fisher BioReagents EZRun Prestained Rec Protein Ladder by Thermo Fisher Scientific was used as a marker.

Table 16: SDS gels composition

	Composition	
15 % SDS-PAGE (running)	Acrylamide	15 %
	Tris-HCl pH 8.8	375
	SDS	0h%
	APS	0.05 %
	TEMED	
	2,2,2-Trichloroethanol (TCE)	0.5 %
	In H_2O	
SDS-PAGE (stacking)	Acrylamide	4 %
	Tris-HCl pH 6.8	160 mM
	SDS	0.1 %
	APS	0.05 %
	TEMED	
	In H_2O	

5.13 TCE staining

Protein carrying tryptophan residue can be easily visualized using 2,2,2-Trichloroethanol (TCE) as described previously [73]. In order detect total protein amounts; we added 0.5 % to our SDS acrylamide gel before casting. Directly after electrophoresis and before transfer, the gels were imaged with ChemiDoc™ (stain free gel protocol, 1 min activation, and automatic exposure).

5.14 Western blot

Following SDS-PAGE, proteins were transferred onto a 0.2 µm nitrocellulose membrane. Blots were then blocked with 5 % milk in TBS-T and probed 1h with appropriate antibodies. Membranes were then washed 3 times 5 min with TBS-T and incubated 30 min in Immun-Star Goat anti-mouse HRP or goat anti-HRP secondary antibodies (1:20,000 in 5 % milk in TBS-T; BioRad). After washing with TBS, membranes were developed using Clarity™ Western ECL (BioRad) and imaged with ChemiDoc™ imaging system (BioRad) using the Chemi Hi-resolution protocol.

5.15 Stripping of Western blot membrane

As previously described, the signal of tagged highly hydrophobic membrane protein can be enhanced by stripping the membrane directly after transfer [74]. This process was used for HA and FLAG tagged FliP and FliO. Nitrocellulose or PVDF membranes were incubated in stripping buffer in a 60 °C incubator for 15 to 20 minutes, with occasional shaking. Membranes were then rinsed abundantly with water followed by three times 5 min washing with TBS-T. After washing, blots were blocked and probed as usual.

5.16 Protein levels quantification

Images were acquired with the ChemiDoc™ imaging system (BioRad). ImageJ was used for protein quantification. Intensities of the signal were measured for FliP, DnaK and total proteins stained with TCE. For each time point, FliP protein levels were normalized to DnaK levels for chromosomally encoded FliP and to total protein amount for plasmid encoded FliP. At least three different experiment were used for quantification. The ratio FliP/control was then expressed relatively to the average value obtained for T_0.

5.17 Large scale crude membrane preparation

To perform Blue Native PAGE, crude membranes were prepared on a large scale as described by Zilkenat *et al* (in preparation). Overnight culture was diluted 1:100 into 1 l of fresh LB and cells were grown at 37 °C until OD_{600} reached 0.8 - 0.9. All following steps were performed at 4 °C except when stated otherwise. 800 OD_{600} units of culture were harvested and centrifuged at 6,000 x g for 15 min in a Beckmann JLA-8. Supernatant was discarded and pellet was resuspended in 35 ml cold PBS, transferred in a 50-ml falcon tube and centrifuged 10 min at 6,000 x g. cells were resuspended in 10-15 ml of buffer K supplemented with cOmplete™ mini EDTA free protease inhibitors cocktail, 10 µg/ml DNase, 10 µg/ml lysozyme and 1 mM EDTA. After 30 min incubation, cells were lyzed by passing three times through a French Press at 18,000 psi. After lysis, 1 mM $MgCl_2$ was added to activate DNase and lysates were centrifuged at 24,000 x g for 20 min to eliminate cell debris. Crude membranes were pelleted by centrifugation at 200,000 x g for 50 min, resuspended in 500 µl of buffer M (1 X), and homogenized in a 1 ml Dounce homogenizer. Membrane were then stored on ice before separation on sucrose gradient.

5.18 Sucrose gradient

All steps were performed at 4 °C. Sucrose gradient was prepared from a 55 % sucrose solution in buffer M, as described in Table 17.

Table 17: Sucrose gradient composition

Percentage of sucrose (w/w)	Sucrose	Buffer M (2 X)	55% Sucrose solution	Buffer M (1 X)
55%	19.25 g	13.5 ml		
50%			4.55 ml	0.45 ml
45%			4.1 ml	0.91 ml
40%			3.6 ml	1.36 ml
35%			3.2 ml	1.8 ml
30%			2.7 ml	2.3 ml

The different layers of the gradient were manually poured on top of each other in an ultracentrifuge glass tube, from 55 % at the bottom to 30 % at the top, with a 5-ml glass pipette. Crude membrane extracts previously homogenized were carefully deposed at the surface of the gradient, and were centrifuge for 14 h at 150,000 g in a

Beckmnan Optima L-90K centrifuge. 8 fractions of 1 ml were collected by carefully pipetting 1 ml slightly under the meniscus along the gradient. Fractions were then diluted 1:3 with buffer M and membranes were centrifuged at 200,000 x g for 45 min. supernatant was discarded and membranes were resuspended in 200 µl buffer L. 10 µl of each fraction were loaded on a 15 % SDS-PAGE, TCE imaging and Western blot were performed as described above. Based on the Western blot results, the 3 to 4 fractions exhibiting the best FliP-FLAG signal and which were relatively pure were pooled together. Protein concentration was measured using Bradford protein assay (BioRad) according to user's manual instructions, and the concentration of each sample was adjusted to 3.0 $mg \cdot ml^{-1}$. Membranes were then solubilized with 1 % DDM for 1h under gentle shaking and centrifuged 20 min at 20,000 x g to eliminate unsolubilzed membranes. The supernatant was collected and analyzed by Blue Native PAGE as described below.

5.19 FliP pull down

All steps described below were performed at 4 °C. Crude membranes prepared in large scale, but not separated on sucrose gradient, were solubilized with 0.5 % DDM for 1 h under smooth shaking and centrifuged 20 min at 20,000 x g to pellet cell debris. Supernatant was collected and 25 µl of ANTI-FLAG M2 affinity gel (Sigma), previously washed with PBS / 0.1 % DDM according to the manufacturer's instructions, were added and incubated for 4h on a rotating wheel. The supernatant and the beads were then transferred onto a 2-ml disposable column, (Pierce™), the flow through was collected and the beads were washed twice with 50 µl PBS / 0.01 % DDM. Proteins were eluted by addition of 25 µl PBS / 0.01 % DDM / $150 \mu g \cdot ml^{-1}$ 3 x FLAG peptides. This operation was repeated 6 times. Fractions were then analyzed by SDS-PAGE and Western blot, and the purest fractions were pooled together analyzed by Blue Native PAGE as described below.

5.20 Blue Native PAGE

Crude membranes or pull down elations were prepared as described above. 45 µl of sample were mixed to 5 µl of native loading dye and 25 µl were loaded on a 3 - 12 % NativePAGE (Thermo Fisher scientific) placed in a mini gel tank (Thermo Fisher scientific) filled with 1 X anode buffer and 1 X cathode buffer I, in the anode and cathode chamber respectively. Samples were run for 50 min at 130 V before 80 % of the cathode buffer I was replaced by cathode buffer II. The gel was run 1.5 h more at 250 V at 4 °C. After electrophoresis, the gel was opened and equilibrated in 1 X SDS running buffer for 10 min, and transferred onto a 0.2 µm PVDF membrane, previously activated in Methanol. Transfer was performed at 30 V for 2 h in transfer buffer supplemented with 0.025 % SDS at 4 °C. After transfer, the membrane was washed in methanol to eliminate the Coomassie, rinsed 5 min in MQ water, stripped, blocked in 5 % milk, probed and developed as usual.

5.21 Mass spectrometry analysis

To determine the composition of the protein complexes, samples were loaded twice on the same BN-PAGE. After electrophoresis, Western blot was performed on one half of the gel and the other one was stained with Coomassie for 30 minutes, washed three times, and stored at 4 °C in 5 % acetic acid until further use. To avoid contamination, all tools and recipients were previously washed with fresh 100 % ethanol. Each lane of the Coomassie stained gel was then cut, and gel pieces were extracted with a clean razor blade from both WT and Δ*fliO* at the height of the complexes detected by Western blot. These gels fragments were stored in 5 % acetic acid until analysis.

In-gel digestion and MS analysis were performed by Mirita Franz-Wachtel and Boris Macek. at the University of Tübingen. In-gel digestion was performed using ProteaseMAX™ surfactant. Proteins were digested using trypsin and chymotrypsin (12.5 ng·µl^{-1} each) in 20 mM ammonium bicarbonate and 0.01 % ProteaseMAX™ surfactant according to the user's manual. Peptides were desalted with C18 StageTips as described by Rappsilber *et al.* [75]

LC-MS/MS analysis was performed using an Easy nano-LC (Thermo Scientific) and a LTQ Orbitrap XL mass spectrometer (Thermo Scientific) as previously described (35). Peptides were run in a HPLC and eluted with a gradient of 5 – 33 – 50 – 90 % gradient. The 10 most intense precursor ions were fragmented using collision-induced dissociation (CID). The masses of the sequenced precursors were excluded from further selection for 90 s.

The target values for MS/MS fragmentation were 5000 charges and 10^6 charges for the MS scan. The MaxQuant software suite v.1.5.2.8. was used for data processing and the MaxQuant module Andromeda was used for database search. The mass spectrometry data have been deposited to the ProteomeXchange Consortium (http://proteomecentral.proteomexchange.org) via the PRIDE partner repository with the data set identifier PXD###.

5.22 FliO localization by super-resolution microscopy

For FliO localization studies, HaloTag and SNAP-Tag fusions were constructed by λ red recombination and the super resolution microscopy analysis was carried out by Britta Peters in Michael Hensel's laboratory in Osnabrück as described below. Bacteria were diluted 1:100 in fresh LB medium and grown for 2.5 h at 30 °C. After 1.75 h, fluorescent HaloTag ligands (HTL) were added, i.e. 20 nM HTL-TMR (Promega) or 150 nM HTL-Atto655 (self-synthesized) for HaloTag fusions and washed at least 5 times with minimal medium by centrifugation at 8,000 x g for 2 min to remove unbound ligand and LB medium. Bacteria were diluted to approx. OD_{600}=0.5 and 15 µl were added to agarose-coated glass cover slips freshly prepared with 1 % agarose and a second glass slide was place atop the agarose. total internal reflection fluorescence (TIRF) microscopy was performed using an inverted microscope (IX71, Olympus) equipped with a motorized 4-line TIRF condenser (cell^TIRF, Olympus), a 150 x oil immersion TIRF objective (UAPON 150 x OTIRF, Olympus) and high power lasers: 488 nm, 150 mW (LuxX, Omicron, Germany); 561 nm, 150 mW (Jive, Cobolt, Sweden); 640 nm, 140 mW (LuxX, Omicron, Germany). Acquisition was performed using an electron multiplying back-illuminated frame transfer CCD camera (iXon Ultra 897, Andor), a fluorescence filter cube containing a polychroic beamsplitter (R405/488/561/647, Semrock) and a quad-band emission/blocking filter (FF01 446/523/600/677, Semrock). For each cell, 500 frames were recorded with an exposure time of 31 ms for 561 nm and 640 nm laser and laser power of 5 mW. For dual color dSTORM bacteria were stained as indicated, washed and fixed with 3 % PFA in PBS for 15 min at room temperature. After fixation, bacteria were washed again 3 times and immobilized on Poly-L-Lysine coated cover slides. As redox system 100 mM ß-Mercaptoethylamine, 4.5 $mg \cdot 10^{-1}$ ml D-Glucose, 40 $\mu g \cdot 10^{-1}$ ml Catalase and 0.5 $\mu g \cdot 10^{-1}$ ml Glucose-Oxidase were added in 1 ml PBS. 500 frames were recorded with an exposure time of 31 ms for 561 nm and 640 nm laser, cycle time 67 and laser power of 40 mW and 50 mW, respectively.

5.23 Single molecule localization and tracking

Localization of single molecules as well as single molecule tracking was carried out by a graphical user interface written in Matlab R2012 (MathWorks) by Britta Peters. Single molecule localization is based on the multiple-target tracing algorithm published by Serge *et al.* and single molecule tracking is performed by the utrack algorithm published by *Jaqaman et al*. (online available: MTT: http://ciml-e12.univ-mrs.fr/App.Net/mtt/, utrack: http://lccb.hms.harvard.edu/doc/u-track-2.1.3.zip).

5.24 Single cysteine labelling

FliP folding state was studied using the substituted-cysteine accessibility method (SCAM) Periplasmic residues A32 and S117 were substituted by cysteine residues. Bacteria were grown until OD_{600} reached 0.6, 25ml were collected by centrifugation at 5,000 x g for 5 minutes and pellets were washed with Tris-HCl at pH 7. Cells were permeabilized by resuspension and incubation for 30 min at 4 °C in 1ml spheroplast buffer. Samples were then centrifuged at 5,000 x g for 10 min, washed once and resuspended in 500 µl spheroplast buffer. Spheroplast were aliquoted in three samples of 50µl supplemented with either 5 mM PEG maleimide (5 kDa) (sample), 1 % SDS and 5 mM PEG maleimide (positive control), or nothing (negative control). Samples were shortly agitated and incubated for 1.5 h at 37 °C. Maleimide was quenched with 50 mM DTT. Samples were diluted in 500 µl of water, precipitated with TCA as described above, resuspended in 50µl SDS sample buffer and analyzed by Western blot.

6. References

1. Hays JN. Epidemics and pandemics : their impacts on human history [Internet]. ABC-CLIO; 2005. Available: https://books.google.de/books?id=GyE8Qt-kS1kC&printsec=frontcover&source=gbs_summary_r&redir_esc=y#v=twopage&q&f=false

2. Perry RD, Fetherston JD. Yersinia pestis--etiologic agent of plague. Clin Microbiol Rev. 1997;10: 35–66. Available: http://www.ncbi.nlm.nih.gov/pubmed/8993858

3. Snowden FM. Emerging and reemerging diseases: a historical perspective. Immunol Rev. 2008;225: 9–26. doi:10.1111/j.1600-065X.2008.00677.x

4. Pitout JDD, Nordmann P, Laupland KB, Poirel L. Emergence of Enterobacteriaceae producing extended-spectrum -lactamases (ESBLs) in the community. J Antimicrob Chemother. Oxford University Press; 2005;56: 52–59. doi:10.1093/jac/dki166

5. Glynn JR. Resurgence of tuberculosis and the impact of HIV infection. Br Med Bull. 1998;54: 579–593. Available: http://www.ncbi.nlm.nih.gov/pubmed/10326286

6. Navin TR, McNabb SJN, Crawford JT. The continued threat of tuberculosis. Emerg Infect Dis. Centers for Disease Control and Prevention; 2002;8: 1187. doi:10.3201/eid0811.020468

7. WHO | Global priority list of antibiotic-resistant bacteria to guide research, discovery, and development of new antibiotics. WHO. World Health Organization; 2017; Available: http://www.who.int/medicines/publications/global-priority-list-antibiotic-resistant-bacteria/en/

8. Agbaje M, Begum RH, Oyekunle MA, Ojo OE, Adenubi OT. Evolution of Salmonella nomenclature: A critical note. Folia Microbiol (Praha). 2011;56: 497–503. doi:10.1007/s12223-011-0075-4

9. Larsson JT, Torpdahl M, Petersen RF, Sorensen G, Lindstedt BA, Nielsen EM. Development of a new nomenclature for Salmonella typhimurium multilocus variable number of tandem repeats analysis (MLVA). Euro Surveill Bull Eur sur les Mal Transm = Eur Commun Dis Bull. 2009;14.

10. Grimont PAD, Weill F-X. WHO Collaborating Centre for Reference and Research on Salmonella. Available: http://www.scacm.org/free/Antigenic Formulae of the Salmonella Serovars 2007 9th edition.pdf

11. Fierer J, Guiney DG. Diverse virulence traits underlying different clinical outcomes of Salmonella infection. J Clin Invest. American Society for Clinical Investigation; 2001;107: 775–80. doi:10.1172/JCI12561

12. Coburn B, Grassl GA, Finlay BB. Salmonella, the host and disease: a brief review. Immunol Cell Biol. Nature Publishing Group; 2007;85: 112–118. doi:10.1038/sj.icb.7100007

13. Crump JA, Luby SP, Mintz ED. The global burden of typhoid fever. Bull World Heal Organ. 2004;82: 346–353. Available: http://www.ncbi.nlm.nih.gov/pubmed/15298225

14. Majowicz SE, Musto J, Scallan E, Angulo FJ, Kirk M, O'Brien SJ, et al. The global burden of nontyphoidal Salmonella gastroenteritis. Clin Infect Dis. 2010;50: 882–889. doi:10.1086/650733

15. Ao TT, Feasey NA, Gordon MA, Keddy KH, Angulo FJ, Crump JA. Global Burden of Invasive Nontyphoidal *Salmonella* Disease, 20101. Emerg Infect Dis. 2015;21: 941–949. doi:10.3201/eid2106.140999

16. WHO | Drug-resistant Salmonella. WHO. World Health Organization; 2011;

17. Glynn MK, Bopp C, Dewitt W, Dabney P, Mokhtar M, Angulo FJ. Emergence of multidrug-resistant Salmonella enterica serotype typhimurium DT104 infections in the United States. N Engl J Med. 1998;338: 1333–1338. doi:10.1056/NEJM199805073381901

18. Fabrega A, Vila J. Salmonella enterica serovar Typhimurium skills to succeed in the host: virulence and regulation. Clin Microbiol Rev. 2013;26: 308–341. doi:10.1128/CMR.00066-12

19. Lazova MD, Butler MT, Shimizu TS, Harshey RM. Salmonella chemoreceptors McpB and McpC mediate a repellent response to L-cystine: a potential mechanism to avoid oxidative conditions. Mol Microbiol. NIH Public Access; 2012;84: 697–711. doi:10.1111/j.1365-2958.2012.08051.x

20. Falke JJ, Hazelbauer GL. Transmembrane signaling in bacterial chemoreceptors. Trends Biochem Sci. NIH Public Access; 2001;26: 257–65. Available: http://www.ncbi.nlm.nih.gov/pubmed/11295559

21. Rosier BT, Lazova MD, McGuckin M, Sylvester P, Arul S, Pignatelli M. Dose-Response Analysis of Chemotactic Signaling Response in Salmonella typhimurium LT2 upon Exposure to Cysteine / Cystine Redox Pair. Pandey G, editor. PLoS One. ASM; 2016;11: e0152815. doi:10.1371/journal.pone.0152815

22. Wadhams GH, Armitage JP. Making sense of it all: bacterial chemotaxis. Nat Rev Mol Cell Biol. Nature Publishing Group; 2004;5: 1024–1037. doi:10.1038/nrm1524

23. Sourjik V, Wingreen NS. Responding to chemical gradients: bacterial chemotaxis. Curr Opin Cell Biol. NIH Public Access; 2012;24: 262–8. doi:10.1016/j.ceb.2011.11.008

24. Stecher B, Hapfelmeier S, Muller C, Kremer M, Stallmach T, Hardt WD. Flagella and chemotaxis are required for efficient induction of Salmonella enterica serovar Typhimurium colitis in streptomycin-pretreated mice. Infect Immun. 2004;72: 4138–4150. doi:10.1128/IAI.72.7.4138-4150.2004

25. Jones GW, Richardson LA, Uhlman D. The invasion of HeLa cells by Salmonella typhimurium: reversible and irreversible bacterial attachment and the role of bacterial motility. J Gen Microbiol. 1981;127: 351–60. doi:10.1099/00221287-127-2-351

26. Zhao K, Liu M, Burgess RR. Adaptation in bacterial flagellar and motility systems: from regulon members to "foraging"-like behavior in E. coli. Nucleic Acids Res. Oxford University Press; 2007;35: 4441–52. doi:10.1093/nar/gkm456

27. Wagner C, Barlag B, Gerlach RG, Deiwick J, Hensel M. The Salmonella enterica giant adhesin SiiE binds to polarized epithelial cells in a lectin-like manner. Cell Microbiol.

2014;16: 962–975. doi:10.1111/cmi.12253

28. Finlay B, Heffron F, Falkow S. Epithelial cell surfaces induce Salmonella proteins required for bacterial adherence and invasion. Science (80-). 1989;243: 940–943. doi:10.1126/science.2919285

29. Van Der Velden AWM, Bäumler AJ, Tsolis RM, Heffron F. Multiple fimbrial adhesins are required for full virulence of Salmonella typhimurium in mice. Infect Immun. 1998;66: 2803–2808.

30. Corr SC, Gahan CCGM, Hill C. M-cells: origin, morphology and role in mucosal immunity and microbial pathogenesis. FEMS Immunol Med Microbiol. Blackwell Publishing Ltd; 2008;52: 2–12. doi:10.1111/j.1574-695X.2007.00359.x

31. Jones BD. Salmonella typhimurium initiates murine infection by penetrating and destroying the specialized epithelial M cells of the Peyer's patches. J Exp Med. 1994;180: 15–23. doi:10.1084/jem.180.1.15

32. Garcia-del Portillo F, Finlay BB. Salmonella invasion of nonphagocytic cells induces formation of macropinosomes in the host cell. Infect Immun. American Society for Microbiology (ASM); 1994;62: 4641–5. Available: http://www.ncbi.nlm.nih.gov/pubmed/7927733

33. Kubori T, Matsushima Y, Nakamura D, Uralil J, Lara-Tejero M, Sukhan A, et al. Supramolecular Structure of the Salmonella typhimurium Type III Protein Secretion System. Science (80-). 1998;280.

34. Hardt W-D, Chen L-M, Schuebel KE, Bustelo XR, Galán JE. S. typhimurium Encodes an Activator of Rho GTPases that Induces Membrane Ruffling and Nuclear Responses in Host Cells. Cell. 1998;93: 815–826. doi:10.1016/S0092-8674(00)81442-7

35. Raffatellu M, Wilson RP, Chessa D, Andrews-Polymenis H, Tran QT, Lawhon S, et al. SipA, SopA, SopB, SopD, and SopE2 Contribute to Salmonella enterica Serotype Typhimurium Invasion of Epithelial Cells. Infect Immun. 2005;73: 146–154. doi:10.1128/IAI.73.1.146-154.2005

36. Francis CL, Ryan TA, Jones BD, Smith SJ, Falkow S. Ruffles induced by Salmonella and other stimuli direct macropinocytosis of bacteria. Nature. Nature Publishing Group; 1993;364: 639–642. doi:10.1038/364639a0

37. Zhang S, Santos RL, Tsolis RM, Stender S, Hardt W-D, Baumler AJ, et al. The Salmonella enterica Serotype Typhimurium Effector Proteins SipA, SopA, SopB, SopD, and SopE2 Act in Concert To Induce Diarrhea in Calves. Infect Immun. 2002;70: 3843–3855. doi:10.1128/IAI.70.7.3843-3855.2002

38. Shea JE, Hensel M, Gleeson C, Holden DW. Identification of a virulence locus encoding a second type III secretion system in Salmonella typhimurium. Proc Natl Acad Sci U S A. National Academy of Sciences; 1996;93: 2593–7. Available: http://www.ncbi.nlm.nih.gov/pubmed/8637919

39. Uchiya K, Barbieri MA, Funato K, Shah AH, Stahl PD, Groisman EA. A Salmonella virulence protein that inhibits cellular trafficking. EMBO J. European Molecular Biology Organization; 1999;18: 3924–33. doi:10.1093/emboj/18.14.3924

40. Worley MJ, Nieman GS, Geddes K, Heffron F. Salmonella typhimurium disseminates within its host by manipulating the motility of infected cells. Proc Natl Acad Sci U S A. National Academy of Sciences; 2006;103: 17915–20. doi:10.1073/pnas.0604054103

41. Abby SS, Rocha EPC. The non-flagellar type III secretion system evolved from the bacterial flagellum and diversified into host-cell adapted systems. PLoS Genet. Public Library of Science; 2012;8: e1002983. doi:10.1371/journal.pgen.1002983

42. Erhardt M, Namba K, Hughes KT. Bacterial nanomachines: the flagellum and type III injectisome. Cold Spring Harb Perspect Biol. 2010;2: a000299. doi:10.1101/cshperspect.a000299

43. Ellermeier CD, Slauch JM. RtsA and RtsB coordinately regulate expression of the invasion and flagellar genes in Salmonella enterica serovar Typhimurium. J Bacteriol. American Society for Microbiology; 2003;185: 5096–108. doi:10.1128/JB.185.17.5096-5108.2003

44. Takaya A, Erhardt M, Karata K, Winterberg K, Yamamoto T, Hughes KT. YdiV: a dual function protein that targets FlhDC for ClpXP-dependent degradation by promoting release of DNA-bound FlhDC complex. Mol Microbiol. 2012;83: 1268–1284. doi:10.1111/j.1365-2958.2012.08007.x

45. Singer HM, Erhardt M, Hughes KT. RflM functions as a transcriptional repressor in the autogenous control of the Salmonella Flagellar master operon flhDC. J Bacteriol. 2013;195: 4274–4282. doi:10.1128/JB.00728-13

46. Macnab RM. How bacteria assemble flagella. Annu Rev Microbiol. 2003;57: 77–100. doi:10.1146/annurev.micro.57.030502.090832

47. Apel D, Surette MG. Bringing order to a complex molecular machine: the assembly of the bacterial flagella. Biochim Biophys Acta. 2008;1778: 1851–8. doi:10.1016/j.bbamem.2007.07.005

48. Ibuki T, Imada K, Minamino T, Kato T, Miyata T, Namba K. Common architecture of the flagellar type III protein export apparatus and F- and V-type ATPases. Nat Struct Mol Biol. 2011;18: 277–282. doi:10.1038/nsmb.1977

49. Minamino T, Macnab RM. Components of the Salmonella flagellar export apparatus and classification of export substrates. J Bacteriol. 1999;181: 1388–1394. Available: http://www.ncbi.nlm.nih.gov/pubmed/10049367

50. Macnab RM. Type III flagellar protein export and flagellar assembly. Biochim Biophys Acta - Mol Cell Res. 2004;1694: 207–217. doi:10.1016/j.bbamcr.2004.04.005

51. Luirink J, Heijne G von, Houben E, Gier J-W de. BIOGENESIS OF INNER MEMBRANE PROTEINS IN *ESCHERICHIA COLI*. Annu Rev Microbiol. Annual Reviews; 2005;59: 329–355. doi:10.1146/annurev.micro.59.030804.121246

52. Francis NR, Sosinsky GE, Thomas D, DeRosier DJ. Isolation, characterization and structure of bacterial flagellar motors containing the switch complex. J Mol Biol. 1994;235: 1261–70. doi:10.1006/jmbi.1994.1079

53. Hirano T, Minamino T, Macnab RM. The role in flagellar rod assembly of the N-terminal domain of Salmonella FlgJ, a flagellum-specific muramidase. J Mol Biol. 2001;312: 359–

369. doi:10.1006/jmbi.2001.4963

54. Chevance FF V, Takahashi N, Karlinsey JE, Gnerer J, Hirano T, Samudrala R, et al. The mechanism of outer membrane penetration by the eubacterial flagellum and implications for spirochete evolution. Genes Dev. Cold Spring Harbor Laboratory Press; 2007;21: 2326–35. doi:10.1101/gad.1571607

55. Ohnishi K, Ohto Y, Aizawa S, Macnab RM, Iino T. FlgD is a scaffolding protein needed for flagellar hook assembly in Salmonella typhimurium. J Bacteriol. 1994;176: 2272–81. Available: http://www.ncbi.nlm.nih.gov/pubmed/8157595

56. Erhardt M, Hirano T, Su Y, Paul K, Wee DH, Mizuno S, et al. The role of the FliK molecular ruler in hook-length control in Salmonella enterica. Mol Microbiol. 2010;75: 1272–1284. doi:10.1111/j.1365-2958.2010.07050.x

57. Hirano T, Yamaguchi S, Oosawa K, Aizawa S. Roles of FliK and FlhB in determination of flagellar hook length in Salmonella typhimurium. J Bacteriol. American Society for Microbiology (ASM); 1994;176: 5439–49. Available: http://www.ncbi.nlm.nih.gov/pubmed/8071222

58. Van Arnam JS, McMurry JL, Kihara M, Macnab RM. Analysis of an engineered Salmonella flagellar fusion protein, FliR-FlhB. J Bacteriol. 2004;186: 2495–2498. Available: http://www.ncbi.nlm.nih.gov/pubmed/15060055

59. Ohnishi K, Kutsukake K, Suzuki H, Lino T. A novel transcriptional regulation mechanism in the flagellar regulon of Salmonella typhimurium: an antisigma factor inhibits the activity of the flagellum-specific sigma factor, sigma F. Mol Microbiol. 1992;6: 3149–57. Available: http://www.ncbi.nlm.nih.gov/pubmed/1453955

60. Wagner S, Königsmaier L, Lara-Tejero M, Lefebre M, Marlovits TC, Galán JE. Organization and coordinated assembly of the type III secretion export apparatus. Proc Natl Acad Sci U S A. National Academy of Sciences; 2010;107: 17745–50. doi:10.1073/pnas.1008053107

61. Kubori T, Sukhan A, Aizawa SI, Galán JE. Molecular characterization and assembly of the needle complex of the Salmonella typhimurium type III protein secretion system. Proc Natl Acad Sci U S A. National Academy of Sciences; 2000;97: 10225–30. doi:10.1073/pnas.170128997

62. Diepold A, Wagner S. Assembly of the bacterial type III secretion machinery. FEMS Microbiology Reviews. 2014. doi:10.1111/1574-6976.12061

63. Abrusci P, McDowell MA, Lea SM, Johnson S. Building a secreting nanomachine: a structural overview of the T3SS. Curr Opin Struct Biol. 2014;25: 111–117. doi:10.1016/j.sbi.2013.11.001

64. Hu B, Morado DR, Margolin W, Rohde JR, Arizmendi O, Picking WL, et al. Visualization of the type III secretion sorting platform of Shigella flexneri. Proc Natl Acad Sci U S A. National Academy of Sciences; 2015;112: 1047–52. doi:10.1073/pnas.1411610112

65. Eichelberg K, Ginocchio CC, Galán JE. Molecular and functional characterization of the Salmonella typhimurium invasion genes invB and invC: homology of InvC to the F0F1 ATPase family of proteins. J Bacteriol. American Society for Microbiology (ASM);

1994;176: 4501–10. Available: http://www.ncbi.nlm.nih.gov/pubmed/8045880

66. Kawamoto A, Morimoto Y V, Miyata T, Minamino T, Hughes KT, Kato T, et al. Common and distinct structural features of Salmonella injectisome and flagellar basal body. Sci Rep. 2013;3: 3369. doi:10.1038/srep03369

67. Wee DH, Hughes KT. Molecular ruler determines needle length for the Salmonella Spi-1 injectisome. Proc Natl Acad Sci U S A. National Academy of Sciences; 2015;112: 4098–103. doi:10.1073/pnas.1423492112

68. Snyder LAS, Loman NJ, Fütterer K, Pallen MJ. Bacterial flagellar diversity and evolution: seek simplicity and distrust it? Trends Microbiol. 2009;17: 1–5. doi:10.1016/j.tim.2008.10.002

69. Morimoto Y V, Ito M, Hiraoka KD, Che YS, Bai F, Kami-Ike N, et al. Assembly and stoichiometry of FliF and FlhA in Salmonella flagellar basal body. Mol Microbiol. 2014;91: 1214–1226. doi:10.1111/mmi.12529

70. Suzuki H, Yonekura K, Namba K. Structure of the rotor of the bacterial flagellar motor revealed by electron cryomicroscopy and single-particle image analysis. J Mol Biol. 2004;337: 105–113. doi:10.1016/j.jmb.2004.01.034

71. Kihara M, Minamino T, Yamaguchi S, Macnab RM. Intergenic suppression between the flagellar MS ring protein FliF of Salmonella and FlhA, a membrane component of its export apparatus. J Bacteriol. 2001;183: 1655–1662. doi:10.1128/JB.183.5.1655-1662.2001

72. Minamino T, Morimoto Y V, Hara N, Namba K. An energy transduction mechanism used in bacterial flagellar type III protein export. Nat Commun. 2011;2: 475. doi:10.1038/ncomms1488

73. Minamino T, Shimada M, Okabe M, Saijo-Hamano Y, Imada K, Kihara M, et al. Role of the C-terminal cytoplasmic domain of FlhA in bacterial flagellar type III protein export. J Bacteriol. 2010;192: 1929–1936. doi:10.1128/JB.01328-09

74. Ibuki T, Uchida Y, Hironaka Y, Namba K, Imada K, Minamino T. Interaction between FliJ and FlhA, components of the bacterial flagellar type III export apparatus. J Bacteriol. 2013;195: 466–473. doi:10.1128/JB.01711-12

75. Erhardt M, Wheatley P, Kim EA, Hirano T, Zhang Y, Sarkar MK, et al. Mechanism of type-III protein secretion: Regulation of FlhA conformation by a functionally critical charged-residue cluster. Mol Microbiol. 2017; doi:10.1111/mmi.13623

76. Abrusci P, Vergara-Irigaray M, Johnson S, Beeby MD, Hendrixson DR, Roversi P, et al. Architecture of the major component of the type III secretion system export apparatus. Nat Struct Mol Biol. 2013;20: 99–104. doi:10.1038/nsmb.2452

77. Fraser GM, Hirano T, Ferris HU, Devgan LL, Kihara M, Macnab RM. Substrate specificity of type III flagellar protein export in Salmonella is controlled by subdomain interactions in FlhB. Mol Microbiol. 2003;48: 1043–1057. Available: http://www.ncbi.nlm.nih.gov/pubmed/12753195

78. Ohnishi K, Fan F, Schoenhals GJ, Kihara M, Macnab RM. The FliO, FliP, FliQ, and FliR proteins of Salmonella typhimurium: putative components for flagellar assembly. J

Bacteriol. 1997;179: 6092–6099. Available: http://www.ncbi.nlm.nih.gov/pubmed/9324257

79. Suzuki H, Yonekura K, Murata K, Hirai T, Oosawa K, Namba K. A Structural Feature in the Central Channel of the Bacterial Flagellar FliF Ring Complex Is Implicated in Type III Protein Export. J Struct Biol. 1998;124: 104–114. doi:10.1006/jsbi.1998.4048

80. Fan F, Ohnishi K, Francis NR, Macnab RM. The FliP and FliR proteins of Salmonella typhimurium, putative components of the type III flagellar export apparatus, are located in the flagellar basal body. Mol Microbiol. 1997;26: 1035–1046. Available: http://www.ncbi.nlm.nih.gov/pubmed/9426140

81. Barker CS, Meshcheryakova I V, Kostyukova AS, Samatey FA. FliO regulation of FliP in the formation of the Salmonella enterica flagellum. PLoS Genet. 2010;6: e1001143. doi:10.1371/journal.pgen.1001143

82. Morimoto Y V, Nakamura S, Hiraoka KD, Namba K, Minamino T. Distinct roles of highly conserved charged residues at the MotA-FliG interface in bacterial flagellar motor rotation. J Bacteriol. 2013;195: 474–481. doi:10.1128/JB.01971-12

83. Toker AS, Macnab RM. Distinct regions of bacterial flagellar switch protein FliM interact with FliG, FliN and CheY. J Mol Biol. 1997;273: 623–634. doi:10.1006/jmbi.1997.1335

84. Gonzalez-Pedrajo B, Minamino T, Kihara M, Namba K. Interactions between C ring proteins and export apparatus components: a possible mechanism for facilitating type III protein export. Mol Microbiol. 2006;60: 984–998. doi:10.1111/j.1365-2958.2006.05149.x

85. Bai F, Morimoto Y V, Yoshimura SD, Hara N, Kami-Ike N, Namba K, et al. Assembly dynamics and the roles of FliI ATPase of the bacterial flagellar export apparatus. Sci Rep. 2014;4: 6528. doi:10.1038/srep06528

86. Paul K, Erhardt M, Hirano T, Blair DF, Hughes KT. Energy source of flagellar type III secretion. Nature. 2008;451: 489–492. doi:10.1038/nature06497

87. Akeda Y, Galán JE. Chaperone release and unfolding of substrates in type III secretion. Nature. Nature Publishing Group; 2005;437: 911–915. doi:10.1038/nature03992

88. Minamino T, Namba K. Distinct roles of the FliI ATPase and proton motive force in bacterial flagellar protein export. Nature. 2008;451: 485–488. doi:10.1038/nature06449

89. Namba K. Roles of partly unfolded conformations in macromolecular self-assembly. Genes Cells. 2001;6: 1–12. Available: http://www.ncbi.nlm.nih.gov/pubmed/11168592

90. Macnab RM. Type III flagellar protein export and flagellar assembly. Biochim Biophys Acta. 2004;1694: 207–217. doi:10.1016/j.bbamcr.2004.04.005

91. Erhardt M, Mertens ME, Fabiani FD, Hughes KT. ATPase-independent type-III protein secretion in Salmonella enterica. PLoS Genet. 2014;10: e1004800. doi:10.1371/journal.pgen.1004800

92. Erhardt M, Hughes KT. C-ring requirement in flagellar type III secretion is bypassed by FlhDC upregulation. Mol Microbiol. Blackwell Publishing Ltd; 2010;75: 376–393. doi:10.1111/j.1365-2958.2009.06973.x

93. Konishi M, Kanbe M, McMurry JL, Aizawa S-I. Flagellar formation in C-ring-defective mutants by overproduction of FliI, the ATPase specific for flagellar type III secretion. J Bacteriol. 2009;191: 6186–91. doi:10.1128/JB.00601-09

94. Kihara A, Akiyama Y, Ito K. Different pathways for protein degradation by the FtsH/HflKC membrane-embedded protease complex: an implication from the interference by a mutant form of a new substrate protein, YccA. J Mol Biol. 1998;279: 175–188. doi:10.1006/jmbi.1998.1781

95. Haldimann A, Wanner BL. Conditional-replication, integration, excision, and retrieval plasmid-host systems for gene structure-function studies of bacteria. J Bacteriol. American Society for Microbiology; 2001;183: 6384–93. doi:10.1128/JB.183.21.6384-6393.2001

96. Yen K-M, Serdar CM, Gunsalus IC. Genetics of Naphthalene Catabolism in Pseudomonads. CRC Crit Rev Microbiol. Taylor & Francis; 1988;15: 247–268. doi:10.3109/10408418809104459

97. Feng Y, Cronan JE. Overlapping repressor binding sites result in additive regulation of Escherichia coli FadH by FadR and ArcA. J Bacteriol. American Society for Microbiology (ASM); 2010;192: 4289–99. doi:10.1128/JB.00516-10

98. Diepold A, Armitage JP. Type III secretion systems: the bacterial flagellum and the injectisome. Philos Trans R Soc Lond B Biol Sci. The Royal Society; 2015;370. doi:10.1098/rstb.2015.0020

99. Pallen MJ, Penn CW, Chaudhuri RR. Bacterial flagellar diversity in the post-genomic era. Trends Microbiol. Elsevier; 2005;13: 143–9. doi:10.1016/j.tim.2005.02.008

100. Schoenhals GJ, Kihara M, Macnab RM. Translation of the flagellar gene fliO of Salmonella typhimurium from putative tandem starts. J Bacteriol. 1998;180: 2936–2942. Available: http://www.ncbi.nlm.nih.gov/pubmed/9603885

101. Barker CS, Meshcheryakova I V, Inoue T, Samatey FA. Assembling flagella in Salmonella mutant strains producing a type III export apparatus without FliO. J Bacteriol. 2014;196: 4001–4011. doi:10.1128/JB.02184-14

102. Dietsche T, Tesfazgi Mebrhatu M, Brunner MJ, Abrusci P, Yan J, Franz-Wachtel M, et al. Structural and Functional Characterization of the Bacterial Type III Secretion Export Apparatus. Coombes BK, editor. PLOS Pathog. Public Library of Science; 2016;12: e1006071. doi:10.1371/journal.ppat.1006071

103. Beitz E. TeXshade: shading and labeling of multiple sequence alignments using LaTeX2e. Bioinformatics. Oxford University Press; 2000;16: 135–139. doi:10.1093/bioinformatics/16.2.135

104. Tsang J, Hoover TR. Requirement of the flagellar protein export apparatus component FliO for optimal expression of flagellar genes in Helicobacter pylori. J Bacteriol. 2014;196: 2709–2717. doi:10.1128/JB.01332-13

105. Langklotz S, Baumann U, Narberhaus F. Structure and function of the bacterial AAA protease FtsH. Biochim Biophys Acta. 2012;1823: 40–48. doi:10.1016/j.bbamcr.2011.08.015

106. Langklotz S, Schäkermann M, Narberhaus F. Control of lipopolysaccharide biosynthesis by FtsH-mediated proteolysis of LpxC is conserved in enterobacteria but not in all gram-negative bacteria. J Bacteriol. American Society for Microbiology (ASM); 2011;193: 1090–7. doi:10.1128/JB.01043-10

107. Simmons LA, Grossman AD, Walker GC. Clp and Lon proteases occupy distinct subcellular positions in Bacillus subtilis. J Bacteriol. American Society for Microbiology; 2008;190: 6758–68. doi:10.1128/JB.00590-08

108. Lush MJ, Li Y, Read DJ, Willis AC, Glynn P. Neuropathy target esterase and a homologous Drosophila neurodegeneration-associated mutant protein contain a novel domain conserved from bacteria to man. Biochem J. 1998;332 (Pt 1: 1–4. Available: http://www.ncbi.nlm.nih.gov/pubmed/9576844

109. Liss V, Barlag B, Nietschke M, Hensel M. Self-labelling enzymes as universal tags for fluorescence microscopy, super-resolution microscopy and electron microscopy. Sci Rep. 2015;5: 17740. doi:10.1038/srep17740

110. Barlag B, Beutel O, Janning D, Czarniak F, Richter CP, Kommnick C, et al. Single molecule super-resolution imaging of proteins in living Salmonella enterica using self-labelling enzymes. Sci Rep. 2016;6: 31601. Available: http://www.ncbi.nlm.nih.gov/pubmed/27534893

111. Dajkovic A, Hinde E, MacKichan C, Carballido-Lopez R. Dynamic Organization of SecA and SecY Secretion Complexes in the B. subtilis Membrane. PLoS One. 2016;11: e0157899. doi:10.1371/journal.pone.0157899

112. Kumar M, Mommer MS, Sourjik V. Mobility of cytoplasmic, membrane, and DNA-binding proteins in Escherichia coli. Biophys J. 2010;98: 552–559. doi:10.1016/j.bpj.2009.11.002

113. Pugsley AP. The complete general secretory pathway in gram-negative bacteria. Microbiol Rev. 1993;57: 50–108. Available: http://www.ncbi.nlm.nih.gov/pubmed/8096622

114. Paetzel M. Structure and mechanism of Escherichia coli type I signal peptidase. Biochim Biophys Acta - Mol Cell Res. 2014;1843: 1497–1508. doi:10.1016/j.bbamcr.2013.12.003

115. Nilsson I, von Heijne G. A signal peptide with a proline next to the cleavage site inhibits leader peptidase when present in a *sec* -independent protein. FEBS Lett. 1992;299: 243–246. doi:10.1016/0014-5793(92)80124-Y

116. Carpenter PB, Zuberi AR, Ordal GW. Bacillus subtilis flagellar proteins FliP, FliQ, FliR and FlhB are related to Shigella flexneri virulence factors. Gene. 1993;137: 243–245. doi:10.1016/0378-1119(93)90014-T

117. Blocker A, Komoriya K, Aizawa S-I. Type III secretion systems and bacterial flagella: insights into their function from structural similarities. Proc Natl Acad Sci U S A. National Academy of Sciences; 2003;100: 3027–30. doi:10.1073/pnas.0535335100

118. Saijo-Hamano Y, Imada K, Minamino T, Kihara M, Shimada M, Kitao A, et al. Structure of the cytoplasmic domain of FlhA and implication for flagellar type III protein export. Mol Microbiol. 2010;76: 260–268. doi:10.1111/j.1365-2958.2010.07097.x

119. Zilkenat S, Franz-Wachtel M, Stierhof YD, Galan JE, Macek B, Wagner S. Determination of the stoichiometry of the complete bacterial type III secretion needle complex using a combined quantitative proteomic approach. Mol Cell Proteomics. 2016; doi:10.1074/mcp.M115.056598

120. Kubori T, Yamaguchi S, Aizawa S. Assembly of the switch complex onto the MS ring complex of Salmonella typhimurium does not require any other flagellar proteins. J Bacteriol. 1997;179: 813–7. Available: http://www.ncbi.nlm.nih.gov/pubmed/9006037

121. Huber R, Swanson R V., Deckert G, Warren P V., Gaasterland T, Young WG, et al. The complete genome of the hyperthermophilic bacterium Aquifex aeolicus. Nature. Nature Publishing Group; 1998;392: 353–358. doi:10.1038/32831

122. Pitulle C, Yang Y, Marchiani M, Moore ERB, Siefert JL, Aragn0 M, et al. Phylogenetic Position of the Genus Hydrogenobacter. Int J Syst Bacteriol. 1994; 620–626.

123. Kröger C, Colgan A, Srikumar S, Händler K, Sivasankaran SK, Hammarlöf DL, et al. An Infection-Relevant Transcriptomic Compendium for Salmonella enterica Serovar Typhimurium. Cell Host Microbe. Elsevier; 2013;14: 683–695. doi:10.1016/j.chom.2013.11.010

124. Kline T, Felise HB, Sanowar S, Miller SI. The type III secretion system as a source of novel antibacterial drug targets. Curr Drug Targets. 2012;13: 338–51. Available: http://www.ncbi.nlm.nih.gov/pubmed/22206256

125. Erhardt M. Strategies to Block Bacterial Pathogenesis by Interference with Motility and Chemotaxis. Curr Top Microbiol Immunol. 2016; doi:10.1007/82_2016_493

126. Karlinsey JE. lambda-Red genetic engineering in Salmonella enterica serovar Typhimurium. Methods Enzym. 2007;421: 199–209. doi:10.1016/S0076-6879(06)21016-4

127. Blank K, Hensel M, Gerlach RG. Rapid and highly efficient method for scarless mutagenesis within the Salmonella enterica chromosome. PLoS One. Public Library of Science; 2011;6: e15763. doi:10.1371/journal.pone.0015763

128. Datsenko KA, Wanner BL. One-step inactivation of chromosomal genes in Escherichia coli K-12 using PCR products. Proc Natl Acad Sci U S A. 2000;97: 6640–6645. doi:10.1073/pnas.120163297

129. Shevchuk NA, Bryksin A V, Nusinovich YA, Cabello FC, Sutherland M, Ladisch S. Construction of long DNA molecules using long PCR-based fusion of several fragments simultaneously. Nucleic Acids Res. Oxford University Press; 2004;32: e19. doi:10.1093/nar/gnh014

130. Cherepanov PP, Wackernagel W. Gene disruption in Escherichia coli: TcR and KmR cassettes with the option of Flp-catalyzed excision of the antibiotic-resistance determinant. Gene. 1995;158: 9–14. Available: http://www.ncbi.nlm.nih.gov/pubmed/7789817

131. Ladner CL, Yang J, Turner RJ, Edwards RA. Visible fluorescent detection of proteins in polyacrylamide gels without staining. Anal Biochem. 2004;326: 13–20. doi:10.1016/j.ab.2003.10.047

132. Kaur J, Bachhawat AK. A modified Western blot protocol for enhanced sensitivity in the detection of a membrane protein. Anal Biochem. 2009;384: 348–349. doi:10.1016/j.ab.2008.10.005

133. Rappsilber J, Mann M, Ishihama Y. Protocol for micro-purification, enrichment, pre-fractionation and storage of peptides for proteomics using StageTips. Nat Protoc. Nature Publishing Group; 2007;2: 1896–1906. doi:10.1038/nprot.2007.261